

AD-A174 851

ADVANCED CONSTRUCTION PROCEDURES: CONFINED BASES FOR
AIRPORT PAVEMENTS (U) ARMY ENGINEER WATERWAYS
EXPERIMENT STATION VICKSBURG MS GEOTE

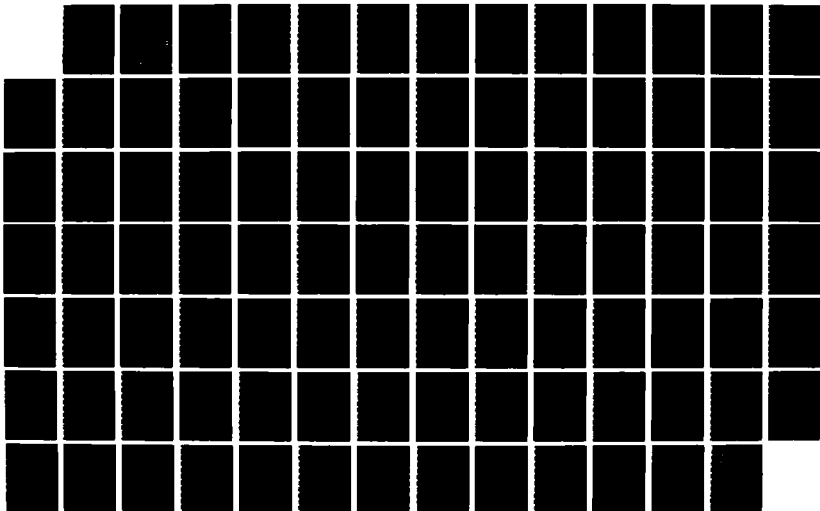
1/1

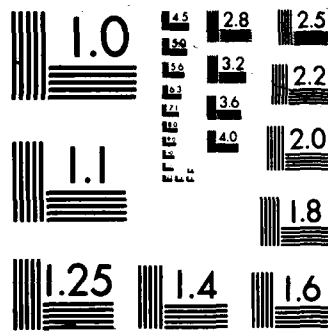
UNCLASSIFIED

J C POTTER ET AL SEP 86 DOT/FAA/PM-86/9

F/G 13/3

NL





XEROCOPY RESOLUTION TEST CHART

2

DOT/FAA/PM-86/9

Program Engineering
and Maintenance Service
Washington, D.C. 20591

Advanced Construction Procedures: Confined Bases for Airport Pavements

John C. Potter
Philip C. Lambe

Geotechnical Laboratory
DEPARTMENT OF THE ARMY
Waterways Experiment Station
Corps of Engineers
Vicksburg, Mississippi 39180

September 1986

Final Report

DTIC
ELECTE
DEC 5 1986
S B D

AD-A174 851

DTIC FILE COPY

This Document is available to the public
through the National Technical Information
Service, Springfield, Virginia 22161.



U.S. Department of Transportation
Federal Aviation Administration

86 12 04 004

NOTICE

This document is disseminated under the sponsorship of the Department of Transportation in the interest of information exchange. The United States Government assumes no liability for its contents or use thereof.

The United States Government does not endorse products of manufacturers. Trade or manufacturers' names appear herein solely because they are considered essential to the object of this report.

1. Report No. DOT/FAA/PM-86/9	2. Government Accession No. <i>AD-A174 851</i>	3. Recipient's Catalog No.	
4. Title and Subtitle ADVANCED CONSTRUCTION PROCEDURES: CONFINED BASES FOR AIRPORT PAVEMENTS		5. Report Date September 1986	6. Performing Organization Code
7. Author(s) John C. Potter, Philip C. Lambe		8. Performing Organization Report No.	
9. Performing Organization Name and Address US Army Engineer Waterways Experiment Station Geotechnical Laboratory PO Box 631, Vicksburg, MS 39180-0631		10. Work Unit No. (TRAIS)	11. Contract or Grant No. IA DTFA01-83-Y-30606
12. Sponsoring Agency Name and Address US Department of Transportation Federal Aviation Administration 800 Independence Avenue, SW Washington, DC 20591		13. Type of Report and Period Covered Final Report September 1983 to March 1986	
15. Supplementary Notes The US Army Engineer Waterways Experiment Station conducted this study sponsored by the Federal Aviation Administration under Inter-Agency Agreement No. DTFA01-83-Y-30606.		14. Sponsoring Agency Code APM-740	
16. Abstract <p>→ Airports for light aircraft must often be built in areas where base course material is inadequate or economically unavailable. Sand grids may provide an economical solution in these cases. Previous work with sand grids has identified optimum grid-cell geometry based on ultimate bearing capacity. Past observations also suggest the nature of sand-grid behavior for small stresses and strains. From these a model was formulated for analyzing the performance of sand grids in pavement systems and spot-checked using field data from a full-scale, accelerated-traffic sand-grid test section. <i>Keywords:</i></p>			
17. Key Words → Airfield pavement, Confined base, Elastic layer analysis, Pavement design, → Soil confinement Sand grids, system		18. Distribution Statement This document is available to the public through the National Technical Information Service, Springfield, Virginia 22161.	
19. Security Classif. (of this report) Unclassified	20. Security Classif. (of this page) Unclassified	21. No. of Pages 94	22. Price

METRIC CONVERSION FACTORS

Approximate Conversions to Metric Measures		Approximate Conversions to Metric Measures	
When You Know	Multiply by	To Find	Symbol
LENGTH			
inches	* 2.5	centimeters	cm
feet	30	centimeters	cm
yards	0.9	meters	m
miles	1.6	kilometers	km
AREA			
square inches	6.5	square centimeters	cm ²
square feet	0.09	square meters	m ²
square yards	0.8	square meters	m ²
square miles	2.6	square kilometers	km ²
acres	0.4	hectares	ha
MASS (weight)			
ounces	28	grams	g
pounds	0.45	kilograms	kg
short tons (2000 lb)	0.9	tonnes	t
VOLUME			
teaspoons	5	milliliters	ml
tablespoons	15	milliliters	ml
fluid ounces	30	milliliters	ml
cups	0.24	liters	l
pints	0.47	liters	l
quarts	0.96	liters	l
gallons	3.8	liters	l
cubic feet	0.03	cubic meters	m ³
cubic yards	0.76	cubic meters	m ³
TEMPERATURE (exact)			
Fahrenheit temperature	5/9 after subtracting 32)	Celsius temperature	°C
TEMPERATURE (exact)			
Celsius temperature	9/5 (then add 32)	Fahrenheit temperature	°F

* 1 in. = 2.54 (exactly). For other exact conversions and more detailed tables, see NBC Misc. Publ. 286, Units of Weights and Measures, Price \$2.25. SD Catalog No. C13.10.286.

LIST OF FIGURES

<u>Figure No.</u>		<u>Page</u>
1	Typical HDPE sand grid	2
2	Effect of grid thickness and elastic modulus on permanent deformation	7
3	Elastic layered pavement idealization	11
4	Westergaard pavement idealization	11
5	Pavement idealization using a finite element program	13
6	Permanent deformation as a function of traffic repetitions	15
7	Comparison of subgrade strain criteria	16
8	Schematic of the sand-grid system	18
9	Flow chart for the analysis	20
10	Grain-size distribution	23
11	K_o data	25
12	Variation of shear modulus with shear strain for sands	26
13	Direct shear test results	28
14	Subgrade pressure as a function of K	30
15	Applied pressure distribution	31
16	Deflection profile	32
17	Sand-grid schematic	33
18	SGRID flow chart	35
19	SGRID data, case 4-3	36
20	Input and output pressures, case 4-1	41
21	Input and output pressures, case 4-2	42
22	Input and output pressures, case 4-3	43

<u>Figure No.</u>		<u>Page</u>
23	Conceptual design chart	46
24	General layout, sand-grid test section	48
25	Average rut depth as a function of vehicle passes . .	49
26	Equivalent single wheel load in percent of axle load versus depth	51
27	Test section data and predicted performance	52

LIST OF TABLES

<u>Table</u>		<u>Page</u>
1	Summary of Input Data	27
2	Results for Case 2	38
3	Results for Case 3	39
4	Results for Case 4	40
5	Summary of Results	44

INTRODUCTION

BACKGROUND

In many cases, airports are located on river banks or in floodplains which do not possess good subgrade characteristics. In some instances, the subgrade can only be improved at great expense by replacing weak material with imported soil, or by stabilization. Further, base course materials may also be inadequate or economically unavailable. For remote areas where suitable substitute soils cannot be obtained and where an airport pavement is required, a technique by which native material can be used to support light commercial or general aviation aircraft needs to be developed. The resulting criteria and methodology may provide greater economies in the construction of remote airports by utilization of certain on-site materials.

Soil confinement systems have evolved from the use of geotextiles in soil construction. The tensile strength of geotextiles make them a logical complement to soils, which exhibit little or no tensile strength. Mass strength can be increased by using geotextile cells to supply additional confining stress. Most effective with granular materials, this concept has been employed for many years in the form of sandbags. Recently, the US Army Corps of Engineers has experimented with mechanical confinement of loose or weak cohesionless materials to strengthen them for use in temporary roads. Developmental work has been conducted using grids forming interconnected confining cells, open top and bottom (see Figure 1). Various materials have been tried, including paper, aluminum, and plastic. High-density polyethelene (HDPE) has been found to provide the best combination of strength, service life, and economy. The cell system contributes to the composite, vertical compressive strength by increasing the horizontal confining stress acting on the cell filler material. When the filler material is sand, these grid systems are sometimes known as sand-grid confinement systems, or simply sand grids.

SCOPE

This report presents a discussion of previous work on confined soil systems for pavements and the development of a performance model. Previous and concurrent work on soil confinement systems, existing pavement system performance models, and basic soil mechanics theories and practices form the basis of this analysis. Laboratory testing and field verification of the design methodology and construction procedure are being considered in a continuation of this research effort.

OBJECTIVE

The objective of this report is to develop an analysis of the behavior of soil confinement systems, identify a mode of behavior appropriate to sand grids in pavement systems, and describe the formulation of a mathematically based model to predict sand-grid pavement performance (serviceability). Performance is to be determined as a function of aircraft landing gear configuration, wheel loads and tire pressures, traffic intensity, and increased strength of the confined material.

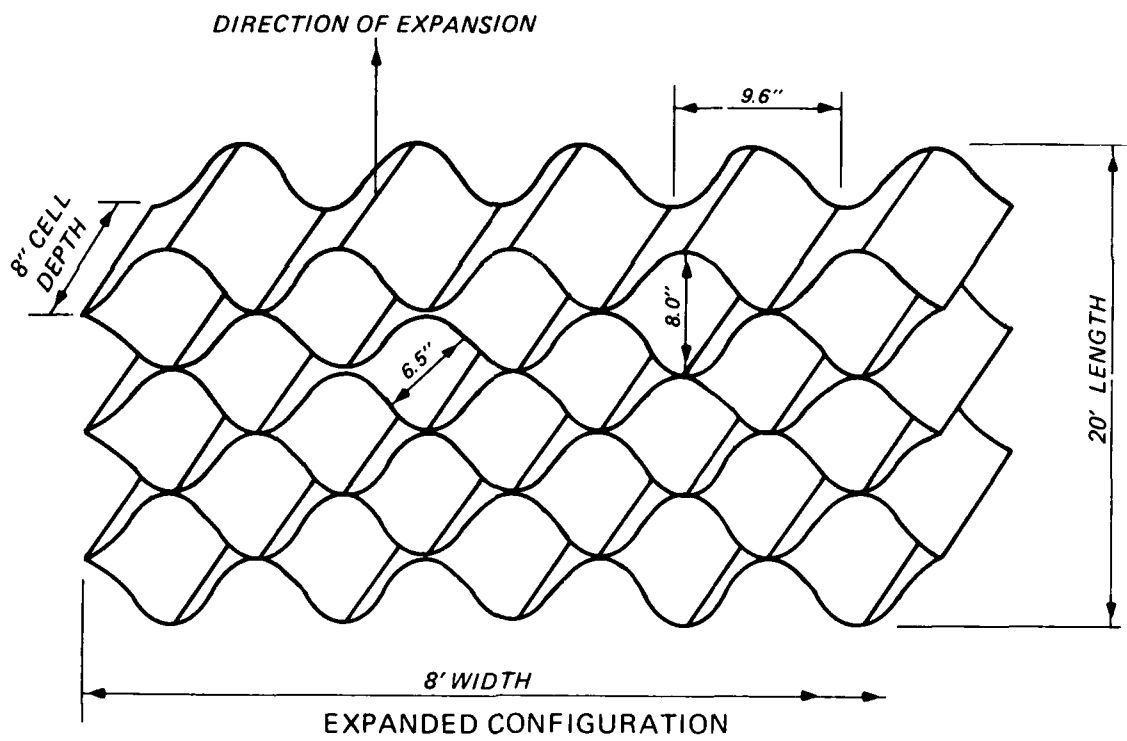
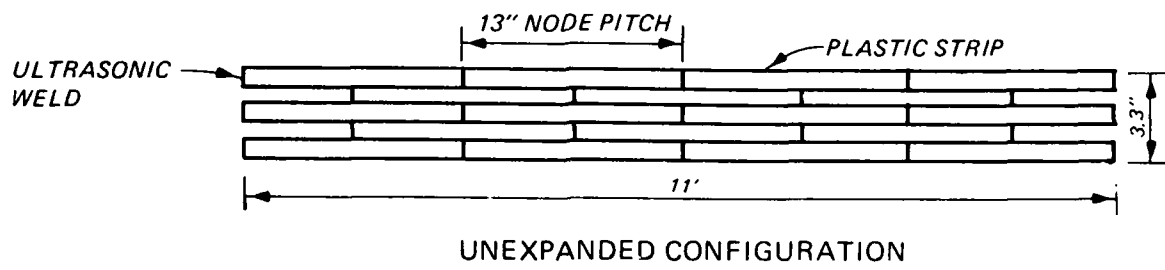


Figure 1. Typical HDPE sand grid

CONSTRAINTS

Pavements are traditionally analyzed in layers according to material strength. Soil confinement systems, because of their moderate strength, may find application in the base course or subbase elements of traditional pavement systems, or even as surface layers.

As noted earlier, soil confinement systems are most effective with granular materials. This is because an increase in strength with increased confining pressure is characteristic of granular materials. Both coarse and fine granular materials are suitable for use in soil confinement systems. Fine aggregate is often readily available even when coarse aggregate is scarce or unavailable. Hence, this study concentrates on fine aggregate or sand as the cell filler material.

These material constraints are typical of remote areas with relatively undeveloped transportation networks and many light utility airports. Air traffic at these airports is characterized by gross weights of less than 30,000 lb,* and usually less than 12,500 lb. Various aircraft can be related to existing pavement performance models and data using an equivalent single-wheel load (ESWL) concept, such as the one developed and used by the US Army Corps of Engineers.²³ The ESWL is applied to the pavement, including the sand-grid system, through the pavement surfacing or wearing course, if any. Light utility airport pavements frequently include a 2-in. asphaltic concrete wearing course. This surfacing serves to distribute both the vertical contact stress from aircraft tires and the horizontal shear stresses generated by aircraft braking and turning. The base course is thus protected from localized material displacements or failures caused by high tire contact pressures or aircraft braking and turning forces.

Pavement performance is most usefully evaluated in terms of serviceability. The end of a pavement's service life is usually marked by excessive permanent deformation (rutting) or cracking. Brabston, Barker, and Harvey³ found that a strain-based criteria provided the most accurate and consistent prediction of flexible pavement service life. Their design method is based on limiting vertical compressive strain at the top of the subgrade and horizontal tensile strain at the bottom of the bituminous concrete layer. A review of various strain criteria is given by Barker and Brabston.²

* A table of factors for converting non-SI units of measurement to SI (metric) units is presented on page ii.

PREVIOUS WORK

DESCRIPTION

Early attempts²¹ to model the behavior of sand grids have been hampered by a lack of quantitative data describing actual behavior.

Mitchell, Kao, and Kavazanjian,²¹ however, proposed several possible failure modes. These included (a) cell penetration into the subgrade, (b) cell rupture, (c) cell wall buckling, (d) simple bearing capacity, (e) beam or raft bending, (f) deterioration with time, and (g) rutting under traffic. They then conducted a series of model tests to gather additional quantitative data. This series formed an extension of earlier work by Rea and Mitchell.²⁶ Like the tests conducted by Rea and Mitchell,²⁶ these experiments were primarily concerned with the plate-bearing capacity of sand grids for various grid geometries.

Rea and Mitchell²⁶ and Mitchell, Kao, and Kavazanjian²¹ suggested optimum geometrical relationships based on their experiments. They concluded that the width of the grid cells should be about two-thirds the width of the loaded area, and the height of the grid cells should be about four-thirds the width of the loaded area. These relationships are consistent with classical soil mechanics theory. According to Prandtl's theory,¹⁸ the zone of shearing failure under a loaded area extends to a depth of less than four-thirds the width of the loaded area in soils whose angles of internal friction are less than about 30 deg. An angle of internal friction of 30 deg is a typical design value for sands.

From the standpoint of repetitive loading due to traffic, the plate-bearing capacity of a sand grid can be thought of as the maximum load for one repetition. Thus, these optimum geometrical relationships can be used to estimate the cell dimensions required for a particular type of traffic. Cell dimensions can then be adjusted based on the performance of sand grids under traffic. After numerous tests using truck traffic³⁰⁻³³ Webster* has adopted a cell height of 8 in. and a mean cell diameter of 7 in. The typical truck tire has a width of about 8 in. Thus, Webster has adjusted his cell width to approximately seven-eighths the width of the loaded area, and his cell height to approximately equal the width of the loaded area. These dimensions have proven satisfactory under extended traffic tests, and have become the de facto industry standard. They are therefore used as a basis for analysis and point of departure for this study.

ANALYSIS

Rea and Mitchell²⁶ noted that sand grid layers produce a greater lateral distribution of vertical stress than unconfined layers of granular materials. This indicates that they behave like beams or plates which, unlike layers of unconfined granular materials, can carry tensile

* S. L. Webster. 1983. Private Communication, US Army Engineer Waterways Experiment Station, Vicksburg, Miss.

stresses. This observation suggests that the sand in the unloaded sand grid is held in compression by the grid cells much like concrete is held in compression by the prestressing tendons of a prestressed concrete beam. Then, under moderate loads, the composite, sand-grid layer is able to perform as a flexural element without developing tensile strains in the sand.

Mitchell, Kao, and Kavazanjian²¹ reported that the load-settlement behavior of plates on sand grids is approximately linear up to moderate (50 psi) stress levels, and that grid cells can increase the effective modulus of the sand filler material by a factor of 2 to 3. They also suggested a qualitative model for predicting the modulus of elasticity of a sand-grid layer. Their test results indicated that the significant parameters are layer geometry, loaded area-grid geometry, sand modulus, grid-material modulus, subgrade modulus, and the number of grid joints per unit area.

Hicks¹⁵ concluded that the apparent Young's modulus of granular materials, E_s as observed in triaxial tests can be represented by equations

$$E_s = k_1 \sigma_3^{k_2} \quad (1)$$

and

$$E_s = k_3 \ell^{k_4} \quad (2)$$

where

k_1, k_2, k_3, k_4 = regression constants

σ_3 = minor principal stress

ℓ = bulk stress (sum of the three principal stresses)

Further, Poisson's ratio, ν , as observed in triaxial compression stress states can be described as

$$\nu = a_1 + a_2 \left(\frac{\sigma_1}{\sigma_3} \right) + a_3 \left(\frac{\sigma_1}{\sigma_3} \right)^2 + a_4 \left(\frac{\sigma_1}{\sigma_3} \right)^3 \quad (3)$$

where

a_1, a_2, a_3, a_4 = regression constants

σ_1 = major principal stress

$\sigma_3 = \sigma_2$ = minor principal stress

Parameters affecting the values of the regression constants in these equations include aggregate density, gradation, soil type, degree of saturation, and particle angularity. Thus the apparent E_s and ν can be estimated from the results of laboratory tests on a particular material prepared to simulate the anticipated field conditions.

The problem is complicated by the fact that stresses in pavement layers, during the passage of traffic wheel-loads, vary widely in both magnitude and orientation. Stress conditions under passing wheel-loads are an area currently not well understood. The reasonably well developed earth-pressure theory applies to static conditions at failure.

The presence of grid cells in the sand layer modifies the apparent E_s and ν by altering the stress state of the soil. The combination of the grid cells and compaction (by rollers during construction and by traffic) apparently increases the horizontal stress in the sand, and changes the shape of the shear zone. The magnitude of this stress increases and the modified shape of the shear zone is uncertain. However, the significant parameters influencing the process include the elastic modulus of the grid material, the geometry and dimensions of the grid cells and the loaded area, the degree of densification of the grid filler aggregate, and the intensity of the load. Preliminary data from Webster* (Figure 2) indicate that the product of the thickness and the modulus of elasticity of the grid material is a dominant parameter influencing the rutting of a sand-grid pavement. Additional data are required to completely define this relationship, even for a limited combination of sand, traffic, and grid type.

Finally, the apparent, composite modulus of sand-grid layers has been observed by Mitchell, Kao, and Kavazanjian²¹ to depend upon the modulus of the material supporting the sand grid layer. This behavior cannot be modeled by a methodology which considers only the physical characteristics of the materials in the sand-grid layer. Sand-grid layers must be analyzed as part of a system.

A predictive model for sand-grid moduli must consider three categories of parameters: (a) sand-grid materials, (b) support conditions, and (c) loading conditions. As previously noted, each of these categories consists of many parameters having a significant impact on the performance of a sand-grid pavement system.

EVALUATION

The composite modulus of elasticity of sand-grid pavements can be obtained from test sections using nondestructive testing (NDT) methods.⁶ This has been done using a sand-grid test section at US Army Engineer Waterways Experiment Station (WES). The test section is part of a concurrent WES research project. It consists of an 8-in.-thick sand-grid layer over a compacted sand subgrade.

* Webster, *ibid.*

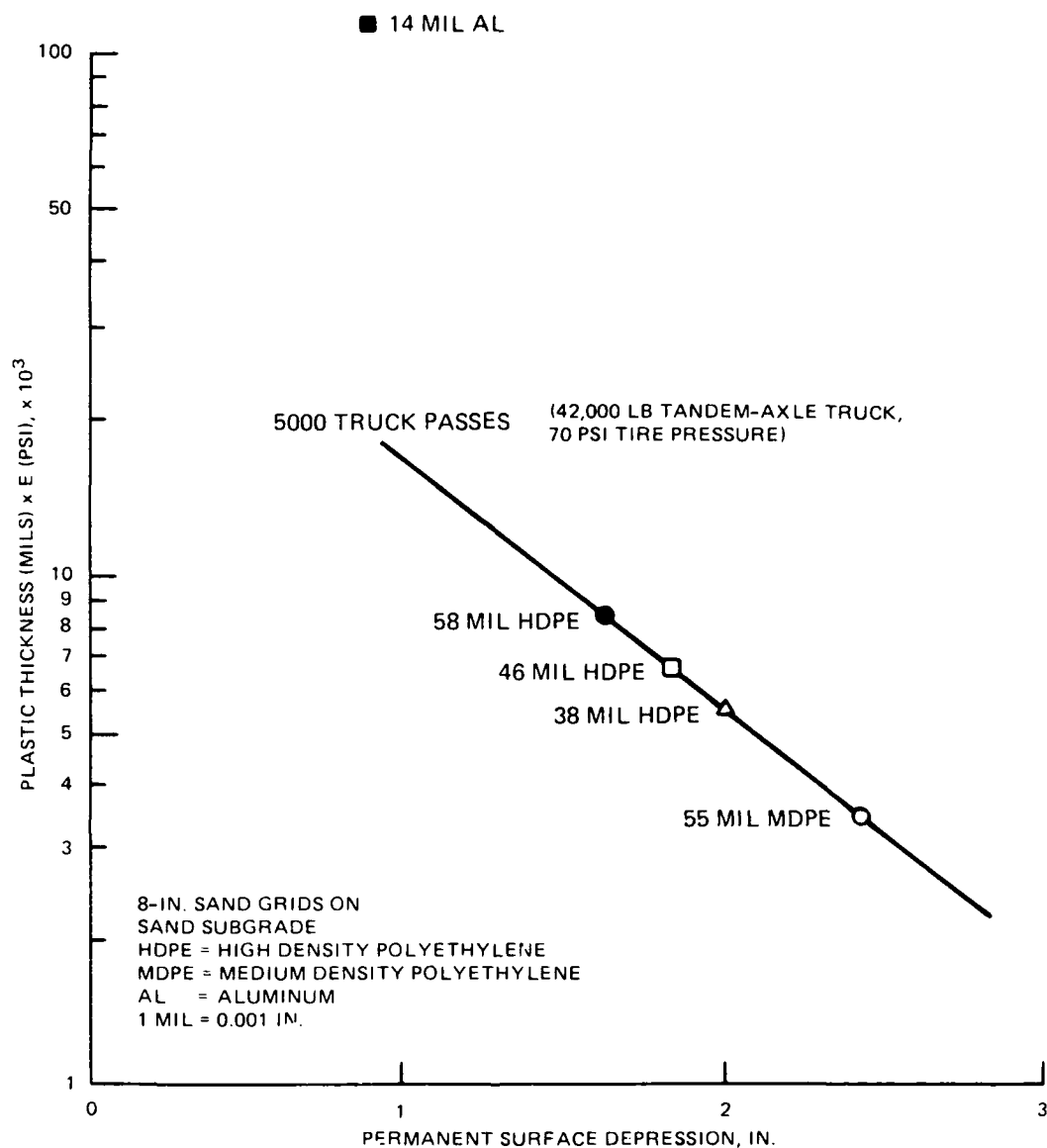


Figure 2. Effect of grid thickness and elastic modulus on permanent deformation*

A Falling Weight Deflectometer (FWD)⁵ was used to generate deflection data for the BISDEF layered elastic computer program. This proprietary program is similar to the CHEVDEF programs,⁶ except that BISDEF uses the BISAR subroutine¹⁹ as the response model to compute predicted deflections. Values for the layer moduli are varied to match the deflections predicted by the BISAR program to those measured by the FWD. Best agreement between actual and predicted deflections was obtained using modulus values of 26,000 psi for the sand-grid layer and 16,000 psi for the subgrade.

* Webster, *ibid.*

APPLICATION

Webster* concluded that sand grids can provide soft subgrades as much protection against the effects of large vertical stresses applied at the surface as unconfined gravel layers up to 1.6 times as thick. A simplified design procedure thus consists of substituting an 8-in. sand-grid layer for 12 in. of gravel in any conventional design procedure.

Coatzee⁸ has suggested that the 8-in. sand-grid layer is equivalent to at least 6 in. of crushed aggregate, based on a layered elastic analysis comparing sand-grid pavement systems to conventional pavement systems. He checked the layered elastic stress predictions using a simplified three-dimensional finite element computer program.

Nixon and Partners²² have adapted a design procedure based on limiting the maximum allowable vertical compressive strain in the granular layers beneath the sand grids. Stresses, and hence strains, are computed by modeling a transformed pavement section as a semi-infinite, homogeneous, elastic half-space. They assumed an elastic modulus of 58,000 psi for the sand-grid layer.

Webster³² has demonstrated a construction procedure for temporary access roads subject to heavy truck traffic. Nixon and Partners²² have outlined construction procedures incorporating sand grids as base courses or subbases under a variety of pavement surfacings and for various types of car and truck traffic. These were used as a basis for airport pavement construction procedures developed during this study.

* Webster, *ibid.*

DESIGN MODEL FORMULATION

PAVEMENT RESPONSE MODELS

Crawford and Katona⁹ have prepared a state-of-the-art report on the prediction of pavement response. In their discussions, they refer to three types of idealizations of pavement structures. These are the Westergaard, layered elastic, and finite element idealizations. To these primary idealizations should be added several significant mutations and combinations of the three primary idealizations.

Hudson and Matlock¹⁷ developed a model that essentially follows the Westergaard idealization but uses a numerical technique for solving the equations of bending for the thin elastic slab representing the surface layer which overlies a Winkler foundation. The numerical technique is based on finite difference approximations of continuous functions, and the corresponding physical idealization of the elastic pavement element is similar to the finite element idealization. This idealization will be referred to as the discrete element idealization. A model developed by Saxena²⁷ combines the discrete element idealization of the elastic pavement element with an elastic solid idealization of the underlying material rather than a dense liquid idealization (Winkler foundation). The elastic solid idealization (Boussinesq) is a simplified version of the layered elastic idealization⁴ in that only one semi-infinite layer is considered.

Huang and Wang¹⁶ developed a model that combines the finite element idealization for thin elastic pavement elements with the dense liquid idealization for the underlying material. This model has been modified and extended for Corps of Engineer use by Chou⁷. A model developed by Eberhardt and Willmer¹² is similar to that developed by Huang and Wang, but with an additional feature that considers an intermediate layer. A procedure was developed in which the top two layers are modeled as an equivalent thin elastic plate. The finite element idealization is then used for the equivalent plate and the dense liquid idealization for the remainder of the structure.

As stated previously, these four models are simply mutations or combinations of the three primary idealizations and are subject to similar limitations. Therefore, the following discussions are limited to the three primary idealizations.

Crawford and Katona⁹ provide detailed discussions of the three primary idealizations and include discussions of various material characterization procedures that are necessary for quantification of properties of the pavement structures. For the reader interested in an in-depth comparison, the report by Crawford and Katona⁹ is recommended. However, a brief comparison follows which includes the primary reasons for selecting a response model based on the layered elastic idealization.

In 1942, Burmister⁴ described a pavement system as being composed of an elastic layer overlying a semi-infinite elastic subgrade. This concept has been adopted and refined by many researchers. For the layered elastic idealization (Figure 3), the pavement structure is represented as a series of horizontal, uniform, elastic layers with properties defined by (a) E_i , the modulus of elasticity of the i^{th} layer; (b) ν_i , the Poisson's ratio of the i^{th} layer, and (c) h_i , the thickness of the i^{th} layer. These layers extend horizontally to infinity, and the n^{th} layer also extends vertically to infinite depth. Computer solutions can be obtained for practically any multilayer system. The Westergaard idealization (Figure 4) represents the pavement element as a thin elastic plate with properties defined by E_p , ν_p , and h_p , over a dense liquid (Winkler) foundation. The liquid foundation is characterized as a bed of springs having a certain stiffness. Each individual spring represents the effect of the support provided over a unit area. This support is quantified by a constant k , which is the ratio of pressure on the unit area divided by the deflection. In the basic Westergaard idealization, loads were represented as uniform circular pressure distributions, but procedures developed by Pickett et al.²⁴ and Pickett and Ray²⁵ permit pressure distribution with any shape to be handled.

The elastic layered idealization would appear to be a more realistic representation of a real pavement structure since pavements are truly layered systems, although the materials may not be truly elastic. For practical loadings, however, the materials can be represented by quasi-elastic properties. The representation of the top layer as a thin elastic plate (Westergaard idealization) or as an elastic layer is equally valid when the top layer is a portland cement concrete (PCC) slab, as in rigid pavements. The major difference lies in the representation of the remainder of the structure. The use of fundamental constants E and ν to represent the properties of underlying layers is theoretically more sound than a single constant k . The Westergaard idealization also suggests that there is no lateral shear transfer in the underlying layers, an unrealistic assumption. From a practical standpoint, the elastic layered idealization is also more valid. The determination of k is made with a plate test and represents the response of the material to a particular loading condition (i.e., 30-in.-diam plate and 10-psi vertical pressure), which may be different from that actually experienced in the pavement.

Experience has shown that, for gears with closely spaced wheels on relatively thin slabs (less than about 15 in.), modeling of the underlying layer with a modulus of soil reaction, k , produces reasonable estimates of the response of the pavement. However, for larger loads transmitted to the pavement through a number of widely spaced wheels, for relatively thin, high-strength (large stiffness) base courses, and for thick PCC slabs, the validity of the idealization decreases. For the thicker slabs and widely spaced wheels, the zone of influence (stresses in the underlying material) becomes much larger than that under the 30-in.-diam plate normally used in measurement of k , although the

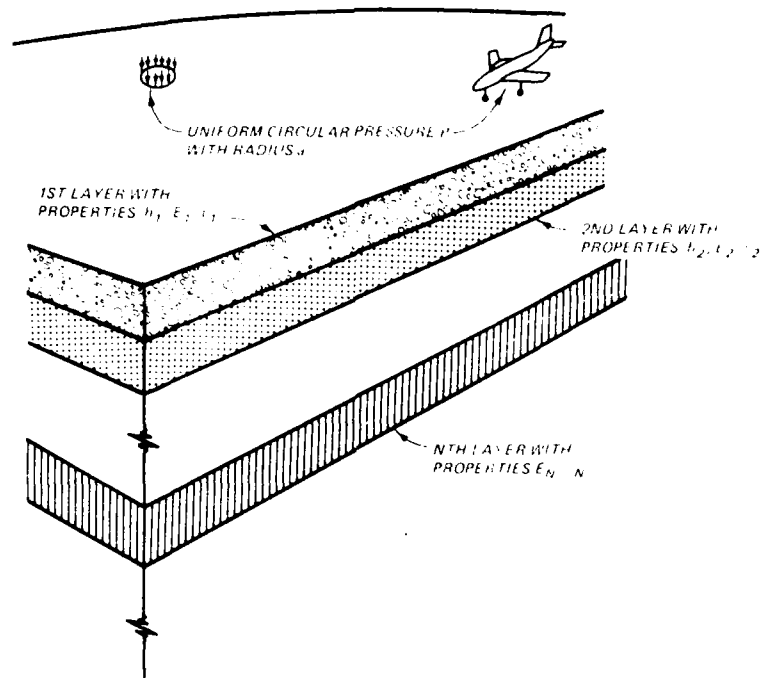


Figure 3. Elastic layered pavement idealization⁹

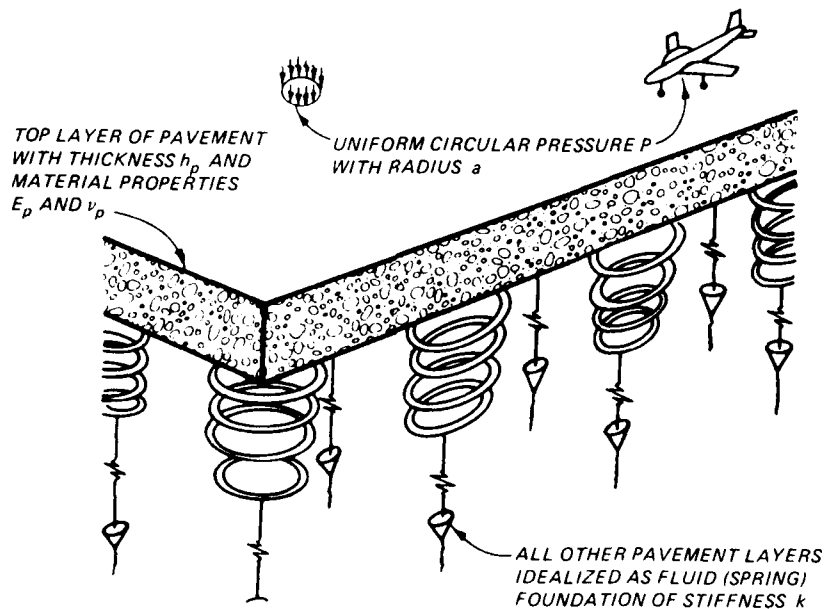


Figure 4. Westergaard pavement idealization⁹

10-psi contact pressure used may in fact be valid for both conditions. The effect of a thin, high-strength (stiffness) base course will be more pronounced on the load deformation response of a 30-in.-diam plate than on the load deformation response of a thick PCC slab. The response of the 30-in.-diam plate will be significantly reduced by the thin base,

whereas the reduction in the response of the pavement will not be as significant.

Another situation in which the use of an elastic layered idealization may be more representative occurs when different types of materials at relatively shallow depths exist within the subgrade (less than 20 ft). For instance, a stiff or a soft layer in the subgrade may not significantly affect the load deformation response of a 30-in.-diam plate, but the effect may be significant on the load deformation response of a thick slab under a large load on widely spaced wheels.

Characterization of each layer with elastic constants obtained from laboratory tests, rather than one elastic constant obtained from field tests, provides the designer greater flexibility. Note that the materials in pavements may behave neither elastically nor linearly, but the assumption of linear elasticity is made for practical application. The state of stress under which the material is tested in the laboratory may be changed to conform to the most critical state of stress under which it may exist in the pavement. This is contrasted with the constant state of stress at which the modulus of soil reaction is selected. There is also the flexibility of being able to readily change the physical condition of the specimen (moisture, pore pressures, density, etc.), whereas this cannot be so easily accomplished on in situ material. Thus, the use of an indirect correction for the effect of saturation (as is done for the modulus of soil reaction¹⁰) is not necessary.

The use of laboratory procedures makes it possible to test a more representative sample of the existing subgrade and a larger variety of available base course materials. With the present design procedure, extensive plate-bearing testing is uncommon. Another factor to be considered is the repetitive nature of the loads applied to a pavement. Certainly, the use of laboratory tests will more readily permit consideration of the effects of repeated load applications than will use of field plate-bearing tests.

The assumption of completely bonded or completely frictionless layer interfaces is not considered to be a significant weakness. A similar assumption is made by the Westergaard idealization: the interface between the pavement element and the underlying material is assumed to be frictionless. The interface between a pavement element and the second layer is most likely intermediate between a completely bonded and completely frictionless condition. Between all other layers, the assumption of full bonding is probably more valid, being dependent on the type material and construction procedure. However, no data exist to adequately quantify the interface conditions, although there is a response model that can analytically consider intermediate conditions. The computation of the various response parameters will certainly be affected by the selection of the interface condition.

The comparison of the finite element idealization with the Westergaard and elastic layered idealizations may not be valid since the finite element idealization is basically a computation procedure rather than a mathematical representation of the physical structure. As noted

previously, the finite element idealization may be employed for the upper layer, with a dense liquid or elastic solid representation for the remainder of the structure. Nevertheless, consideration as a separate idealization has merit for comparisons between available techniques for computing the response of a pavement to loads. As discussed here, the finite element representation considers the entire structure to be broken into a number of finite elements (Figure 5).

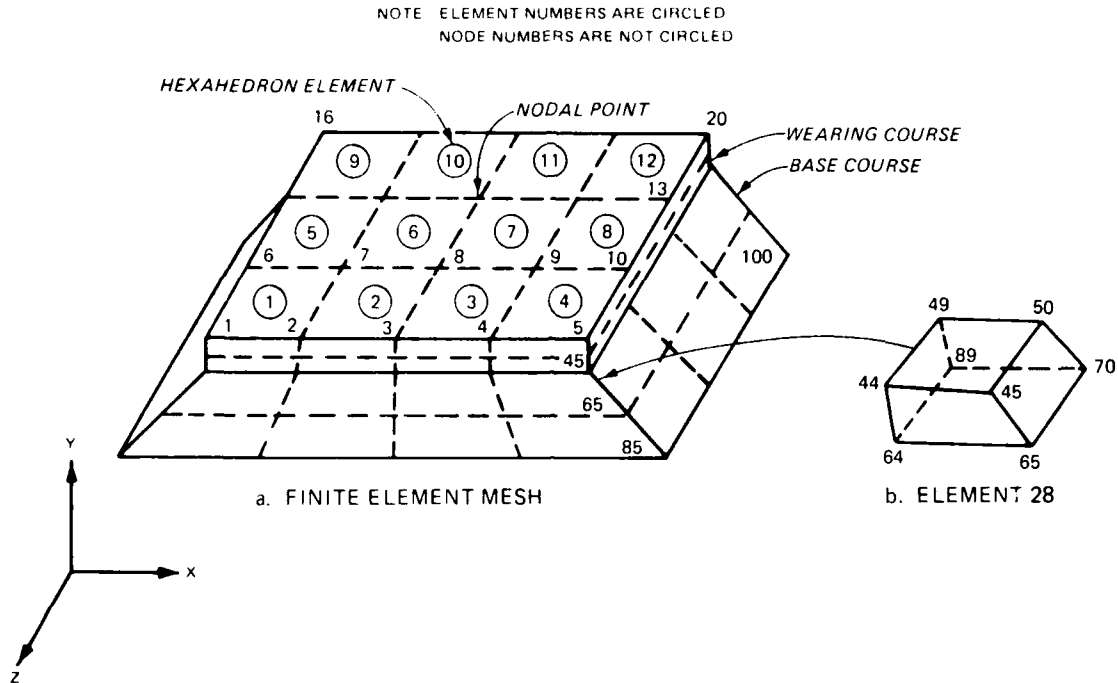


Figure 5. Pavement idealization using a finite element program⁹

In the finite element idealization, the continuous pavement structure is broken into a number of elements connected at nodal points. The material in each element is assigned properties that may vary from element to element. The number of elements and nodal points that may be considered are limited by computer capacity, and thus boundary conditions must be specified. The loads are applied as concentrated forces at the nodal points. With the aid of special types of elements, discontinuities, special interface conditions, reinforcing steel, and dowel bars may be modeled. Special computational techniques permit consideration of voids and temperature and moisture gradients within the pavement structure. In addition, variable layer properties (thickness and load deformation properties) and nonlinear material response may also be treated.

However, there are limitations. For a three-dimensional idealization with only a minimum number of elements and refinements (Figure 5), the required time and cost involved in applying the procedure to pavement problems become prohibitive.

There are plane strain, axisymmetric, and prismatic solid finite element idealizations, but with all of these idealizations certain

constraints are introduced. If the time, effort, and cost to apply the models are reduced to manageable levels, the applicability to a general design procedure and improvements over simpler models are likewise reduced.

ELASTIC LAYERED MODEL

The previous observations suggest that an elastic axisymmetric layered model subjected to a uniform circular loaded surface area is appropriate. This model appears to describe the behavior of both conventional pavement systems and subgrade layers. Using a limiting strain criteria for pavement design constrains stresses and strains, determined by the elastic layered analysis, to moderate levels. Linear load-settlement behavior can thus be maintained. This model, which is available in closed form solutions, can also be incorporated into a workable design procedure.

Larger loads or pass levels can be accommodated by adding a structural surfacing (e.g., more than 4 in. of asphaltic concrete) over the sand-grid layer. A three-layer analysis is then required to compute strains and determine the maximum allowable aircraft load. Such an analysis is used in the structural design procedure developed by Barker and Brabston.²

Sand-grid pavements can accommodate much larger strains than comparatively brittle bituminous concrete pavements and still retain their structural integrity. They are also characterized by large (1- to 2-in.) initial deflections due to densification of the grid filler material. The degree to which permanent deflection occurs can be controlled by proper attention to compaction. Since most sand grid applications to date have been for military expedient low-speed roads over beaches, little attention has been given to achieving high degrees of compaction in either the underlying layer or in the sand within the grid itself. Deflections resulting from sand densification occur under the first several hundred traffic coverages. Thereafter, permanent deflections accumulate much more slowly* (Figure 6). Thus, sand-grid pavements will be structurally sound at levels of total, permanent surface deflections considered unsatisfactory for bituminous concrete pavements. The horizontal tensile strain criteria, then, do not control the performance of sand-grid pavements.

Limiting the vertical compressive strain at the top of the subgrade provides a sufficient failure criteria for sand-grid pavements. An analysis of the data summarized by Barker and Brabston,² and shown in Figure 7, suggests that limiting the resilient strain to 0.6×10^{-3} will ensure satisfactory performance for up to 1,000,000 strain repetitions. Alternately, the number of coverages to failure can be included as an additional design parameter by using one of the relationships shown in Figure 7, to relate the calculated subgrade strain to the number of allowable coverages.

* Webster. *ibid.*

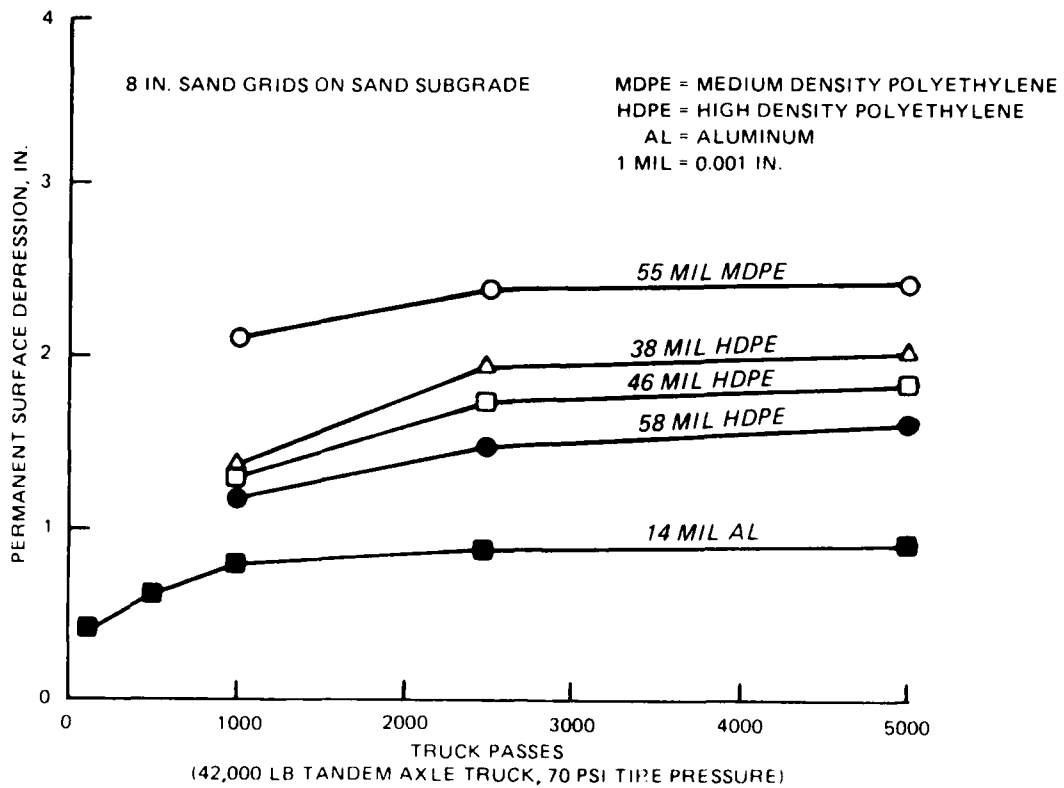


Figure 6. Permanent deformation as a function of traffic repetitions*

The construction procedure must be designed to prevent development of unacceptable surface roughness under traffic. One alternative is to apply a large compactive effort during construction. Initial tests indicate that the sand filler material should be compacted to about 80 percent of its laboratory maximum dry density. Another alternative is to consider the first several hundred traffic coverages as the last step in the construction and reducing surface roughness, as necessary, by applying a thin wearing surface process.

* Webster, *ibid.*

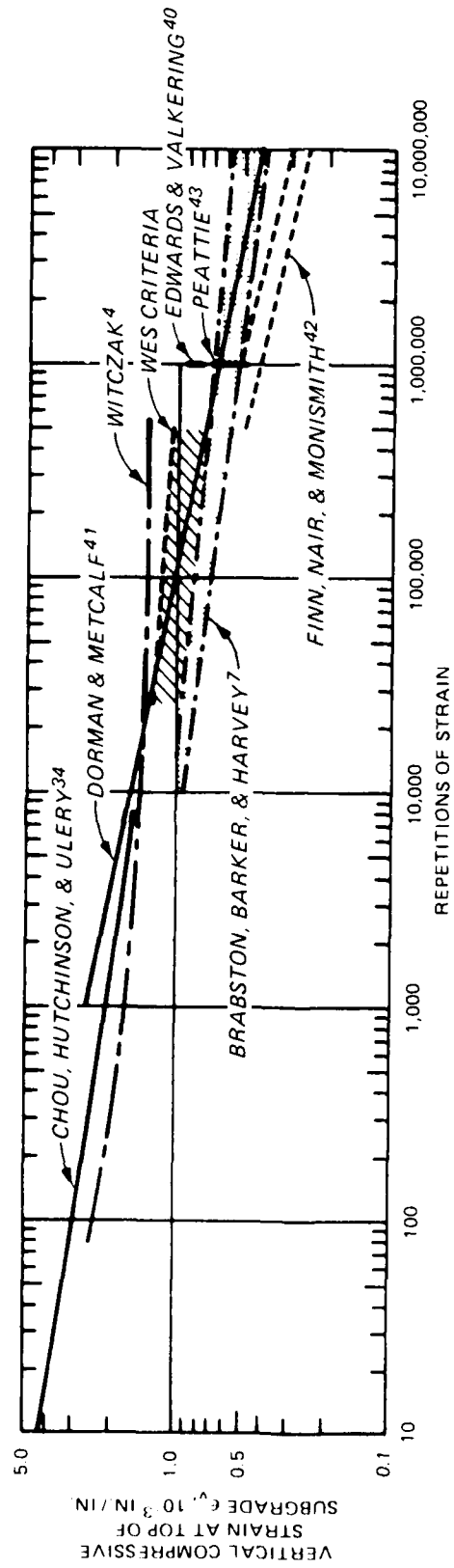


Figure 7. Comparison of subgrade strain criteria²

SAND GRID BEHAVIOR

INTRODUCTION

As stated earlier, a model for sand grid behavior must consider three general features of the problem:

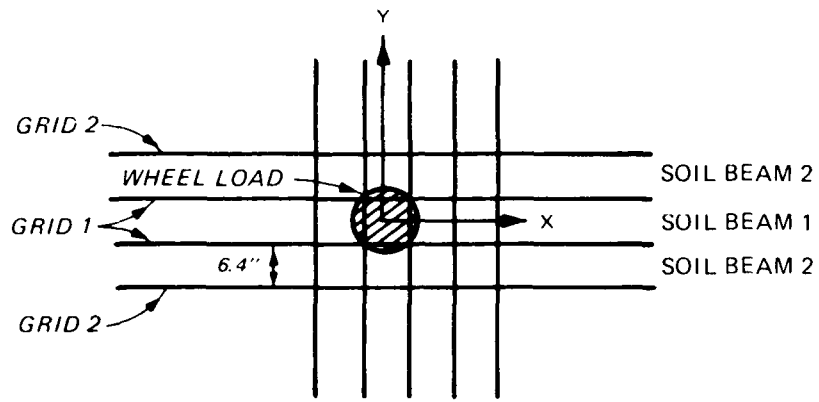
- (a) Sand-grid materials
- (b) Support conditions or subgrade
- (c) Loading conditions

The model described in this section treats the sand grid and subgrade separately and then compares the interface conditions for consistency.

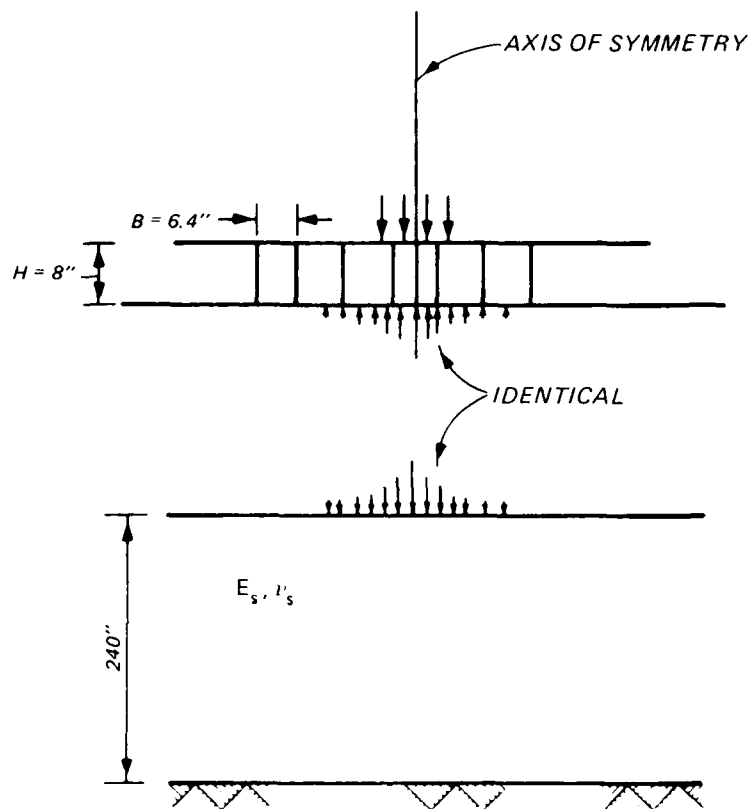
The sand grid forms a composite structure, and the load gets divided between the sand and the plastic (Figure 8). In the analysis of the upper layer, both the sand and plastic follow the deflection bowl of the subgrade surface computed from an assumed pressure distribution. A computer program calculates the subgrade pressures that act on the sand grid layer to deflect it in the shape of the subgrade deflection bowl. These deflections are modeled by a piecewise linear relationship. The distributed forces are compared to the assumed pressure distribution applied to the top of the subgrade. The calculation is then repeated until the two pressure distributions are equal. The final solution has both equal vertical stresses and equal vertical displacements acting at both the base of the sand grid and the top of the subgrade (Figure 8). This interface condition corresponds to a frictionless or smooth interface in a two-layer elastic system.

The sand grid layer has several characteristics of behavior that must be addressed to successfully analyze its response.

- (a) The plan view of the individual grid cells are not simple plane figures as shown in Figure 8.
- (b) The assumed wheel load has axisymmetry while the sand grid geometry has symmetry about two axes.
- (c) The sand-plastic interface on the vertical sides of the grid cells provide a reduced friction surface in the layer making the sand grid noncontinuous above some maximum stress level.
- (d) The repeated loading and unloading of the confined sand in the grid cells by compaction and traffic lock in lateral stresses.
- (e) Since the stress state in the sand grid at some depth below the wheel load varies with the radial distance from the application point, the modulus of the medium also varies in the horizontal plane.



a. Plan



b. Profile

Figure 8. Schematic of the sand-grid system

By analyzing the sand grid separately from the subgrade all five of these characteristics are treated, although with differing levels of refinement.

Figure 8 shows the simplified plan view of the sand grid that was analyzed with the complex cell geometry treated as a series of square cells each measuring 6.4 by 6.4 in., standing 8 in. tall, and having a wall thickness of 0.055 in. By aligning the sides of the squares along the x and y axes the behavior could be analyzed separately in the x and y directions and then combined to describe the layer. Treating the 8-in. deep sand grid layer as a series of four independent one dimensional (1-D) beams indicated as soil beam 1, soil beam 2, grid 1, and grid 2 greatly simplified calculations for this analysis. The assumption of superposition of the solutions for orthogonal beams is made for ease of solution. In reality the actual behavior is probably more like that of a four-way slab. Fully utilizing symmetry about the x and y axes, only the x direction beams in the positive x-y quadrant were actually analyzed. The complete solution involved adding the x direction beams to the results of the y direction beams which were also obtained from the x direction calculations.

This analysis did not explicitly include the influence of the sand-plastic interface in the calculations. Applying a theoretical analysis proposed by Hadala¹³ to calculate the side friction along the vertical sides of a cylindrical pressure chamber provided guidelines for the minimum possible subgrade pressure distribution directly below the most heavily loaded grid cell. This minimum pressure was less than the value calculated from the model, using values of interface friction measured in a direct shear test.

The stress-strain behavior of sand is the key feature in the sand-grid response. The shear modulus of sand depends upon the initial density, the initial stress level, the strain level, and the stress path. This analysis employs a procedure developed for dynamic analysis that determines a secant shear modulus during simple shear for a particular shear strain level and initial octahedral stress state. For the sand-grid problem, response is treated as a two step process; first the wheel load increases the initial stress level and then the layer deforms under the load. This provides an approximation to the actual stress path experienced by the sand, which is different from the stress path felt by sand during a simple shear loading. The octahedral stress is calculated using vertical stresses computed for the applied load and the lateral stress coefficients computed from a relation proposed by Mayne and Kulhawy,²⁰ which is described later. The sand grid is initially analyzed using a low strain shear modulus. Following the first calculation step new moduli are computed from the computed shear strains and compared to original shear modulus values. The procedure iterates until the moduli values used in the program are consistent with the computed shear strains.

Figure 9 shows a flow chart describing the whole calculation process involved in the sand-grid model. To start the process, a pressure distribution acting on the surface of the subgrade is assumed.

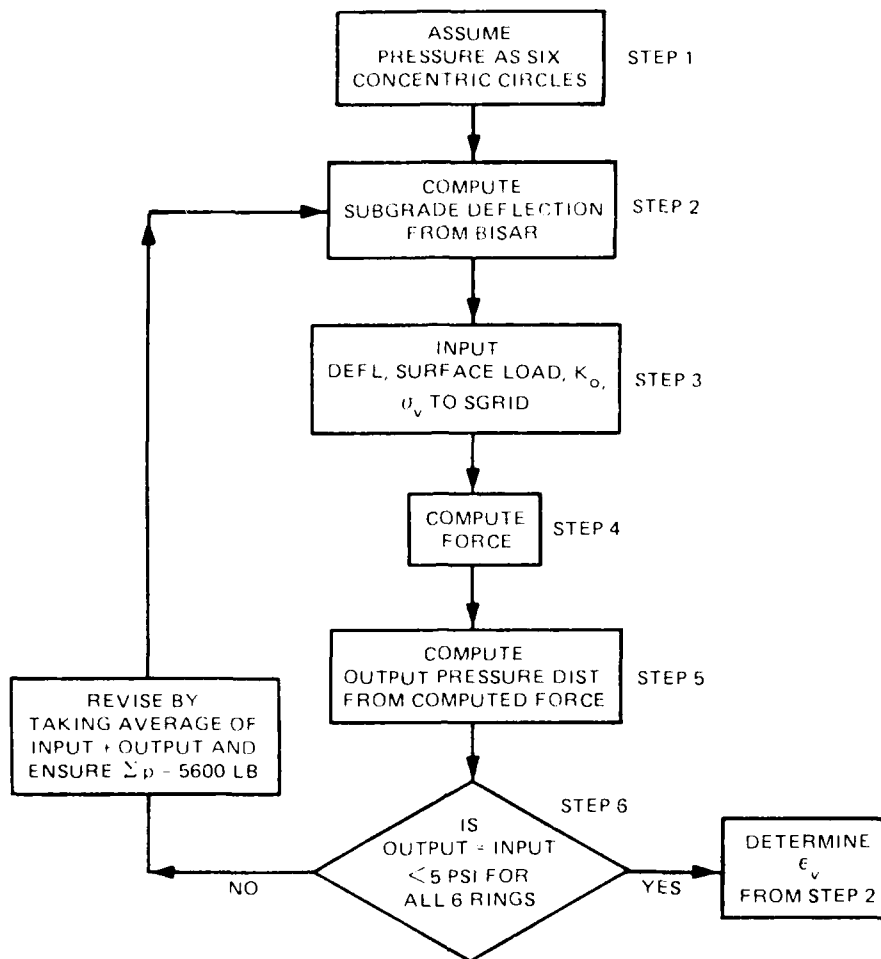


Figure 9. Flow chart for the analysis

Describing this distribution as a series of six concentric constant pressure circles, a layered elastic program computes the subgrade deflection bowl in step 2. (The results reported in this report used the computer program BISAR, since it is considered a "benchmark" for layered elastic programs. However, any of several available layered elastic programs could be used.) In step 3 the computed deflection profile, the surface load from the applied wheel load, the resulting vertical stresses, and the K_o values are input into the program SGRID (Appendix A). The weighting factors for load input to the program SGRID are given in Appendix B. During step 4 the computer program SGRID uses an iterative procedure to calculate the pressure distribution acting along the bottom of the sand-grid layer when deformed to follow the subgrade deflection basin. The program is used to analyze the response for soil beams 1 and 2 in addition to calculating the response of the grid beams 1 and 2 using a simplified version of the SGRID program. The output pressures acting on the base of the sand-grid layer are compared in step 5 to the subgrade pressure assumed in step 1. In step 5 a simple computer program CAL (Appendix A) performs the process of combining the x direction and y direction beams so that the output pressure distribution can be compared to

the input pressure on a common basis. In step 6 the two pressure distributions are compared; when input (step 1) and output (step 5) stresses were within ± 5 psi, the iteration process stops. The sand-grid response is then characterized by the maximum vertical subgrade strain computed during step 2.

The second general feature of the problem is considered by analyzing the sand grid response for three different subgrade modulus values. The three solutions are called case 2, case 3, and case 4 representing subgrade modulus values of 16,000, 8,000, and 32,000 psi, respectively. Each reported case is also assigned a second number that gives the iteration number. For example, case 3-2 refers to the second iteration for the situation with a subgrade modulus of 8,000 psi.

The final general feature of the problem, the surface loading condition, was not varied for analyses reported. Calculations assumed a 5,600-lb single-wheel load at 100 psi tire pressure acting on 2-in. layer of asphalt overlying the sand grid. This load would be typical for a single-wheel, light-utility aircraft having a gross weight of approximately 12,000 lb. The load on the surface of the sand grids was represented by a 10.5 in. diameter, 65 psi uniform load, and by assuming a simple pyramidal pressure distribution (with 2:1 side slopes) in the asphalt layer.

All of the above calculations were performed on a mainframe computer. The computer capacity required to perform these computations is governed by the mathematical precision necessary to obtain accurate solutions for the numerical methods employed by each of the programs. The minimum acceptable capacity was not determined during this study.

PROPERTIES OF THE COMPONENT PARTS

The plastic grid performs two functions:

(a) It increases initial confining stress of sand (and hence, the E and G used in the program SGRID).

(b) It carries some of the load.

In this analysis, function 1 influenced the initial stress conditions, while function 2 was computed from the modified version of the program SGRID. The plastic-beam modulus values were measured in the laboratory.

The shear modulus was measured in a torsion test according to ASTM Standard D 1043. At a temperature of 70° F, the shear modulus, G , equals 32,000 psi. Using a Poisson's ratio of 0.5 to describe the plastic yields a stiffness, E , equal to 96,000 psi. When tested in bending using ASTM D 747, the measured E value equals 120,000 psi for a shear modulus of 40,000 psi. In analyses presented in this report, the plastic is described using the values of G equal to 40,000 psi and E values equal to 120,000 psi.

The soil properties for the analyses presented in this report represent the concrete sand that filled sand grid cells in field tests performed at WES. Figure 10 shows the grain size distribution.

Al-Hussaini and Perry¹ reported the following properties for this sand:

Specific gravity = 2.66
 Maximum dry density = 117.7 pcf
 Minimum dry density = 98.2 pcf
 Coefficient of uniformity = 2
 Mean diameter = 0.5 mm

The particles have subangular to angular shape. Nuclear density tests performed after testing on a short section of sand-grid roadway measured a dry density of 113 to 115 pcf at a water content of 4 to 7 percent; these densities represented a relative density varying from 76 to 86 percent. This study used a dry density of 114 pcf, for a D_r equal to 81 percent. To analyze the sand-grid beam, the shear modulus, Poisson's ratio and sand-plastic friction angle must be determined. The shear modulus and Poisson's ratio were based upon test results and proposed relations reported in the literature^{28,14} while the sand-plastic friction was measured in a direct shear test.

The shear modulus for a sand depends upon both the initial stress state and upon the shear strain magnitude. These influences can be treated separately using a stress dependent maximum shear modulus and then decreasing it consistent with the shear strain. Hardin and Black¹⁴ found laboratory shear moduli measured at low shear strains were fit by the following equation:

$$G_{\max} = 1230 \frac{(2.973 - e)^2}{1 + e} (\sigma_{\text{oct}})^{1/2} \quad (4)$$

where

G_{\max} = shear modulus, psi

e = void ratio, psi

σ_{oct} = octahedral normal stress, psi

For the concrete sand used in this study, which has a void ratio equal to 0.45, this expression becomes:

$$G_{\max} = 5400 (\sigma_{\text{oct}})^{1/2} \quad (5)$$

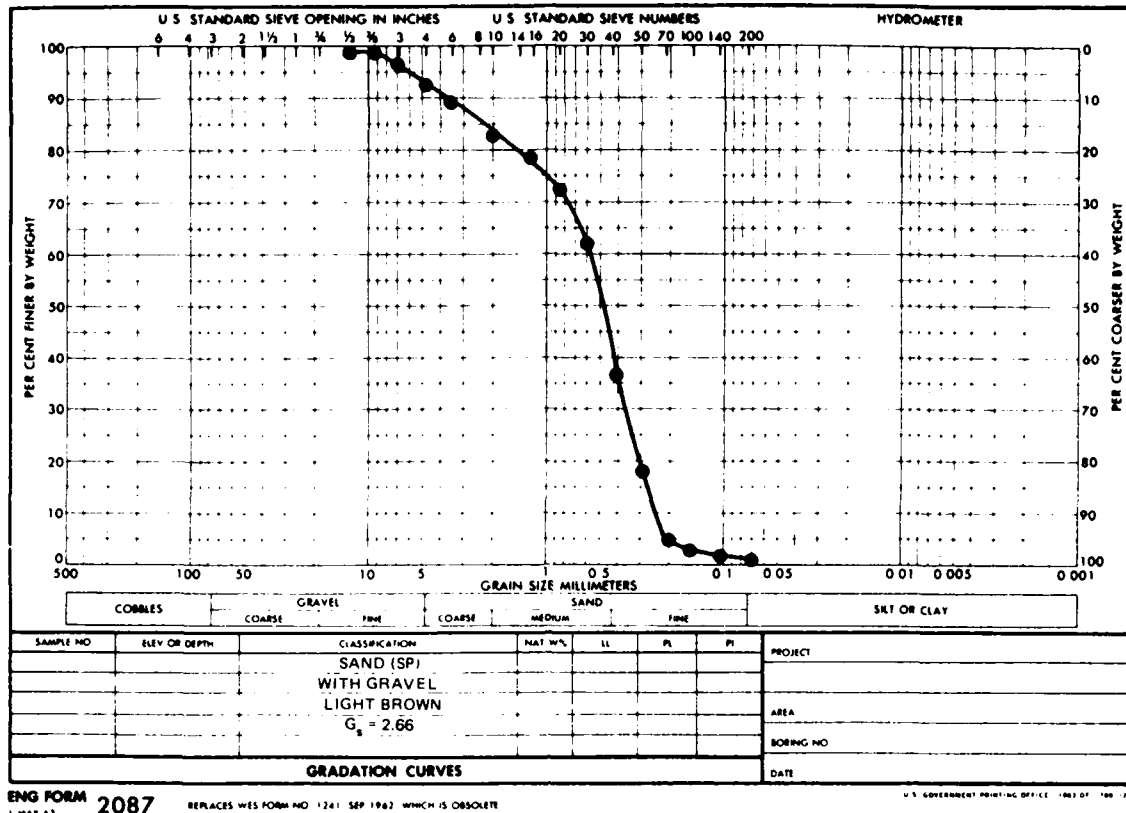


Figure 10. Grain-size distribution

Seed and Idriss²⁸ used equation 6 to give G and σ_{oct} in psf:

$$G = 1000 K_2 (\sigma_{oct})^{1/2} \quad (6)$$

The constant K_2 is a function of both shear strain and relative density. At the small shear strain value of 10^{-6} in./in., K_2 equals 64 for a sand having a relative density equals to 80 percent. If both G and σ_{oct} are given in psi, equation 6 becomes:

$$G_{max} = 5300 (\sigma_{oct})^{1/2} \quad (7)$$

Preliminary computations were made using equation 8:

$$G_{max} = 5500 (\sigma_{oct})^{1/2} \quad (8)$$

to model the higher relative density expected under aircraft loads.

The initial stress required to compute G_{\max} is:

$$\sigma_{\text{oct}} = (1 + 2K_o) \frac{\sigma_v}{3} \quad (9)$$

where K_o is the ratio of horizontal to vertical stress. The vertical stress at a point equals the initial vertical stress caused by the overlying soil and asphalt plus the added stress from the applied wheel load. Mayne and Kulhawy²⁰ empirically related the value of K_o in soils to the friction angle, ϕ , and the stress history by equation 10.

$$K_o = (1 - \sin \phi) \left[\frac{\text{OCR}}{\text{OCR}_{\max} (1 - \sin \phi)} + \frac{3}{4} \left(1 - \frac{\text{OCR}}{\text{OCR}_{\max}} \right) \right] \quad (10)$$

The quantities OCR and OCR_{\max} refer to the stress history. The OCR value equals the ratio of the maximum vertical stress to the current vertical stress. For the sand filling the sand grid cells the maximum vertical stress is assumed to have occurred during construction, when a 5,600 lb wheel load compacted the soil. The OCR_{\max} equals the ratio of the maximum vertical stress to the minimum vertical stress. During the first unloading cycle for a soil, OCR equals OCR_{\max} while for later load/unload cycles the OCR_{\max} value remains constant at about 40 while the OCR value varies. Figure 11 compares the results of equation 10 to the measured horizontal stresses during a load-unload-reload test on filter sand reported by Mayne and Kulhawy.²⁰

The response of soil in simple shear is nonlinear when shear strains exceed 10^{-6} in./in., with the tangent shear modulus decreasing. Seed and Idriss²⁸ developed the relationship shown in Figure 12 to describe the secant shear modulus as a function of shear strain. For these analyses, the average curve, shown as a dashed line in Figure 12, was used to find the ratio G/G_{\max} as a function of shear strain, γ . Combining G/G_{\max} with equation 8, the shear modulus for the sand is given in equation 11.

$$G = 5500 \frac{G}{G_{\max}} \sqrt{\sigma_{\text{oct}}} \quad (11)$$

For calculations, the Poisson's ratio, ν , equals 0.35. Table 1 summarizes the material input properties used in each of the three analyzed cases or references the appropriate equation.

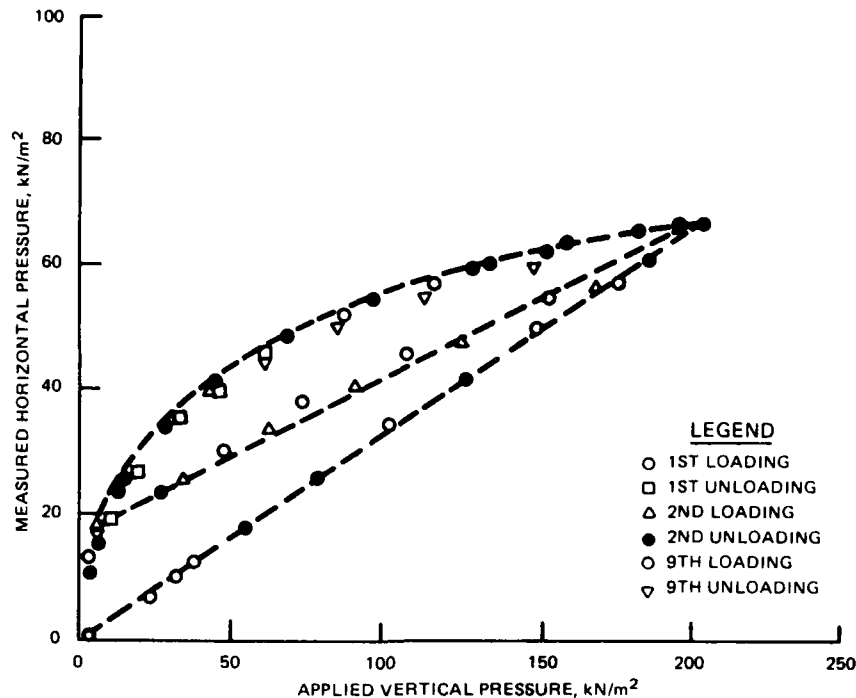


Figure 11. K_0 data²⁰

The analysis for sand grid response uses an elastic approach and assumes no developed plastic failure mechanisms. This holds true when the maximum vertical shear stress does not exceed the frictional strength between the sand and the plastic grid. Therefore, the friction of the interface was measured in direct shear tests. Figure 13 shows the strength envelope for sliding of sand on sections of plastic grid trimmed from a completed field test, and compares it to the strength envelope for sand. For plastic-sand sliding, the angle of friction, δ , equals 21 deg, while for sand, the angle of internal friction, ϕ , equals 40 deg. The ratio $\tan \delta / \tan \phi$ equals 0.46. The plastic significantly reduces the sand layer's capacity to transmit shear stresses along vertical planes. In the next section the significance of this reduced friction surface upon subgrade pressure distributions will be examined.

SUBGRADE ANALYSIS

The deflection profile of the subgrade was computed for an assumed pressure distribution. The initial pressure distributions used in the analyses were based upon results computed for a two-layer system with an 8 in. layer overlying a subgrade. The area under the assumed pressure distribution equals the total wheel load of 5,600 lb.

The pressure distribution underlying the sand grid cell loaded by the wheel is controlled by the frictional force acting along the vertical sand plastic interface. Hadala¹³ presented an analysis to compute the vertical stress acting at the base of a sand sample confined by a cylindrical chamber. Modifying his analysis for the rectangular prismatic

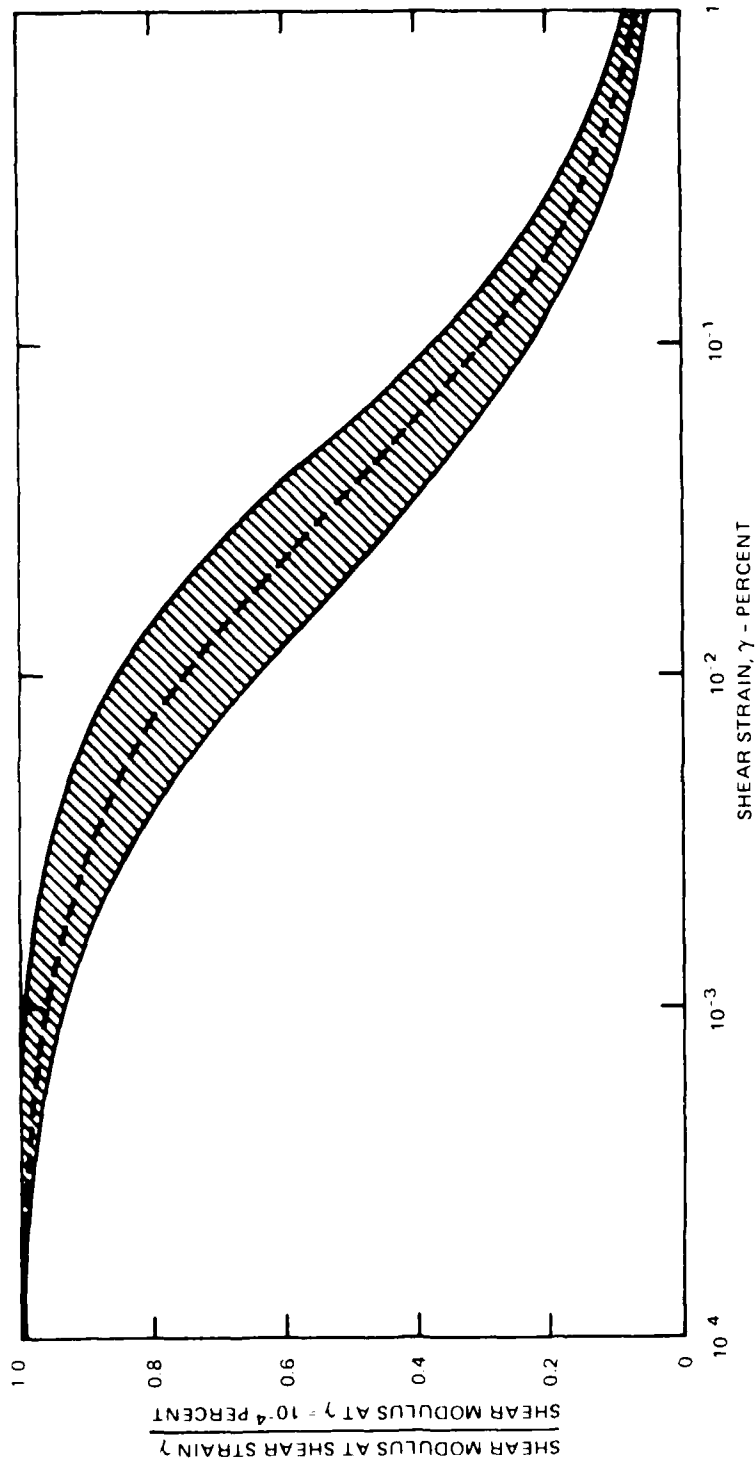


Figure 12. Variation of shear modulus with shear strain for sands²⁸

Table 1

Summary of Input Data

Case	Plastic			Subgrade			Sand			
	E psi	G psi	ν	t in.	E _s psi	ν	G	ν	K _o	γ_d pcf
2	120,000	40,000	0.5	0.055	16,000	0.35	Eq. 5-7	0.35	Eq. 5-6	114
3	120,000	40,000	0.5	0.055	8,000	0.35	Eq. 5-7	0.35	Eq. 5-6	114
4	120,000	40,000	0.5	0.055	32,000	0.35	Eq. 5-7	0.35	Eq. 5-6	114

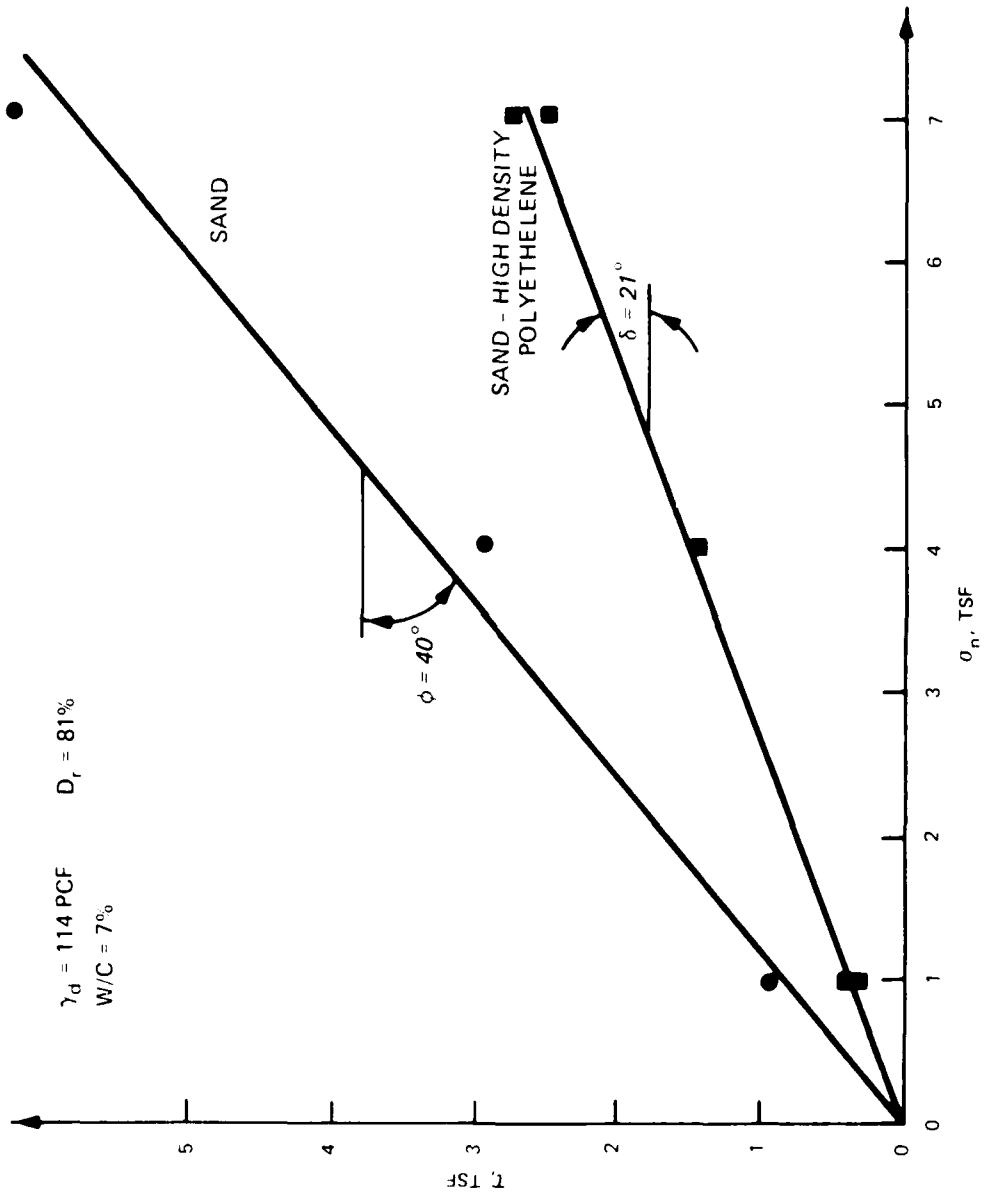


Figure 13. Direct shear test results

confining chamber formed by the simplified version of the sand grid cells leads to equation 12.

$$\sigma_v = \sigma_o \exp (-4K \tan \delta H/B) \quad (12)$$

where

σ_o = applied surface load

K = ratio between the horizontal and vertical stress

$\tan \delta$ = the coefficient of friction between the sand and plastic grid

Figure 14 shows the value of σ_v at the base of the sand grid cell loaded by a 65 psi wheel load plotted as a function of K. For the minimum value of K used in the analysis of 0.38, the minimum subgrade pressure equals 31.3 psi. For the three cases evaluated, the central subgrade pressure always exceeds 34 psi. Therefore the subgrade values exceeded the minimum allowable values. Since other grid cells carried small surface pressures, the minimum limit only applies for the pressures underlying the central cell.

The subgrade deflection profiles were computed using the computer program BISAR although any layered elastic program could be used. As noted earlier, BISAR was chosen for this study because it is considered a "benchmark" for layered elastic programs. Figure 15 shows a profile of the geometry analyzed. A rigid base under the subgrade was located at a 20 ft depth as recommended by Barker and Brabston.² The subgrade pressure distribution was approximated by six concentric circular pressure rings to satisfy the input limitations of the program BISAR, and this procedure led to the step shaped pressure pattern pictured in Figure 15.

Figure 16 shows the computed deflection profile used for one of the analyzed cases. Output values correspond to the required input locations for the program SGRID, described in the next section. Displacements were computed at points along all four of the beams that were analyzed. The results of the subgrade analysis reflect the fact that the pressure was step shaped instead of continuous. The calculated shear strains reach their maximum values at x values representing the edges of load steps.

SAND GRID ANALYSIS

For analysis the sand-grid layer was divided into a series of 1-D beams. Each of the beams was in turn subdivided into a series of subcells. The displacements and forces were calculated at only the corner points of the subcells. Figure 17 shows a schematic of the analyzed geometry. Fully utilizing the symmetry of the problem, only the positive quadrant of the x-y plane was analyzed. The responses of the four different beams in the x direction were calculated and doubled to get the full solution for the contributions from both the x and y directions.

$$\sigma_v = (65) e^{-4 K \text{TAN} \delta H/B} \quad \text{HADALA}^{12}$$

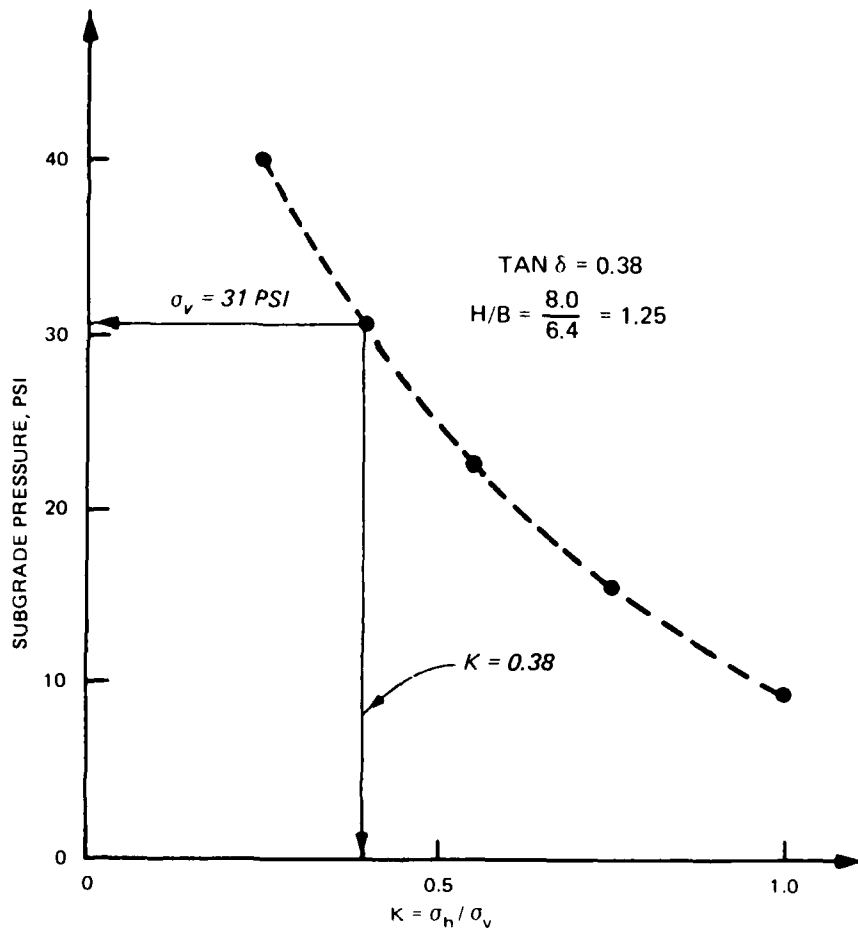


Figure 14. Subgrade pressure as a function of K

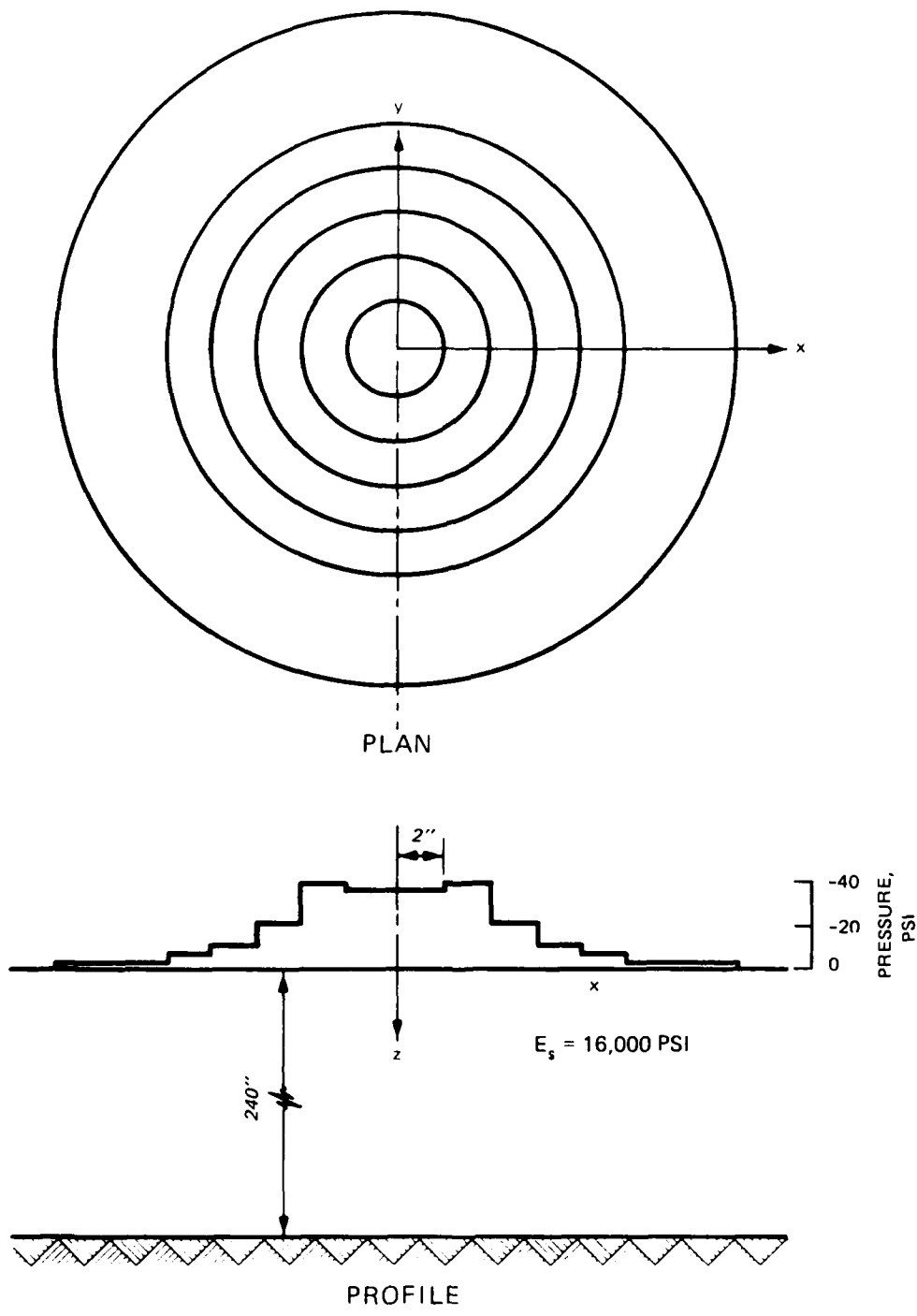
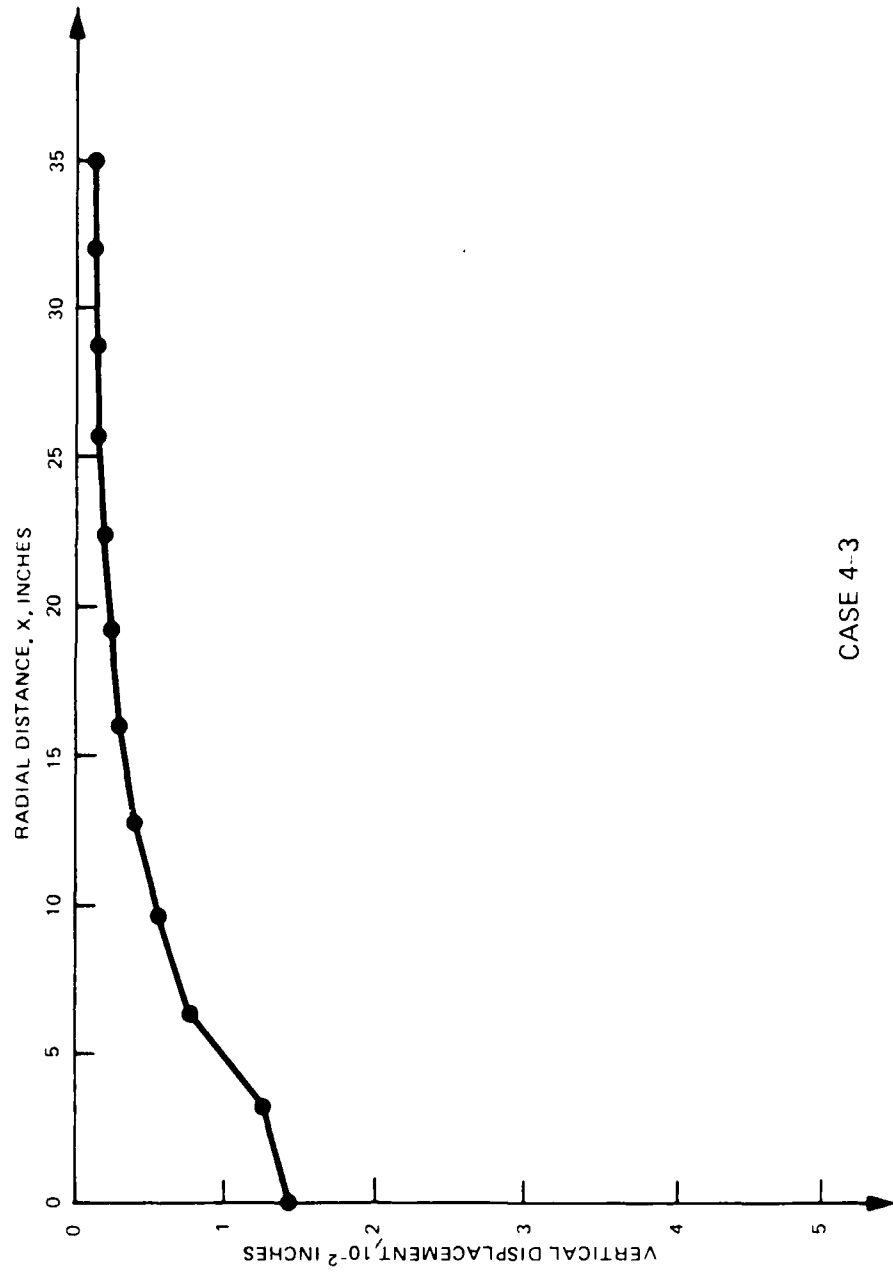
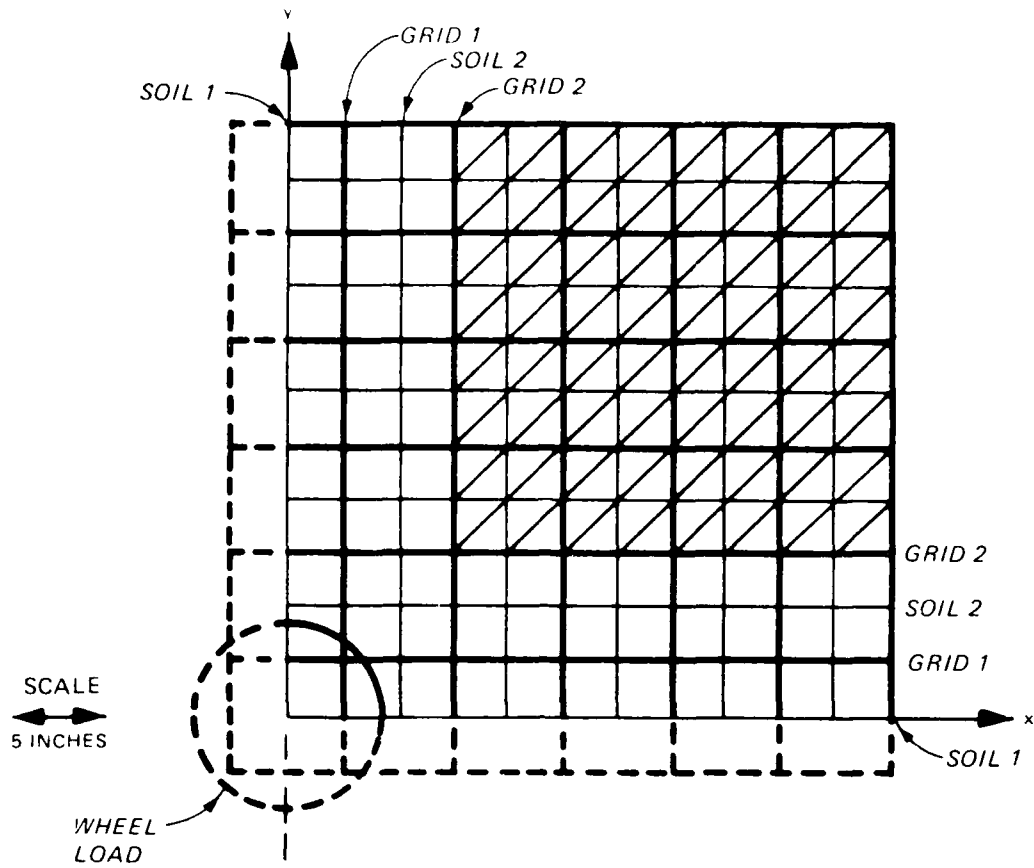


Figure 15. Applied pressure distribution

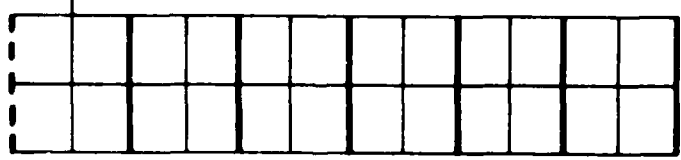


CASE 4-3

Figure 16. Deflection profile



a. Plan view



b. Cross section

Figure 17. Sand-grid schematic

For both soil beams 1 and 2, the deflections computed along the center line of the respective grid cell lines were used as input. In the case of soil beam 1, only a half-width beam was treated because of symmetry, while in the case of soil beam 2, the appropriate width was the full width of the individual grid cells. The behavior of the plastic grid was modeled by means of two grid beams labeled grid 1 and grid 2. The calculated response for the x direction beams was used to describe the y direction behavior. The analysis neglected the influence of the

cross-hatched area shown in Figure 17 because they contribute an insignificant proportion of the total load.

The cross section shown in Figure 17 portrays the geometry of the analyzed beams. Each grid cell was subdivided into four subcells with the response computed at the subcell corner points. The soil beams were analyzed assuming plane strain behavior while plane stress applied for the grid beams. Distributed loads were converted to point loads acting at the subcell corners. Each subcell corner carried the distributed load applied over a region extending from the midpoint between that corner and the preceding corner to the midpoint between that corner and the following corner.

Figure 18 shows the flow chart for the computer program SGRID used to model the response of each soil beam. In step 1, two sets of information are input: first, the data needed to characterize the response of the soil, and second, the prescribed corner forces imposed by the wheel load and the corner deflections computed from the subgrade analysis. Figure 19 shows the input and output data for the SGRID computer program. Figure 19a shows the information input for the analysis of soil beam 1 in case 4. For each sand subcell, the K_0 value, the vertical stress level, and the Poisson's ratio are required. In step 2 the low-strain shear modulus values are computed for each subcell using the input values in equation 8. In step 3 the stiffness matrix $[K]$ is computed from the geometry of the problem and from the material properties. Using the methods described by Smith²⁹ the subcell corner forces $\{F\}$ can be related to the subcell corner displacements $\{U\}$ in equation 13.

$$\{F\} = [K] \{U\} \quad (13)$$

In step 4 the appropriate, known displacement and force values are included in equation 13, and the remaining unknown displacement and force values are calculated. The subcell shear strains are then computed from the calculated values of displacements and forces. Using these shear strain values in step 5, new values for shear modulus values, G_{i+1} , are computed from equation 11. In step 6, the new G values are compared to the values, G_i , used to construct the $[K]$ matrix in step 3. If the G_{i+1} values are more than 10 percent different from the G_i values, the program performs steps 3 through 6 using the G_{i+1} values. Iteration proceeds until the two G values are less than 10 percent different, at which time the results are output. Figure 19b shows the final results for beam 1 in case 4-3. The values for all three cases are portrayed in Appendix C.

ITERATION AND CONVERGENCE

The SGRID output loads must be converted to a pressure distribution before comparing them to the input pressure distribution. The load for each subcell corner along the base of the soil beams acts over an area

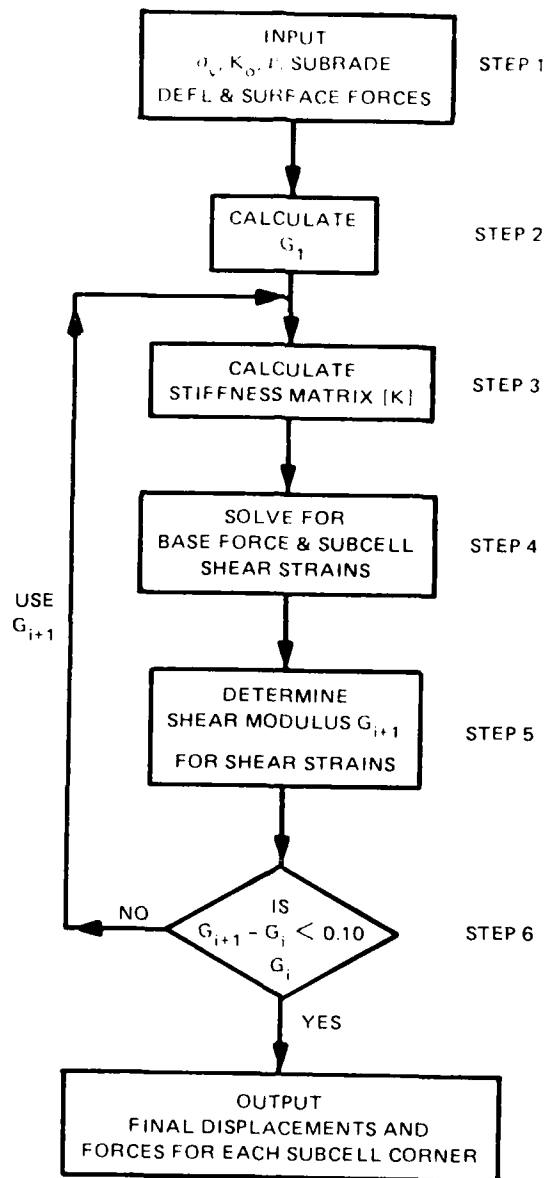
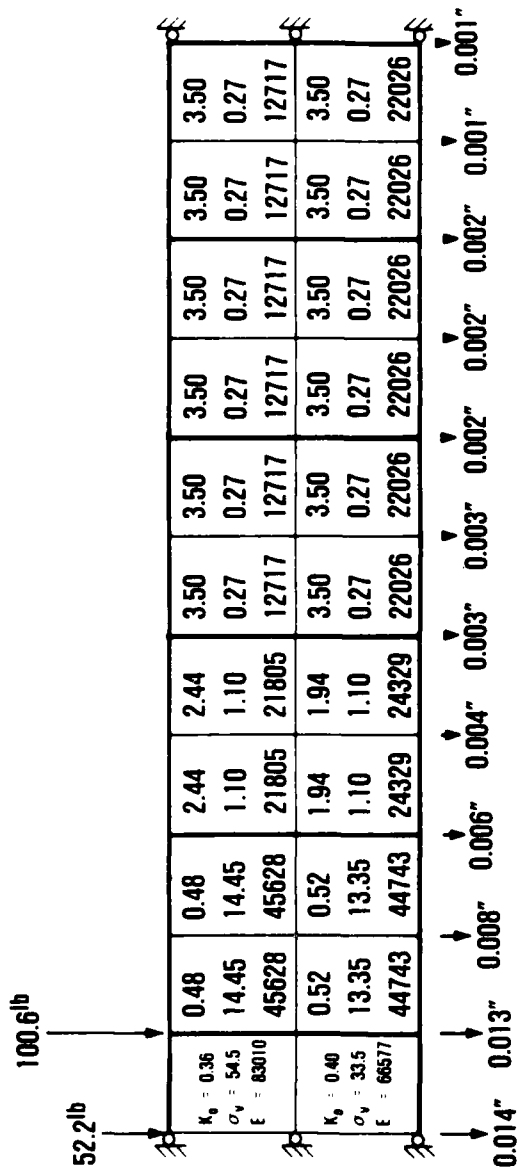
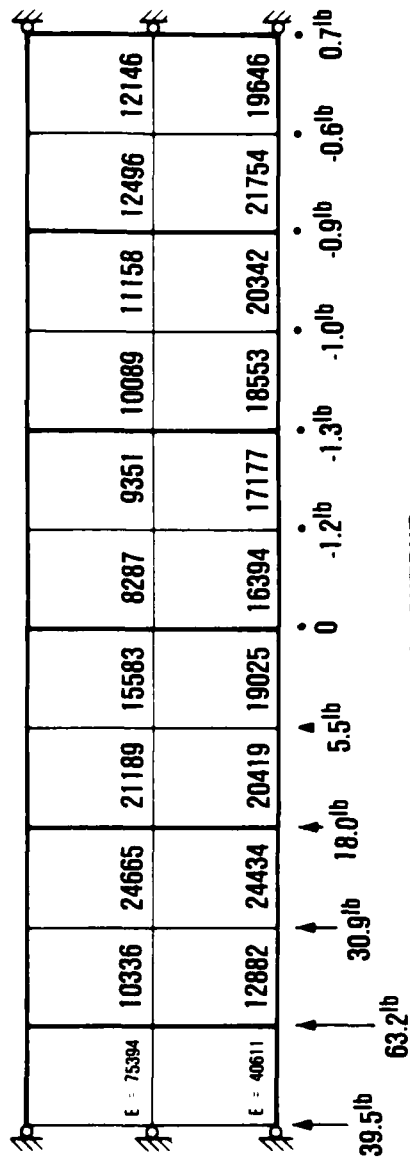


Figure 18. SGRID flow chart



a. INPUT



b. OUTPUT
CASE 4-3 BEAM 1

Figure 19. SGRID data, case 4-3

whose width equals the beam width and whose length equals the distance from the preceding midpoint to the following midpoint. The load calculated for the plastic grid beam subcell corners was distributed only along the length from the preceding midpoint to the following midpoint, assuming negligible width. To compare these rectangular and linear regions of constant stress to the ring shaped regions of constant stress input to BISAR, the SCRID results were transformed to square regions selected to correspond with the rings. The computer program CAL combined the subcell corner loads using weighting factors calculated from the portion of the acting subcell rectangular area lying within each square region. The square regions making up each ring were then averaged to obtain the output pressure distribution for that ring. Tables 2, 3, and 4 summarize the input and output pressures for each iteration of cases 2, 3, and 4.

The iteration procedure involved selecting the average of the input and the output pressures to be used for the input pressure to the next iteration. Before these values could be used, the total area under the pressure distribution was adjusted to give an area equal to the 5,600 lb wheel load. Figure 20 graphically portrays the input and output pressures used in case 4, iteration 1. The output values for the center two rings are high by 15 and 10 psi, respectively. Horizontal arrows show the pressure values selected for the second iteration. Figure 21 compares the input pressures to the output pressures for iteration 2. Finally, Figure 22 compares the pressures for iteration 3. Note that the output values fall above the input values by less than 4 psi.

The key decision during an iteration process involves the level of agreement between the input and output values. For this analysis, iteration continues until the input and output pressures agree to within ± 5 psi. Early experience showed both that it is difficult to get better agreement criteria than this, given the scale of discretization for the model, and that additional refinement does not significantly influence the maximum vertical subgrade strain computed from BISAR.

RESULTS

Table 5 summarizes the results of the final iteration for each of the cases analyzed. The maximum vertical subgrade strain represents the feature of performance recommended by Barker and Brabston for design of flexible airport pavements. Their design plot showing the repetitions of strain, as a function of maximum vertical strain at the top of the subgrade, was presented in an earlier section. The design discussion in this section uses the lower bound to the range proposed by Brabston, Barker, and Harvey³ and extrapolates it to low repetitions of strain. Table 5 shows that the allowable number of passes by a 5,600 lb wheel (repetitions of strain) varies from 70 to 400,000 as the subgrade modulus increases from 8,000 to 32,000 psi.

The calculated values of subgrade strain versus the subgrade modulus value have been plotted in Figure 23. This plot provides the basis of a design plot for a single wheel load acting on an 8 in. thick sand-grid layer having an average cell width equal to 6.4 in. The vertical

Table 2

Results for Case 2

<u>Case</u>	<u>Ring 1</u>	<u>Ring 2</u>	<u>Ring 3</u>	<u>Ring 4</u>	<u>Ring 5</u>	<u>Ring 6</u>	<u>ϵ_v</u>
2-1							
Input	37.5	37.5	17.5	9.5	7.5	2.5	
Output	41.7	43.0	18.6	11.8	9.3	3.4	0.95×10^{-3}
Difference	+3.2	+5.5	+1.1	+2.3	+1.8	0.9	
2-2							
Input	32.0	32.0	18.0	10.0	8.0	3.0	
Output	46.8	40.8	15.8	9.7	9.1	4.0	0.81×10^{-3}
Difference	+14.8	+8.8	-2.2	-0.3	+1.1	1.0	

Table 3

Results for Case 3

<u>Case</u>	<u>Ring 1</u>	<u>Ring 2</u>	<u>Ring 3</u>	<u>Ring 4</u>	<u>Ring 5</u>	<u>Ring 6</u>	<u>ϵ_v</u>
3-1							
Input	37.5	37.5	17.5	9.5	7.5	2.5	
Output	29.7	28.8	13.2	8.5	9.2	5.5	0.19×10^{-2}
Difference	-7.8	-8.7	-4.3	-1.0	+1.7	+3.0	
3-2							
Input	33.6	33.2	15.4	9.0	8.4	3.2	
Output	32.3	38.3	16.8	9.2	8.0	4.1	0.17×10^{-2}
Difference	-1.3	+5.1	+1.4	+0.2	-0.4	+0.9	

Table 4
Results for Case 4

<u>Case</u>	<u>Ring 1</u>	<u>Ring 2</u>	<u>Ring 3</u>	<u>Ring 4</u>	<u>Ring 5</u>	<u>Ring 6</u>	<u>ϵ_v</u>
4-1							
Input	37.5	37.5	17.5	9.5	7.5	2.5	
Output	52.9	47.7	18.1	11.2	9.4	3.6	0.48×10^{-3}
Difference	+15.4	+10.2	+0.6	+1.7	+1.9	+1.1	
4-2							
Input	44.2	41.6	16.8	9.3	7.4	2.0	
Output	47.9	50.6	20.6	11.9	9.1	2.9	0.56×10^{-3}
Difference	+3.7	+9.0	+3.8	+2.6	+1.7	+0.9	
4-3							
Input	46.0	46.0	17.0	10.0	7.5	2.0	
Output	48.8	49.9	20.3	11.8	9.1	2.8	0.58×10^{-3}
Difference	+2.8	+3.9	+3.3	+1.8	+1.6	+0.8	

CASE 4-1

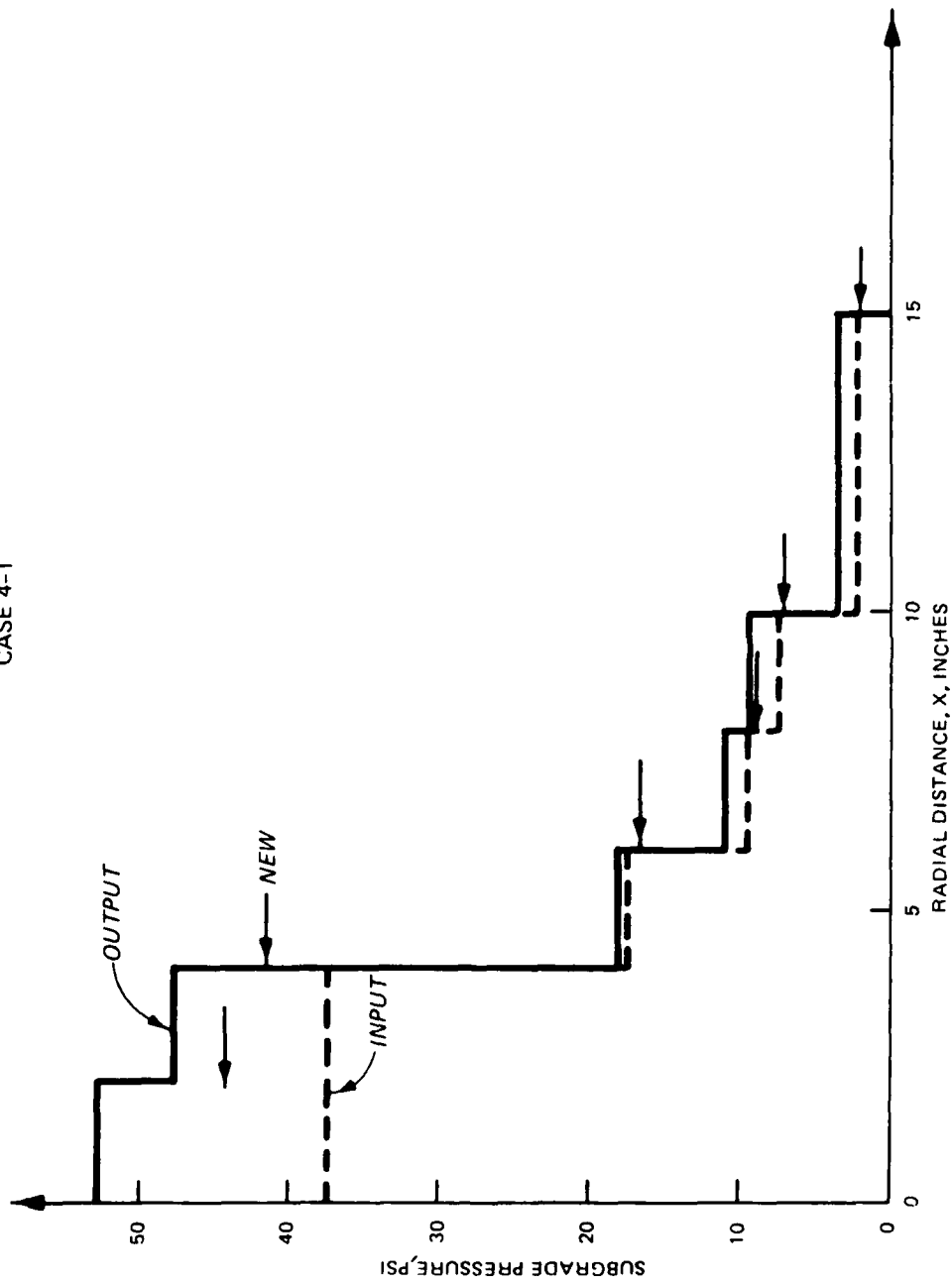


Figure 20. Input and output pressures, case 4-1

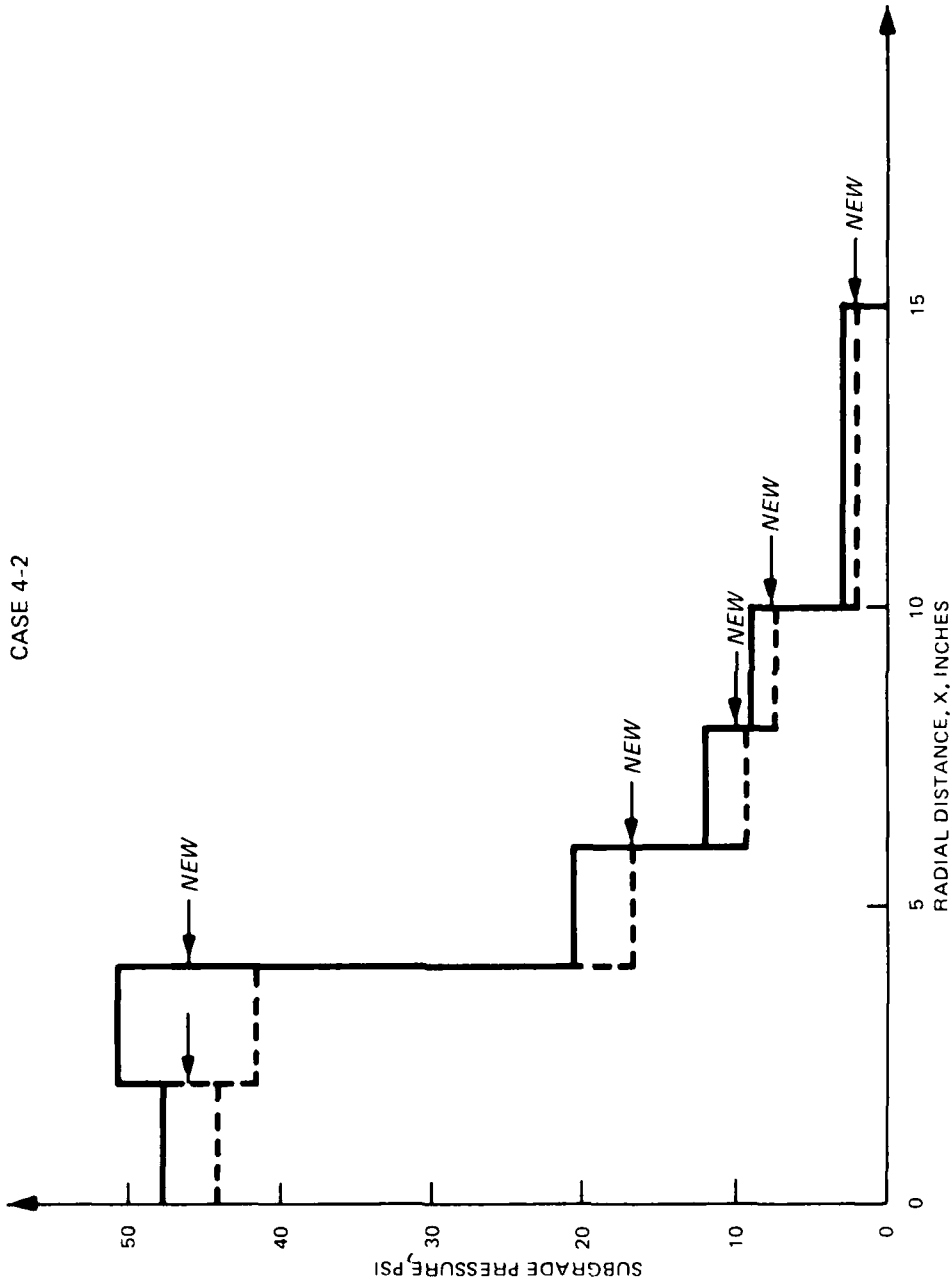


Figure 21. Input and output pressures, case 4-2

CASE 4-3

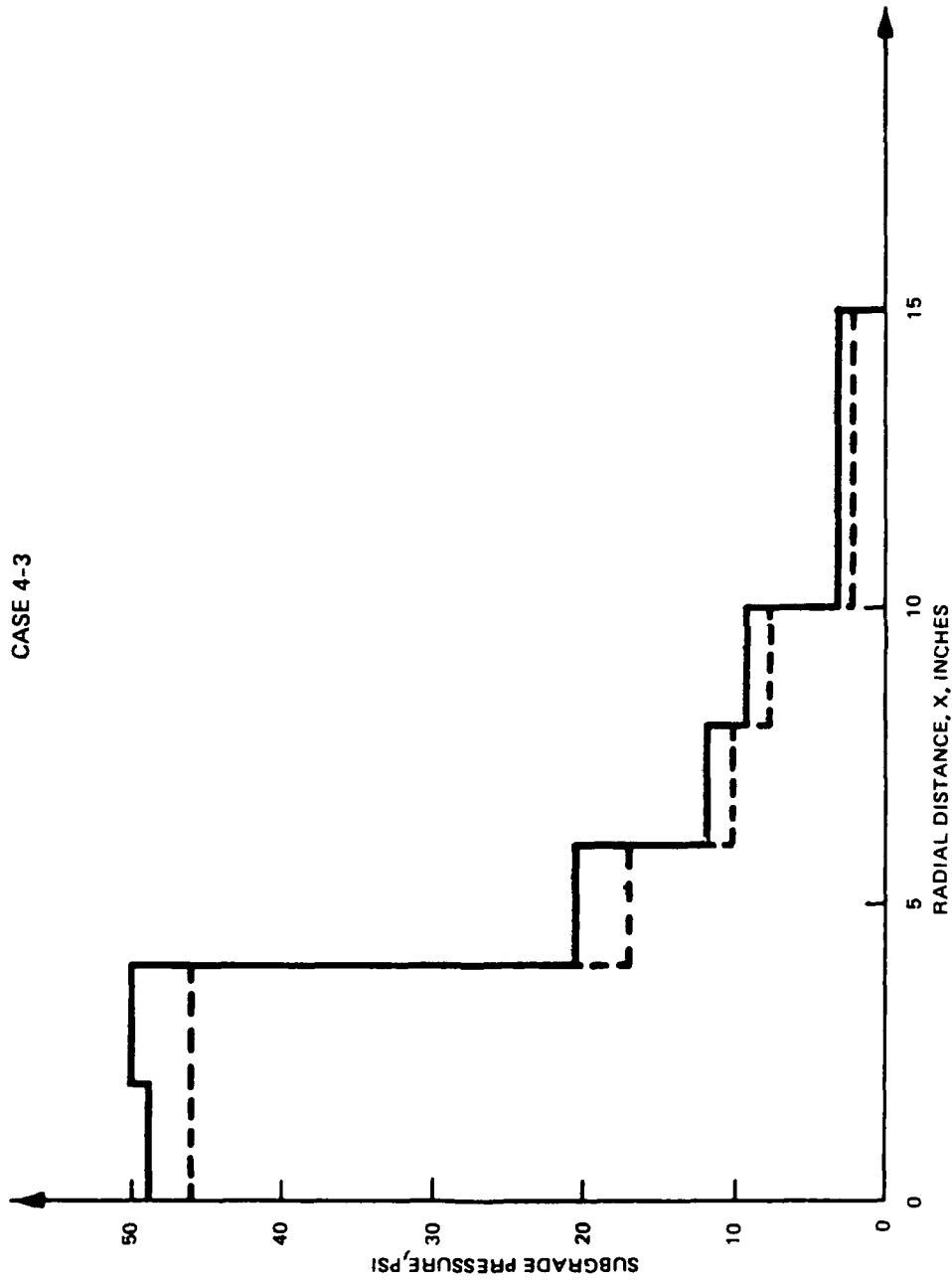


Figure 22. Input and output pressures, case 4-3

Table 5

Summary of Results

<u>Case</u>	<u>Subgrade Modulus psi</u>	<u>Maximum Subgrade Strain in./in.</u>	<u>Number of Coverages</u>
2	16,000	0.95×10^{-3}	7,750
3	8,000	1.7×10^{-3}	71
4	32,000	0.58×10^{-3}	415,000

subgrade strain axis can also be shown as the number of passes by using the Brabston, Barker, and Harvey³ relationship to relate subgrade strain to low repetitions. This is an appropriate relationship, since it is also based on an elastic model for subgrade behavior. Additional dashed lines have been added to Figure 23 to represent, conceptually, the single wheel load as a third design parameter. These lines were positioned approximately, by scaling the strains computed for a 5,600 lb wheel load, by the ratio of the wheel loads. Many additional analyses of the type described in this report are required to complete the design curves.

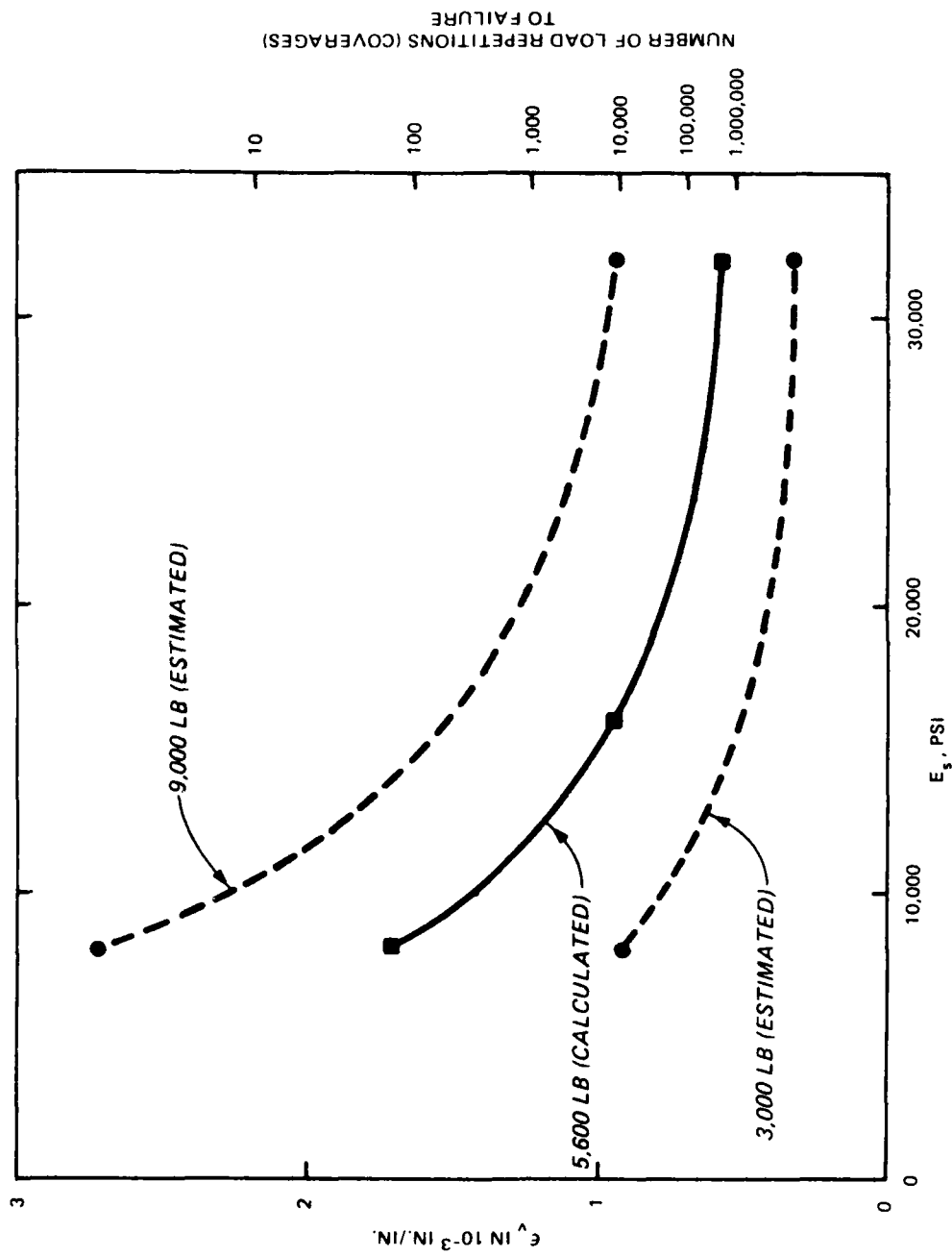


Figure 23. Conceptual design chart

FIELD VALIDATION

FIELD DATA

Two full-scale test sections were used to generate data for the analytical model described in the previous section. The first was an un-surfaced test section constructed under a previous WES project. This test section provided material for laboratory and field testing of the physical properties of the sand, grid, and subgrade. These properties are those described and summarized in the previous section. The second test section was part of a larger test section which was built as a joint project to provide field validation of the analytical model under this project and to study the performance of various surfacings and grid-fill materials under a separate WES project.

The general layout of the second test section is shown in Figure 24. Item 3 was constructed to match the input parameters used in the hypothetical case studies described in the previous section. Items 4 and 12 are similar. Item 4 has a thicker asphalt wearing course, which changes the ESWL on the top of the sand grid. Item 12 has a different type of sand for both grid fill and subgrade, which changes both the subgrade modulus and the distribution of stresses (k-values) in the sand-grid layer. Although they were built primarily to address the objectives of the other WES project, they could provide data for additional, future case studies and refinement of the analytical model. Considerable expenditures of additional engineering and computer time would be required to develop the conceptual design charts for comparison with these test items.

Item 3 consisted of 2 in. of asphalt wearing course over an 8-in. sand-grid layer placed on a compacted sand subgrade. Asphalt thickness was checked by taking core samples. Actual thicknesses ranged from 1.5 to 2.25 in. The dimensions and properties of the HDPE grids are as shown in Figure 1 and described in the previous section, except that the thickness of the plastic was 0.05 in. for the test section. As production tolerances of about ± 0.005 in. are considered reasonable, this difference will be ignored for the purposes of the analysis to follow. The sand used to build the subgrade and to fill the sand-grid cells is from the same source as that described in the previous section. Its grain-size distribution is shown in Figure 10. The sand was compacted in the grid cells to a dry density of 105 pcf. The moisture content ranged from 4 to 7 percent. The subgrade stiffness was evaluated using a FWD after construction was completed. The initial subgrade modulus was calculated to be 14,000 psi, densifying and stiffening to the expected 16,000 psi after the first 500 passes of the test vehicle.

The test vehicle was a standard 5-ton, tandem-axle, M51 military dump truck carrying the maximum highway payload of 20,000 lb. The resulting gross vehicle weight was 42,000 lb. The truck was fitted with standard, military, off-road tires inflated to the maximum cold inflation pressure of 70 psi.

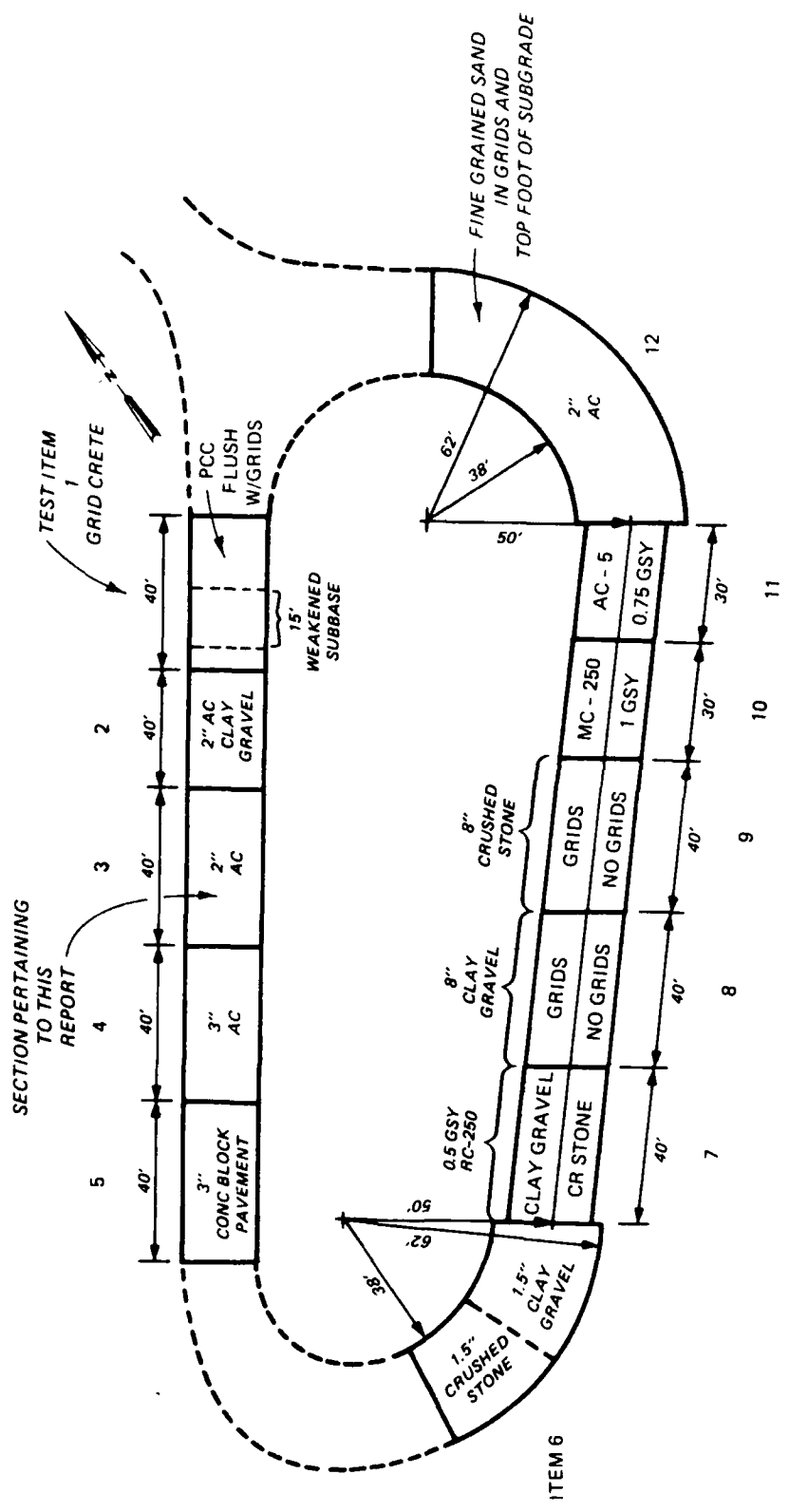


Figure 24. General layout, sand-grid test section

Natural vehicle wander was allowed, and a reversal of vehicle direction every 100 passes was used to ensure a more symmetrical pattern of vehicle wander.

Cross-section data were collected at 0, 100, 500, 1,000, 2,000, 3,000, 4,000, and 5,000 passes, and supplemented by photographs and FWD measurements. Damage to pavement systems is generally a function of the logarithm (base 10) of traffic intensity. A great deal of additional trafficking would therefore be required to produce significant additional data beyond that obtained at 5,000 passes. Hence, traffic was halted at 5,000 passes.

No destructive field testing was done, and additional trafficking by other vehicles is anticipated under the other project. The average, permanent, differential surface deflection or rut depth was obtained from the cross-section data. It is plotted as a function of vehicle passes in Figure 25.

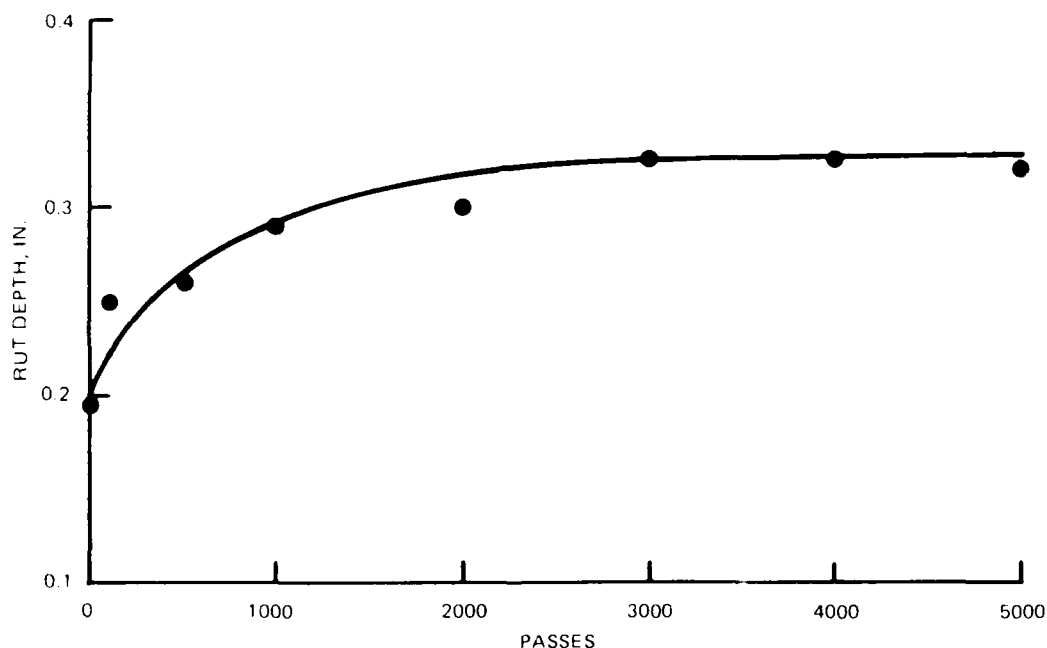


Figure 25. Average rut depth as a function of vehicle passes

ANALYSIS

The data presented in Figure 25 suggest that initial consolidation or shakedown has occurred with the rut depth stabilizing at 0.3 in. A pavement failure (rut depth ≥ 1.0 in.) has not occurred and does not appear imminent. This information can be used to check the conceptual design chart shown in Figure 23, if the test-section traffic can be expressed in terms of coverages of a single wheel load.

The effect of the test vehicle on the test section can be described in terms of ESWL as noted earlier. Based on the concepts presented by Pereira,²³ an ESWL curve for the test vehicle's 18,000 lb axle, as shown

in Figure 26, can be constructed. From Figure 26, the ESWL is seen to vary from 31 percent of 5,600 lb at the top of the sand-grid layer to 42 percent or 7,600 lb at the bottom of the sand-grid layer. Thus, the effective load induced by one 18,000 lb axle of the test vehicle is equivalent to the 5,600 lb single-wheel load assumed for the development of the analytical model, at the top of the sand-grid layer. The effective load is somewhat larger at greater depths. The test vehicle thus provides a slightly more severe validation load than a single 5,600 lb wheel. It can be used to provide a conservative validation check of the analytical model developed for a 5,600 lb single wheel load.

Because the test vehicle has two 18,000 lb axles, and because the test vehicle exhibits a lateral wander during trafficking, one vehicle pass does not provide at least one coverage, or strain repetition across the entire width of the test item. A test vehicle "pass-to-coverage" ratio is required to compare the vehicle passes shown in Figure 24 to the coverages used in Figures 7 and 23. Using vehicle wander concepts presented by Pereira²³ a pass-to-coverage ratio for the 18,000 lb axle has been calculated to be 2.64. Since the test vehicle has two 18,000 lb axles, and the effect of the front axle can be ignored because of its relatively small load, the test vehicle pass-to-coverage ratio can be taken as $2.64 \div 2 = 1.32$.

Based on the above, Item 3 of the test section was subjected to more than 5,000 passes $\div 1.32$ per coverage to yield 3,788 coverages of a 5,600 lb equivalent single wheel load without experiencing failure. Figure 27 shows this point superimposed on a portion of Figure 23. An arrow through the data point indicates the direction the point would translate had trafficking been carried to failure. For a subgrade modulus of 16,000 psi, the analytical model predicts satisfactory performance to 7,750 coverages. These two values are quite close in terms of the logarithm (base 10) of coverages commonly used in pavement design. The analytical model predicted satisfactory performance to $\log(7,750) = 3.9$, and the test section demonstrated satisfactory performance to at least $\log(3,788) = 3.6$. It can be inferred from these results that the model is conservative.

These promising results support spending the time and money necessary to construct additional test sections, having various subgrade strengths, and trafficking them to failure with a variety of equivalent single wheel loads. Should additional testing indicate that the model is too conservative, the model is easily calibrated by selecting a less conservative relationship between vertical subgrade strain and allowable coverages.

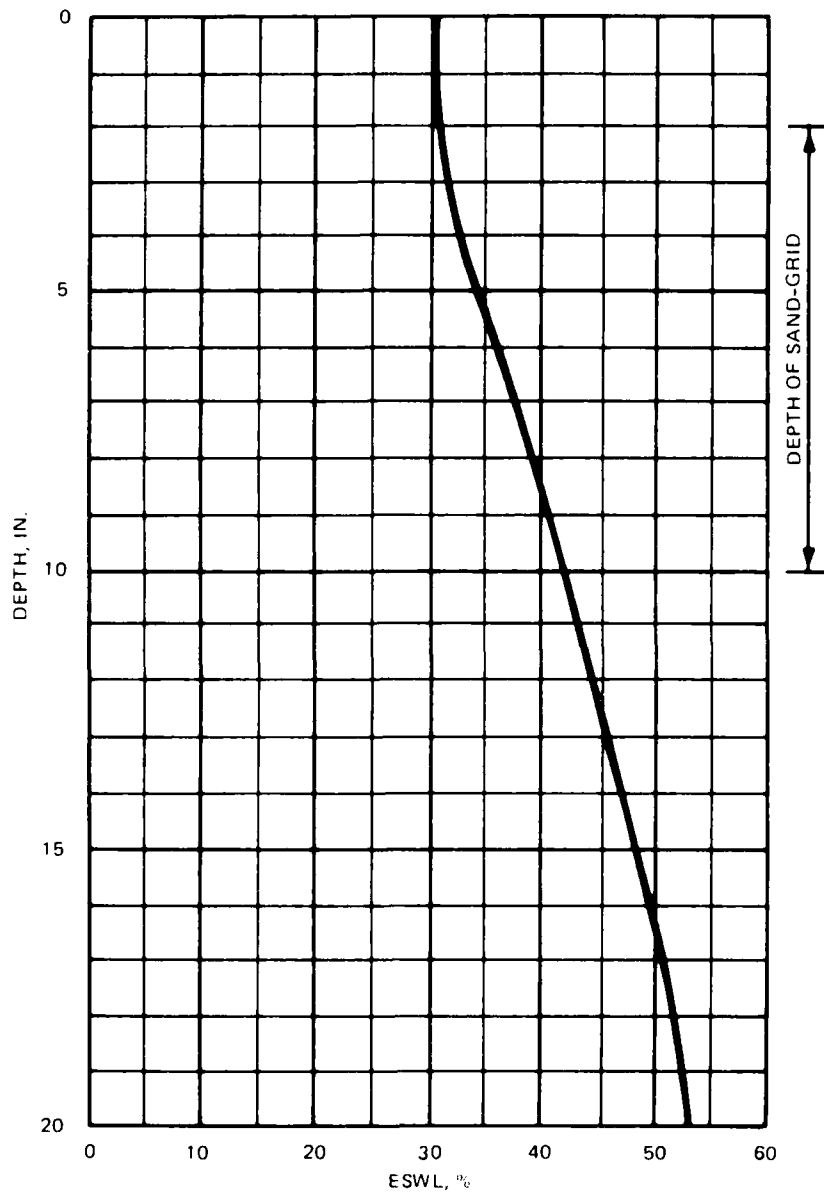


Figure 26. Equivalent single wheel load in percent of axle load versus depth

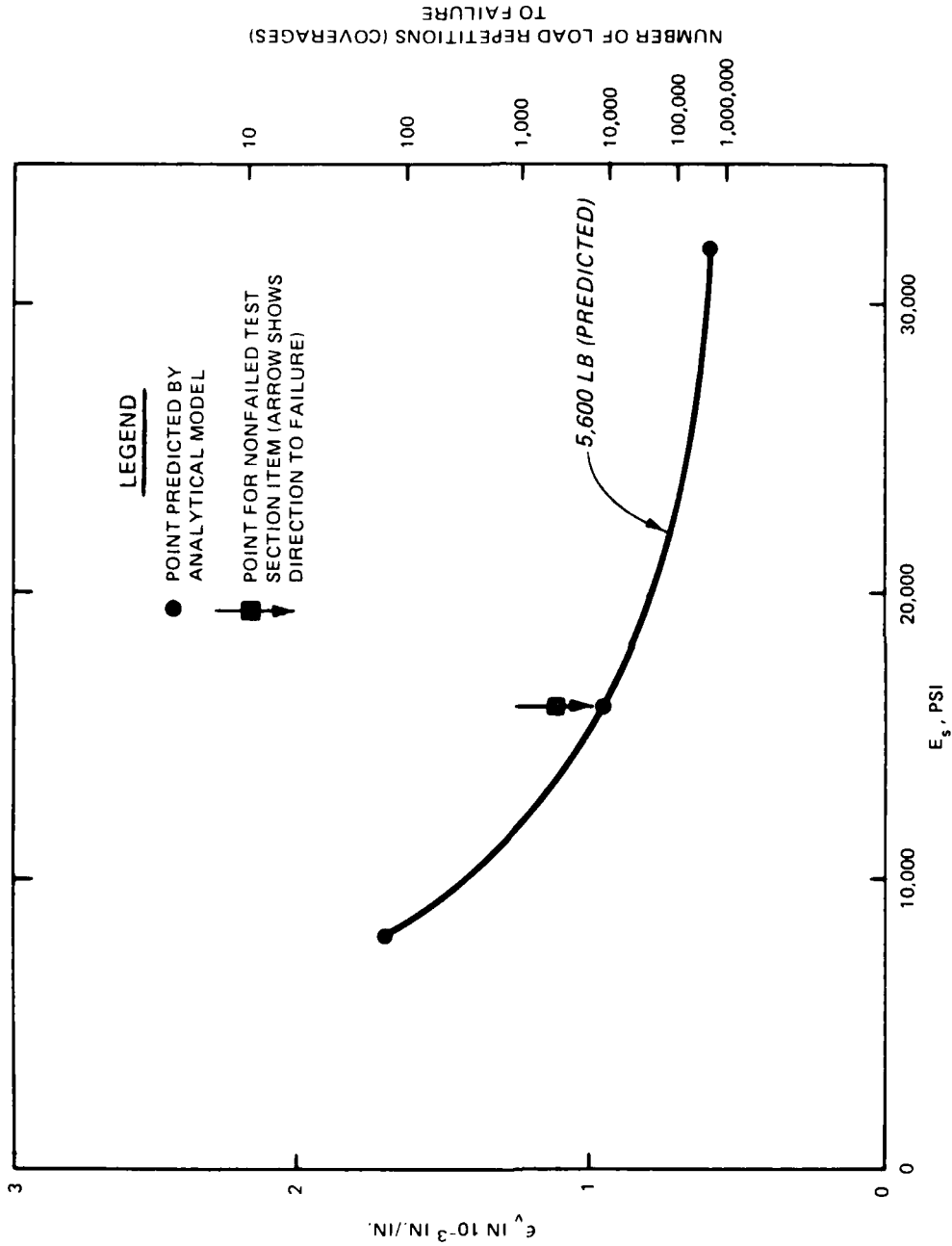


Figure 27. Test section data and predicted performance

CONCLUSION AND RECOMMENDATIONS

The model described in this report provides a means of considering five important characteristics of sand grids. These are: the complex geometry, the different symmetry for the load than for the grid, the vertical sand-plastic interface, the importance of locked-in lateral sand stresses, and the variation of sand modulus in the horizontal plane. The model handles these characteristics with differing levels of sophistication. Although the results reflect the required simplifications, they provide a design result which compares favorably with measured test section behavior.

The flow chart described in the text, and shown in Figure 9, was used to generate a conceptual design chart. Physical properties and dimensions for the sand grid were taken from the commercially available product that is being used to construct sand grid test sections at WES. The material properties for the sand match those of the concrete sand described in the text and Figure 10. Loads on the sand grid were based on a 5600 lb. single wheel load acting through a 2 in. asphalt concrete wearing surface. This conceptual design chart is shown in Figure 23, including estimated lines for 3000 and 9000 lb. single wheel loads. The number of allowable coverages shown on the right-hand vertical axis is obtained by applying the subgrade strain criteria by Brabston, Barker, and Harvey³ to the subgrade strain calculated in the last block of the flow chart.

A design chart similar to Figure 23 can be generated for any particular combination of sand grid and material used to fill the grid cells. Sand grid pavement systems can be designed for multiple-wheel gear configurations by using equivalent single wheel load theory to determine an equivalent single wheel load to use with the single wheel load design chart. The appropriate chart is then entered with the known design parameters, to determine the value of the unknown parameter or acceptable combinations of the design parameters.

For example, suppose a light utility airport pavement is to be constructed using the materials used to develop Figure 23. Further suppose that the subgrade has a modulus of 23,000 psi (approximately CBR 15), and that the design aircraft has an equivalent single wheel load of 5600 lb. Entering Figure 23 with a subgrade modulus of 23,000 psi, the 5600 lb. line is intersected at 100,000 coverages. Hence, the proposed pavement should sustain 100,000 coverages of the design aircraft before developing a 1 in. rut.

Further full-scale testing to include instrumentation of the sand grids to measure the lateral stress distribution inside the cells and the vertical stress distribution at the subgrade's surface will allow appropriate refinement of the analytical model.

Extensive exercising of the design model will allow the development of complete design charts which can be used directly for sand-grid pavement design.

REFERENCES

1. Al-Hussaini, M. M., and Perry, E. B. 1976 (Dec). "Effect of Horizontal Reinforcement on Stability of Earth Masses," Technical Report S-76-11, US Army Engineer Waterways Experiment Station, Vicksburg, Miss.
2. Barker, W. R., and Brabston, W. N. 1975 (Sep). "Development of a Structural Design Procedure for Flexible Airport Pavements," Technical Report S-75-17, US Army Engineer Waterways Experiment Station, Vicksburg, Miss. (Also: Report No. FAA-RD-74-199), Federal Aviation Administration, Washington, DC.
3. Brabston, W. N., Barker, W. R., and Harvey, G. G. 1975 (Jul). "Development of a Structural Design Procedure for All-Bituminous Concrete Pavements for Military Roads," Technical Report S-75-10, US Army Engineer Waterways Experiment Station, Vicksburg, Miss.
4. Burmister, D. M. 1943. "The Theory of Stresses and Displacements in Layered Systems and Application to the Design of Airport Runways," Proceedings, Highway Research Board, Vol 23.
5. Bush, A. J., III. 1980a. "Nondestructive Testing for Light Aircraft Pavements; Phase I, Evaluation of Nondestructive Testing Devices," Report No. FAA-RD-80-9-I, Department of Transportation, Federal Aviation Administration, Washington, DC.
6. Bush, A. J., III. 1980b. "Nondestructive Testing for Light Aircraft Pavements; Phase II, Development of the Nondestructive Evaluation Procedure," Report No. FAA-RD-80-9-II, Department of Transportation, Federal Aviation Administration, Washington, DC.
7. Chou, Y. T. 1981 (May). "Structural Analysis Computer Programs for Rigid Multi-component Pavement Structures with Discontinuities--WESLIQID and WESLAYER; Report 1: Program Development and Numerical Presentations," Technical Report GL-81-6, US Army Engineer Waterways Experiment Station, Vicksburg, Miss.
8. Coatzee, N. F. 1985. "Product Evaluation Presto Roadbase Sand Confinement Grid-Final Report," Alaska Department of Transportation and Public Facilities, Fairbanks, Alaska.
9. Crawford, J. E., and Katona, M. G. 1975 (Oct). "State-of-the-Art for Prediction of Pavement Response," US Army Engineer Waterways Experiment Station, Report No. FAA-RD-75-183 (also CR S-75-8), Federal Aviation Administration, Washington, DC.

10. Department of Defense. 1974 (Dec). "Test Methods for Pavement, Subgrade, Subbase, and Base-Course Materials," Military Standard No. MIL-STD-621A, Method 104, Washington, DC.
11. Eberhardt, A. C. 1973 (Jun). "Aircraft-Pavement Interaction Studies Phase I: A Finite-Element Model of a Jointed Concrete Pavement on a Non-Linear Viscous Subgrade," Preliminary Report S-19, Construction Engineering Research Laboratory, Champaign, Ill.
12. Eberhardt, A. C., and Willmer, J. L. 1973 (Nov). "Computer Program for the Finite Element Analysis of Concrete Airfield Pavements," Technical Report S-26, Construction Engineering Research Laboratory, Champaign, Ill.
13. Hadala, P. F. 1968 (Aug). "Sidewall Friction Reduction in Static and Dynamic Small Blast Load Generator Tests," Technical Report S-68-4, US Army Engineer Waterways Experiment Station, Vicksburg, Miss.
14. Hardin, B. O., and Black, W. L. 1968 (Mar). "Vibration of Normally Consolidated Clay," Journal of the Soil Mechanics and Foundations Division, ASCE, Vol 94, No. SM2.
15. Hicks, R. G. 1971. "Factors Influencing the Resilient Response of Granular Materials," Highway Research Record, No. 345.
16. Huang, Y. H., and Wang, S. T. 1973. "Finite-Element Analysis of Concrete Slabs and Its Implications for Rigid Pavement Design," Highway Research Record No. 466, pp. 55-69.
17. Hudson, W. R., and Matlock, H. 1966 (May). "Discontinuous Orthotropic Plates and Pavement Slabs," Research Report 56-6, Center for Highway Research, Austin, Tex.
18. Jumikis, A. R. 1967. Introduction to Soil Mechanics, D. Van Nostrand Co.
19. Koninklijke/Shell Laboratorium. 1972. "BISAR Users Manual; Layered System Under Normal and Tangential Loads," Amsterdam, Holland.
20. Mayne, P. W. and Kulhawy, F. H. 1982 (Jun). " K_o -OCR Relationship in Soil," Journal of the Geotechnical Engineering Division, ASCE, Vol 108, No. GT6, pp. 851-872.
21. Mitchell, J. K., Kao, T. C. and Kavazanjian, E. 1979 (Jul). "Analysis of Grid Cell Reinforced Pavement Bases," Technical Report GL-79-8, US Army Engineer Waterways Experiment Station, Vicksburg, Miss.
22. Nigel Nixon & Partners. 1983. "Final Report on Presto Geoweb for Presto Products Incorporated," London, U.K.

23. Pereira, A. T. 1977 (Jun). "Procedures for Development of CBR Design Curves," Instruction Report S-77-1, US Army Engineer Waterways Experiment Station, Vicksburg, Miss.
24. Pickett, G. et al. 1951 (Oct). "Deflection, Moments, and Reactive Pressures for Concrete Pavements," Bulletin No. 65, Kansas State College, Manhattan, Kans.
25. Pickett, G., and Ray, G. K. 1951. "Influence Charts for Concrete Pavements," Transactions, American Society of Civil Engineers, Vol 116, pp. 49-73.
26. Rea, C. E., and Mitchell, J. K. 1978 (Apr). "Sand Reinforcement Using Paper Grid Cells," Preprint 3130, American Society of Civil Engineers Spring Convention and Exhibit, Pittsburgh, Penn.
27. Saxena, S. K. 1973. "Pavement Slabs Resting on Elastic Foundation," Highway Research Record No. 466, pp. 163-178.
28. Seed, H. B., and Idriss, I. M. 1970 (Dec). Soil Moduli and Damping Factors for Dynamic Response Analysis, Earthquake Engineering Research Report No. 70-10.
29. Smith, I. M. 1982. Programming the Finite Element Method with Applications to Geomechanics. John Wiley and Sons, Chichester.
30. Webster, S. L. 1979 (Nov). "Investigation of Beach Sand Trafficability Enhancement Using Sand-Grid Confinement and Membrane Reinforcement Concepts; Report 1, Sand Test Sections 1 and 2," Technical Report GL-79-20, US Army Engineer Waterways Experiment Station, Vicksburg, Miss.
31. Webster, S. L. 1981 (Feb). "Investigation of Beach Sand Trafficability Enhancement Using Sand-Grid Confinement and Membrane Reinforcement Concepts; Report 2, Sand Test Sections 3 and 4," Technical Report GL-79-20, US Army Engineer Waterways Experiment Station, Vicksburg, Miss.
32. Webster, S. L. 1986. "Sand Grid Demonstration Roads Constructed for JLOTS II Tests at Fort Story, Virginia" (in preparation), US Army Engineer Waterways Experiment Station, Vicksburg, Miss.
33. Webster, S. L., and Alford, S. J. 1978. "Investigation of Construction Concepts for Pavements Across Soft Ground," Technical Report S-78-6, US Army Engineer Waterways Experiment Station, Vicksburg, Miss.

APPENDIX A
PROGRAM LISTINGS

```

PROGRAM CAL
PROGRAM CAL USED FOR CALCULATING THE STRESS OF THE SQUARE
DIMENSION B1(12), B2(12), G1(12), G2(12), W(3), BEAM1(12), BEAM2(12),
* GRID1(12), GRID2(12)
READ (1,*) (W(I), I=1,3)
READ (1,*) (BEAM1(I), I=1,12)
READ (1,*) (BEAM2(I), I=1,12)
READ (1,*) (GRID1(I), I=1,12)
READ (1,*) (GRID2(I), I=1,12)
WRITE (3,110) (BEAM1(I), I=1,12)
WRITE (3,210) (BEAM2(I), I=1,12)
WRITE (3,220) (GRID1(I), I=1,12)
WRITE (3,230) (GRID2(I), I=1,12)
A1=1.75*1.75
DO 1 I=1,12
  B1(I)=BEAM1(I)*W(1)
  B2(I)=BEAM2(I)*W(2)
  G1(I)=GRID1(I)*1.0
  G2(I)=GRID2(I)*1.0
CONTINUE
WRITE (3,310) (B1(I), I=1,12)
WRITE (3,320) (B2(I), I=1,12)
S1=2.*(.55*B1(1)+.626*B1(2))
SS1=S1/A1
S2=.7*B1(2)+.45*B1(1)+.22*B1(2)+.47*B2(1)+.0022*B2(2)+1.*G1(1)
+ .047*G1(2)
SS2=S2/A1
S3=.22*B1(2)+.077*B1(3)+.27*B2(1)+.013*B2(2)
SS3=S3/A1
S4=.3*B1(3)+.27*B2(1)+.013*B2(2)
SS4=S4/A1
S5=.17*B1(3)+.13*B1(4)+.27*B2(1)+.013*B2(2)
SS5=S5/A1
S6=.42*B1(4)+.38*B1(5)+.13*B2(1)+.006*B2(2)+1.*G2(1)+.047*G2(2)
SS6=S6/14.9
S9=2.*(.25*B1(2)+.0256*B2(2)+.55*G1(2))
SS9=S9/A1
S10=.185*B1(2)+.064*B1(3)+.019*B2(2)+.0066*B2(3)+.149*B2(2)+
+ .406*G2(2)+.141*G2(3)
SS10=S10/A1
S11=.25*B1(3)+.0256*B2(3)+.149*B2(2)+.547*B2(3)
SS11=S11/A1
S12=.142*B1(3)+.106*B1(4)+.015*B2(3)+.011*B2(4)+.313*B2(3)+
+ .234*B2(4)
SS12=S12/A1
S13=.35*B1(4)+.31*B1(5)+.25*B2(4)+.13*B2(2)+.02*B2(3)+
+ .77*G1(4)+.11*G1(5)+.15*G2(2)+.02*G2(3)
SS13=S13/12.25
S16=2.*(.11*B2(2)+.04*B2(3))
SS16=S16/A1
S17=.15*B2(3)+.11*B2(2)+.04*B2(3)

```


PROGRAM

SGRID

LATEST REVISION - MAY 25, 1985 -- MODIFIED BY P.T. CHANG
UNDER THE DIRECTION OF DR. P. LAMBE.

PROGRAM GSAND IS MODIFIED BASED ON I.M. SMITH PROGRAM 5.0
(PLANE STRAIN OF ELASTIC SOLID USING 4-NODE QUADRILATERAL ELEMENTS)
THE MODIFICATIONS ARE FOLLOWS :

1. ECHO INPUT DATA
2. CAN HANDLE DIFFERENT E,V VALUES FOR EACH ELEMENT OR LAYER
3. CAN HANDLE DIFFERENT ELEMENT SIZE
4. CAN ASSEMBLE GLOBAL STIFFNESS MATRIX IN N*N MATRIX
5. CAN HANDLE KNOWN DISPLACEMENT BOUNDARY CONDITION
6. CAN CALCULATE THE FORCE(REACTION) VECTOR
7. PRINT STRESS AND STRAIN AT SAME LINE THROUGH NEW SUBROUTINE
PRINTW FOR EACH GAUSSIAN POINT OR PRINT LOAD DEFOR. FORCE
AS TABULAR FORM FOR EACH DEGREE OF FREEDOM.
8. CAN ITERATE PSEUDO-NONLINER PROBLEM BY SETTING THE
CONVERGENCE CRITERION AS 1/10 THE DIFFERENCE OF THE SHEAR
STRAIN RATIO (G/GMAX) BETWEEN TWO ITERATIONS.

```
REAL E,V,AA,BB,K1,K2,DET,QUOT
INTEGER I,J,K,L,P,Q,NXE,NYE,H,N,W,CDMAX,RN,NL,NN,
*DOF,MOD,NODOF,R,T,GP,IDEF,ICOORD,IJAC,IJAC1,IDERIV,
*IDEE,IBEE,IDREE,IBT,IBTDB,IKM,INF,ISAMP
REAL DEF(8,3),SAMP(7,2),COORD(8,2),JAC(8,2),
*IJAC1(8,2),DER(8,4),DERIV(8,4),BEE(8,8),DBEE(8,8),
*BTDB(8,8),KM(8,8),ELD(8),VOL(8),EPS(3),SIGMA(3),BT(8,3),FUN(4)
INTEGER G(8)
```

ALTER NEXT TWO CARDS TO CHANGE PROBLEM SIZE

```
REAL R(1000),LOAD(100),BIGK(100,100),FORCE(100),GDISP(100),
*BIGKM(100,100),VAL(100),RADIUS(100),DEPTH(100),PROP(100,2),
*GSTRN(23),RATIO(23),STRESSV(22),KO(22),GRATIO(22,10),
*AVGSTRN(22),LOAD(10),GMAX(22),LOADD(100),DISP(100),FORCES(100)
INTEGER NF(100,2),IBIGK,FIX,NO(100),NLOAD(10)
DATA IDEF,ICOORD,IJAC,IJAC1,IDERIV,IDEE/6*8/
DATA IBEE,IDREE,IBT,IBTDB,IKM,DOF/6*8/
DATA ISAMP/7/,NODOF/2/,H/3/,T/2/
DATA GSTRN/.000001,.00001,.0001,.00015,.0002,.0003,.0004,.0005,
* .0006,.0007,.0008,.0009,.0010,.0015,
* .0020,.0030,.0040,.0050,.0060,.0070,
* .0080,.0090,.0100/
DATA RATIO/1.,.95,.74,.67,.62,.53,.43,.43,.39,.36,.34,.32,.30,.27,
* .19,.15,.12,.105,.09,.08,.074,.065,.06/
```

ALTER NEXT CARD TO CHANGE PROBLEM SIZE

```
DATA INF/100/,IBIGK/100/,EPSLON/.1/
```

INPUT AND INITIALISATION

```
READ(1,*)NXE,NYE,N,W,NN,PN,NL,FIX,GP
```

```

WRITE(3,100) NXE,NYE,N,N,N,N,N,N,NL,RY,GP
100 FORMAT(1H1,/, ' NUMBER OF ELEMENTS IN X - DIRECTION'      = ',I4,/,
+      ' NUMBER OF ELEMENTS IN Y - DIRECTION'                = ',I4,/,
+      ' TOTAL NUMBER OF FREEDOMS IN MESH'                    = ',I4,/,
+      ' HALF BAND WIDTH'                                     = ',I4,/,
+      ' NUMBER OF NODES IN MESH'                             = ',I4,/,
+      ' NUMBER OF RESTRAINED NODES IN MESH'                  = ',I4,/,
+      ' NUMBER OF LOADED FREEDOMS'                           = ',I4,/,
+      ' NUMBER OF FIXING PRESCRIBED DISPLACEMENT'           = ',I4,/,
+      ' NUMBER OF GAUSSIAN INTERGRATION ORDER'               = ',I4,/)
NOD=DOF/NODOF
CDMAX=N+1
R=N*CDMAX
M=NXE+1
READ(1,*) (RADIUS(I),I=1,M)
WRITE(3,110) (RADIUS(I),I=1,M)
110 FORMAT(/, ' RADII OF THE MESH LINES = ',2PF5.1)
M=NYE+1
READ(1,*) (DEPTH(I),I=1,M)
WRITE(3,120) (DEPTH(I),I=1,M)
120 FORMAT(/, ' DEPTH OF THE MESH LINES = ',11F6.2 )
CALL GAUSS(SAMP,ISAMP,GP)
CALL FORMMF(NF,INF,NN,NODOF,RN)

```

ELEMENT STIFFNESS INTEGRATION AND ASSEMBLY

```

WRITE(3,145)
145 FORMAT(1H1)
ITER = 0
1 ITER = ITER + 1
CALL NULVEC(3K,R)
CALL NULVEC(LOADS,N)
CALL NULL(BIGK,IPIGK,N,N)
CALL NULL(BIGKM,IPIGK,N,N)
CALL NULL(DEE,IDEE,H,H)
DO 3 P=1,NXE
DO 3 Q=1,NYE
NUMBER = NYE * (P - 1) + Q
IF(ITER .EQ. 1) THEN
READ(1,*) STRESV(NUMBER),KO(NUMBER),V
STPESO = (1.+2.*KO(NUMBER))/3. * STRESV(NUMBER)
GMAX(NUMBER) = 5500. * (STRESO) ** 0.5
E = 2. * (1.+V) * GMAX(NUMBER)
WRITE(3,50) ITER,NUMBER,KO(NUMBER),NUMBER,STRESV(NUMBER),
* STPESO,GMAX(NUMBER),E
ELSE
ITEP1 = ITER - 1
STPESO = (1.+2.*KO(NUMBER))/3. * STRESV(NUMBER)
GG=5500. * GRATIO(NUMBER,ITER1) * (STRESO)**0.5
E = 2. * (1.+V) * GG
WRITE(3,55) ITER,NUMBER,GRATIO(NUMBER,ITER1),STRESV(NUMBER),
* STPESO,GG,E
ENDIF
50 FORMAT(/, ' ITER=',I3,2X, 'KO(',I2,')=',F9.2,2X, 'SV(',I2,')=',

```

```

*          F9.2,2X,'SC=' ,F9.2,2X,'G=' ,F9.2,2X,'E=' ,F9.2)
55  FORMAT (/, ' ITER=' ,I3,2X,'GRATIO(' ,I2,')=' ,F9.2,2X,'SV=' ,F9.2,
*          2X,'SC=' ,F9.2,2X,'G=' ,F9.2,2X,'E=' ,F9.2)
CALL NULL(KM,IKM,DOF,DOF)
CALL FORMD(DFE,IDEF,E,W)
CALL VGEOM(P,Q,NXE,NYE,COORD,ICCOORD,G,NF,INF,RADIUS,DEPTH)
DO 4 I=1,GP
DO 4 J=1,GP
    K1=SAMP(I,2)
    K2=SAMP(J,2)
    CALL FORMLN(DEF,IDER,SUN,SAMP,ISAMP,I,J)
    CALL MATMUL(DEF,IDER,COORD,ICCOORD,JAC,IJAC,T,NOD,T)
    CALL TWBY2(JAC,IJAC,JAC1,IJAC1,DET)
    CALL MATMUL(JAC1,IJAC1,DER,IDER,DERIV,IDERIV,T,T,NOD)
    CALL NULL(BEE,IBEE,H,DOF)
    CALL FORMB(BFE,IBFE,DERIV,IDERIV,VOL,NOD)
    CALL MATMUL(DEF,IDEF,BEE,IBEE,DBEE,IDBEE,H,H,DOF)
    CALL MATRAN(BT,IBT,BEE,IBEE,H,DOF)
    CALL MATMUL(BT,IBT,DBEE,IDBEE,BTDB,IBTDB,DOF,H,DOF)
    QUOT=DET*K1*K2
    DO 5 K=1,DOF
    DO 5 L=1,DOF
5      BTDB(K,L)=BTDB(K,L)*QUOT
    CALL MATADD(KM,IKM,BTDB,IBTDB,DOF,DOF)
4  CONTINUE
    CALL FMBIGK(BIGK,IBIGK,KM,IKM,G,DOF)
    CALL FMBIGK(BIGKM,IBIGK,KM,IKM,G,DOF)
    CALL FORMKV(BK,KM,IKM,G,N,DOF)
3  CONTINUE

```

EQUATION SOLUTION

```

IF(ITER .EQ. 1) THEN
    DO 11 I=1,FIX
        READ(1,*) NO(I),VAL(I)
11     WRITE(3,170) NO(I),VAL(I)
    ENDIF
170  FORMAT (/, ' PRESCRIBED DEFORMATION AT # OF DOF (' ,I2,') =' ,F12.4)
    DO 12 I=1,FIX
        BK(NO(I)) = BK(NO(I)) + 1.0E12
12     BIGKM(NO(I),NO(I)) = BIGKM(NO(I),NO(I)) + 1.0E12
        CALL SAMPED(BK,N,CDMAX)
    DO 13 I=1,FIX
13     LOADS(NO(I)) = BK(NO(I)) * VAL(I)
        IF(ITER .EQ. 1) THEN
            DO 6 I=1,NL
                READ(1,*) NLOAD(I),LOAD(I)
                WRITE(3,180) NLOAD(I),LOAD(I)
6         LOADS(NLOAD(I)) = LOAD(I)
            ENDIF
180  FORMAT (/, ' PRESCRIBED LOAD AT # OF DOF (' ,I2,') =' ,F12.4)
        IF(ITER .GE. 2) THEN
            DO 66 I=1,NL
66         LOADS(NLOAD(I)) = LOAD(I)

```

```

      FND=7
      DO 210 I=1,N
        LOADD(I) = LOADS(I)
    ) CONTINUE
      CALL BACK1(BK,LOADS,N,CDMAX)
      CALL BACK2(BK,LOADS,N,CDMAX)
      DO 310 I=1,N
        DISP(I) = LOADS(I)
    310 CONTINUE
      CALL MMULT(BIGK,IBIGK,LOADS,N,N,FORCE)
      DO 410 I=1,N
        FORCES(I) = FORCE(I)
    410 CONTINUE
      CALL MMULT(BIGKM,IBIGK,LOADS,N,N,FORCE)
      WRITE (3,550)
    550 FORMAT(1H1,' NUMBER',7X,'LOAD',10X,'DISPLACEMENT',6X,'FORCE',/)
      DO 600 I=1,N
        WRITE(3,700) I,LOADD(I),DISP(I),FORCES(I)
    600 CONTINUE
      700 FORMAT(15,5X,3(E12.4,5X))
      REACT = 0.
      DO 800 I=1,FIX
        REACT = REACT + FORCES(NO(I))
    800 CONTINUE
      WRITE(3,850) ITER,REACT
    850 FORMAT(/,' REACTION FORCE FOR ITER. (' ,I2,' ) =',F10.2,/)

```

RECOVER ELEMENT STRAINS AND STRESSES
AT ALL GAUSSIAN INTEGRATION POINTS

```

      NYX = NYE * NYE
      DO 222 I=1,NXY
        AVGSTN(I) = 0.
        GDISP(I) = 0.
    222 CONTINUE
      DIFMAX=0.
      DO 7 P=1,NXE
        DO 7 Q=1,NYE
          CALL NULL(DBE,IDBE,H,H)
          CALL FORMD(DBE,IDE, E, V)
          CALL VGEOM(P,Q,NXE,NYE,COORD,ICOORD,G,NF,INF,RADIUS,DEPTH)
          SEM = 0.
          DO 9 I=1,GP
            DO 8 J=1,GP
              CALL FORMLN(DER,IDER,FUN,SAMP,ISAMP,I,J)
              CALL MATMUL(DER,IDER,COORD,ICOORD,JAC,IJAC,T,NOD,T)
              CALL TWOBY2(JAC,IJAC,JAC1,IJAC1,DET)
              CALL MATMUL(JAC1,IJAC1,DEP,IDER,DERIV,IDERIV,T,T,NOD)
              CALL NULL(BEE,IBEE,H,DOF)
              CALL FORMR(BEE,IBEE,DERIV,IDERIV,VOL,NOD)
              DO 9 M=1,DOF
                IF(G(M).EQ.0) ELD(M)=0.0
                IF(G(M).NE.0) ELD(M)=LOADS(G(M))
              CALL MMULT(BEE,IBEE,ELD,H,DOF,EPS)

```

```

      CALL MMULT (DEF, IDER, PPS, H, H, SIGMA)
      SUM = SUM + PPS (3)
      NUMBER = NYE * (P - 1) + 2
3     CONTINUE
      AVGSTN (NUMBER) = SUM / 4.
      GDISP (NUMBER) = SUM / 4.
      DO 31 K=1, 23
          IF (GSTRN (K) - ABS (AVGSTN (NUMBER))) 81, 82, 82
81     CONTINUE
82     K11=K-1
          IF (K11 .EQ. 0) GO TO 83
          SLOPE=(RATIO (K) -RATIO (K11)) / ALOG (GSTRN (K)/GSTRN (K11))
          TT = SLOPE * ALOG (ABS (AVGSTN (NUMBER)) / GSTRN (K11))
          GRATIO (NUMBER, ITER) =RATIO (K11) -ABS (TT)
83     IF (K11 .EQ. 0) GRATIO (NUMBER, ITER) =RATIO (1)
          IF (ITER .GE. 2) THEN
              ITER1=ITER - 1
              DIFF = ABS (GRATIO (NUMBER, ITER) - GRATIO (NUMBER, ITER1)) /
                  ABS (GRATIO (NUMBER, ITER1))
          *
              IF (ABS (DIFF) .GE. DIFMAX) DIFMAX = ABS (DIFF)
          END IF
          WRITE (3, 1150) NUMBER, AVGSTN (NUMBER), NUMBER, GRATIO
          *
              (NUMBER, ITER), DIFF, DIFMAX
1150    FORMAT (' ** ELEMENT =', I3, 2X, ' AVG. SHEAR STRAIN =', F16.8, 2X,
          * ' GRATIO (' , I2, ') =', F6.2, 2X, ' DIFF =', F10.6, 2X, ' DIFMAX =', F16.8, /)
          7 CONTINUE
          IF (ITER .EQ. 1 .OR. DIFMAX .GT. EPSLON) GO TO 1111
9999   WRITE (3, 1250) ITER
          10 FORMAT (/, ' ITERATION = ', I3)
          STOP
          END

```

SUBROUTINE GEOMET (P, Q, NXE, NYE, AA, BB, COORD, ICOORD, G, NF, INF)

NODAL COORDINATES AND STEERING VECTOR
 FOR A RECTANGULAR MESH OF 4-NODE
 QUADPILATERAL PLANE ELEMENTS
 NUMBERING IN THE Y-DIRECTION

```

INTEGER G (1), INF, NF (INF, 1), P, Q, NXE, NYE, ICOORD, AO, AL, AM, AN
REAL COORD (ICOORD, 1), AA, BB
AO = (P-1) * (NYE+1) + Q
AL = AO + 1
AM = P * (NYE+1) + Q
AN = AM + 1
G (1) = NF (AL, 1)
G (2) = NF (AL, 2)
G (3) = NF (AO, 1)
G (4) = NF (AO, 2)
G (5) = NF (AM, 1)
G (6) = NF (AM, 2)
G (7) = NF (AN, 1)
G (8) = NF (AN, 2)
COORD (1, 1) = (P-1) * AA

```

```

COORD(1,2) = (NYE-Q) * PB
COORD(2,1) = (P-1) * AA
COORD(2,2) = (NYE-Q+1) * PB
COORD(3,1) = P * AA
COORD(3,2) = (NYE-Q+1) * BB
COORD(4,1) = P * AA
COORD(4,2) = (NYE-Q) * BB
RETURN
END
SUBROUTINE NULVEC(VEC,N)
REAL VEC(1)
INTEGER I,N
DO 1 I=1,N
1 VEC(I) = .0
RETURN
END
SUBROUTINE NULL(A,IA,M,N)
INTEGER IA,M,N,I,J
REAL A(IA,1)
DO 1 I=1,M
DO 1 J=1,N
1 A(I,J) = 0.0
RETURN
END
SUBROUTINE FORMD(DEE,IDEE,E,V)

```

STRESS STRAIN MATRIX FOR PLANE ELASTIC STRAIN

```

INTEGER IDEE,I,J
REAL DEE(IDEE,1),E,V,V1,VV
V1=V/(1.0-V)
VV=(1.0-2.0*V)*.5/(1.0-V)
DEE(1,1)=1.0
DEE(2,2)=1.0
DEE(3,3)=VV
DEE(1,2)=V1
DEE(2,1)=V1
DO 1 I=1,3
DO 1 J=1,3
1 DEE(I,J)=DEE(I,J)*E/(2.0*(1.0+V)*VV)
RETURN
END
SUBROUTINE GAUSS(SAMP,ISAMP,GP)

```

GAUSSIAN QUADATURE ABSCISSAE AND WEIGHTS

```

INTEGER ISAMP,GP
REAL SAMP(ISAMP,1)
GO TO(1,2,3,4,5,6,7),GP
2 SAMP(1,1)=1./SQRT(3.)
SAMP(2,1)=-SAMP(1,1)
SAMP(1,2)=1.
SAMP(2,2)=1.
GO TO 1

```

```

3  SAMP (1, 1) = .2*SQRT(15.)
   SAMP (2, 1) = .0
   SAMP (3, 1) = -SAMP (1, 1)
   SAMP (1, 2) = 5./9.
   SAMP (2, 2) = 8./9.
   SAMP (3, 2) = SAMP (1, 2)
   GO TO 1

4  SAMP (1, 1) = .861136311594053
   SAMP (2, 1) = .339981043584856
   SAMP (3, 1) = -SAMP (2, 1)
   SAMP (4, 1) = -SAMP (1, 1)
   SAMP (1, 2) = .347854845137454
   SAMP (2, 2) = .652145154862546
   SAMP (3, 2) = SAMP (2, 2)
   SAMP (4, 2) = SAMP (1, 2)
   GO TO 1

5  SAMP (1, 1) = .906179845938664
   SAMP (2, 1) = .538469310105683
   SAMP (3, 1) = .0
   SAMP (4, 1) = -SAMP (2, 1)
   SAMP (5, 1) = -SAMP (1, 1)
   SAMP (1, 2) = .236926885056189
   SAMP (2, 2) = .478628670499366
   SAMP (3, 2) = .568888888888889
   SAMP (4, 2) = SAMP (2, 2)
   SAMP (5, 2) = SAMP (1, 2)
   GO TO 1

6  SAMP (1, 1) = .932469514203152
   SAMP (2, 1) = .661209386466265
   SAMP (3, 1) = .238619186083197
   SAMP (4, 1) = -SAMP (3, 1)
   SAMP (5, 1) = -SAMP (2, 1)
   SAMP (6, 1) = -SAMP (1, 1)
   SAMP (1, 2) = .171324492379170
   SAMP (2, 2) = .360761573048139
   SAMP (3, 2) = .467913934572691
   SAMP (4, 2) = SAMP (3, 2)
   SAMP (5, 2) = SAMP (2, 2)
   SAMP (6, 2) = SAMP (1, 2)
   GO TO 1

7  SAMP (1, 1) = .949107912342759
   SAMP (2, 1) = .741531185599394
   SAMP (3, 1) = .405845151377397
   SAMP (4, 1) = .0
   SAMP (5, 1) = -SAMP (3, 1)
   SAMP (6, 1) = -SAMP (2, 1)
   SAMP (7, 1) = -SAMP (1, 1)
   SAMP (1, 2) = .129484966168870
   SAMP (2, 2) = .279705391489277
   SAMP (3, 2) = .381930050505119
   SAMP (4, 2) = .417959183673469
   SAMP (5, 2) = SAMP (3, 2)
   SAMP (6, 2) = SAMP (2, 2)
   SAMP (7, 2) = SAMP (1, 2)

```

```

1 CONTINUE
  RETURN
  END
  SUBROUTINE FOR4NF (NF, INF, NN, NODOF, RN)

```

NODE FREEDOM ARRAY FOR MORE
THAN ONE FREEDOM PER NODE

```

  INTEGER INF, NF (INF, 1), NN, NODOF, RN, I, J, K, L
  DO 1 I=1, NN
  DO 1 J=1, NODOF
1  NF (I, J) = 1
    DO 2 I=1, RN
      READ (1, *) K
      DO 3 J=1, NODOF
        READ (1, *) L
3      IF (L.EQ.1) NF (K, J) = 0
2    CONTINUE
      K=1
      DO 4 I=1, NN
      DO 4 J=1, NODOF
      IF (NF (I, J)) 5, 4, 5
5    NF (I, J) = K
      K=K+1
4  CONTINUE
  RETURN
  END
  SUBROUTINE FOR4LN (DER, IDER, FUN, SAMP, ISAMP, I, J)

```

LOCAL COORDINATE SHAPE FUNCTIONS AND THEIR
DERIVATIVES FOR A 4-NODE QUADRILATERAL

```

  INTEGER IDER, ISAMP, I, J
  REAL DER (IDER, 1), FUN (1), SAMP (ISAMP, 1)
  REAL ETA, XI, ETAM, ETAP, XIM, XIP
  ETA=SAMP (I, 1)
  XI=SAMP (J, 1)
  ETAM=.25*(1.0-ETA)
  ETAP=.25*(1.0+ETA)
  XIM=.25*(1.0-XI)
  XIP=.25*(1.0+XI)
  FUN (1)=4.0*XIM*ETAM
  FUN (2)=4.0*XIM*ETAP
  FUN (3)=4.0*XIP*ETAP
  FUN (4)=4.0*XIP*ETAM
  DER (1, 1)=-ETAM
  DER (1, 2)=-ETAP
  DER (1, 3)=ETAP
  DER (1, 4)=ETAM
  DER (2, 1)=-XIM
  DER (2, 2)=XIM
  DER (2, 3)=XIP
  DER (2, 4)=-XIP
  RETURN

```

```

END
SUBROUTINE MATMUL(A,IA,B,IB,C,IC,L,M,N)
INTEGER IA,IB,IC,L,M,N,I,J,K
REAL A(IA,1),B(IB,1),C(IC,1),X
DO 1 I=1,L
DO 1 J=1,N
X=0.0
DO 2 K=1,M
2 X=X+A(I,K)*B(K,J)
C(I,J)=X
1 CONTINUE
RETURN
END
SUBROUTINE TWOBY2(JAC,IJAC,JAC1,IJAC1,DET)
INTEGER IJAC,IJAC1,K,L
REAL JAC(IJAC,1),JAC1(IJAC1,1),DET
DET=JAC(1,1)*JAC(2,2)-JAC(1,2)*JAC(2,1)
JAC1(1,1)=JAC(2,2)
JAC1(1,2)=-JAC(1,2)
JAC1(2,1)=-JAC(2,1)
JAC1(2,2)=JAC(1,1)
DO 1 K=1,2
DO 1 L=1,2
1 JAC1(K,L)=JAC1(K,L)/DET
RETURN
END
SUBROUTINE FORMB(BEE,IBEE,DERIV,IDERIV,VOL,NOD)

```

STRAIN-DISPLACEMENT MATRIX FOR PLANE STRAIN(STRESS)

```

INTEGER IBEE,IDERIV,NOD,K,L,M
REAL BEE(IBEE,1),DERIV(IDERIV,1),VOL(1)
DO 1 M=1,NOD
K=2*M
L=K-1
VOL(L)=DERIV(1,M)
BEE(1,L)=DERIV(1,M)
BEE(3,K)=DERIV(1,M)
VOL(L)=DERIV(2,M)
BEE(2,K)=DERIV(2,M)
BEE(3,L)=DERIV(2,M)
1 CONTINUE
RETURN
END
SUBROUTINE FMBIGK(BIGK,IBIGK,KM,IKM,G,DOF)

```

```

INTEGER IBIGK,IKM,G(1),DOF,I,J
REAL BIGK(IBIGK,1),KM(1)
DO 1 I=1,DOF
IF(G(I).EQ.0) GO TO 1
2 DO 3 J=1,DOF
IF(G(J).EQ.0) GO TO 3
4 BIGK(G(I),G(J))=BIGK(G(I),G(J))+KM(I,J)

```

```

3 CONTINUE
1 CONTINUE
RETURN
END
SUBROUTINE FOPMKV (BK, KM, IKM, G, N, DOF)

```

ASSEMBLES ELEMENT MATRICES INTO SYMMETRICAL BAND
GLOBAL MATRIX (STORED AS A VECTOR)

```

INTEGER G(1), IKM, N, DOF, I, J, CD, VAL
REAL BK(1), KM(IKM, 1)
DO 1 I=1, DOF
IF (G(I) .EQ. 0) GO TO 1
2 DO 5 J=1, DOF
IF (G(J) .EQ. 0) GO TO 5
3 CD=G(J) -G(I) + 1
IF (CD-1) 5, 4, 4
4 VAL=N*(CD-1) +G(I)
BK(VAL) =BK(VAL) +KM(I, J)
5 CONTINUE
1 CONTINUE
RETURN
END
SUBROUTINE MATPAN(A, IA, B, IB, M, N)
INTEGER IA, IB, M, N, I, J
REAL A(IA, 1), B(IB, 1)
DO 1 I=1, M
DO 1 J=1, N
1 A(J, I) =B(I, J)
RETURN
END
SUBROUTINE MATADD(A, IA, B, IB, M, N)
INTEGER IA, IB, M, N, I, J
REAL A(IA, 1), B(IB, 1)
DO 1 I=1, M
DO 1 J=1, N
1 A(I, J) =A(I, J) +B(I, J)
RETURN
END
SUBROUTINE BANDRED(BK, L, KB)
REAL BK(1), SUM
INTEGER L, KB, I, IL1, KBL, IJ, J, NKB, NI, NJ
DO 1 I=2, L
IL1=I-1
KBL=IL1+KB
IF (KBL-L) 3, 3, 2
2 KBL=L
3 DO 1 J=I, KBL
IJ= (J-I) *L+I
SUM=BK(IJ)
NKB=J-KB+1
IF (NKB) 4, 4, 5
4 NKB=1
5 IF (NKB-IL1) 6, 6, 8

```

```

6 DO 7 N=NKB, I1
  VI=(I-N)*L+N
  NJ=(J-N)*L+N
7 SUM=SUM-BK(VI)*BK(NJ)/BK(N)
8 BK(IJ)=SUM
1 CONTINUE
  RETURN
  END
  SUBROUTINE BACK1(BK,R,L,KB)
  REAL BK(1),R(1),SUM
  INTEGER L,KB,I,I1,NKB,JN,K
  R(1)=R(1)/BK(1)
  DO 1 I=2,L
    SUM=R(I)
    I1=I-1
    NKB=I-KB+1
    IF(NKB) 2,2,3
2 NKB=1
3 DO 4 K=NKB,I1
  JN=(I-K)*L+K
  SUM=SUM-BK(JN)*R(K)
4 CONTINUE
  R(I)=SUM/BK(I)
1 CONTINUE
  RETURN
  END
  SUBROUTINE BACK2(BK,R,L,KB)
  REAL BK(1),R(1),SUM
  INTEGER L,KB,JJ,I,I1,NKB,JN,K
  DO 1 JJ=2,L
    I=L-JJ+1
    SUM=0.0
    I1=I+1
    NKB=I-1+KB
    IF(NKB-L) 3,3,2
2 NKB=L
3 DO 4 K=I1,NKB
  JN=(K-I)*L+I
4 SUM=SUM+BK(JN)*R(K)
  R(I)=R(I)-SUM/BK(I)
1 CONTINUE
  RETURN
  END
  SUBROUTINE MVMULT(M,IM,V,K,L,Y)
  INTEGER IM,K,L,I,J
  REAL M(IM,1),V(1),Y(1),X
  DO 1 I=1,K
    X=0.0
    DO 2 J=1,L
2 X=X+M(I,J)*V(J)
  Y(I)=X
1 CONTINUE
  RETURN
  END

```

```

SUBROUTINE PRINTV (V,L)
INTEGER L
REAL V(L)
WRITE (3,1) V
1 FORMAT (1H ,10F12.4)
RETURN
END

```

```

SUBROUTINE PRINTU (V,L)
INTEGER L
REAL V(L)
DO 10 I=1,L
WRITE (3,1) I,V(I)
1 FORMAT (1H ,1I2,' ' NUMBER OF FREEDOM (' ,I2,' ) = ',E12.4)
10 CONTINUE
RETURN
END

```

```

SUBROUTINE VGEOM (P,Q,NXF,NYE,COORD,ICOORD,G,NF,INF,
*RADIUS,DEPTH)

```

NODAL COORDINATES AND STEERING VECTOR
 FOR A VARIABLE RECTANGULAR MESH OF 4-NODE
 QUADRILATERAL PLANE ELEMENTS

```

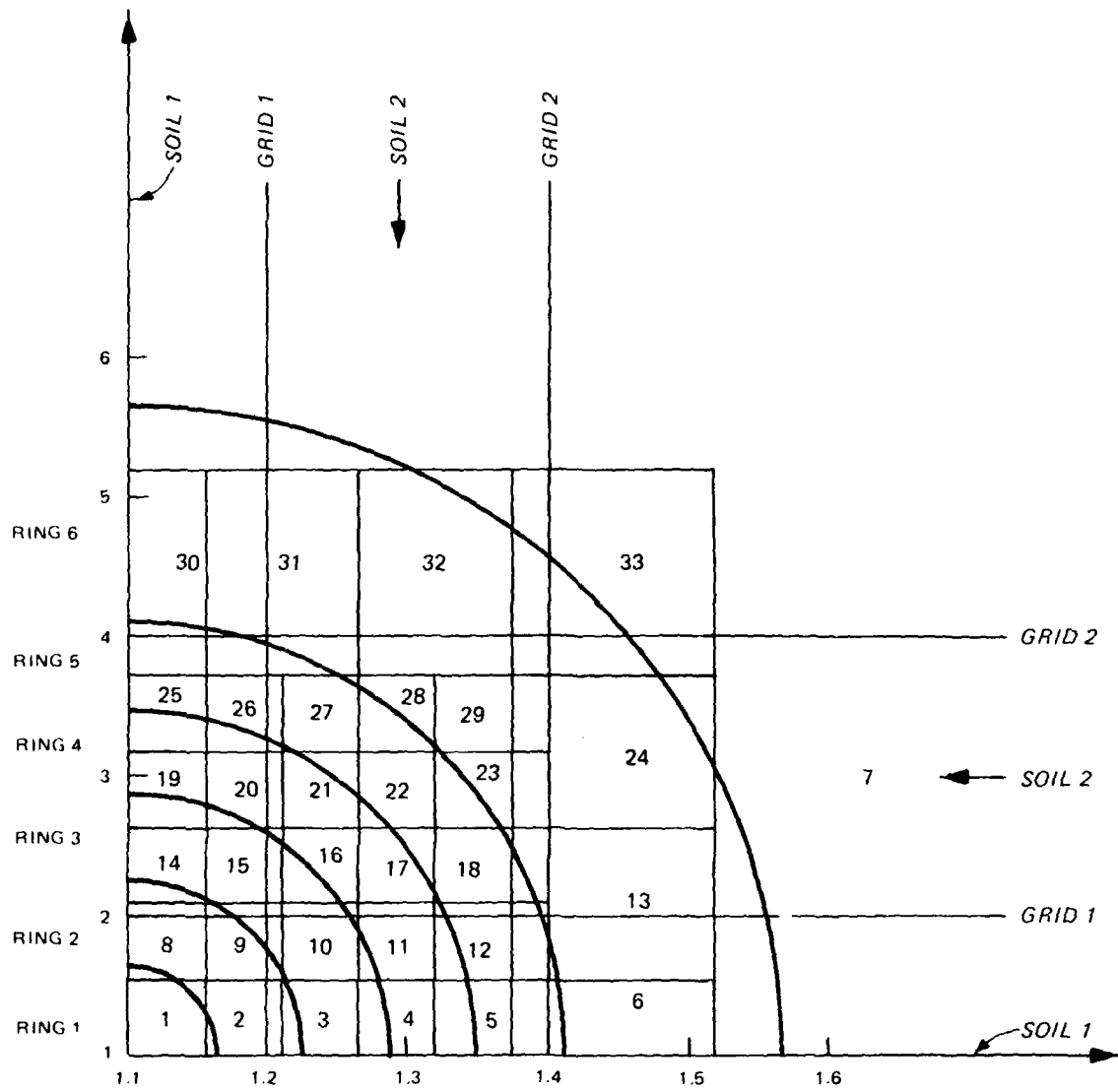
INTEGER P,Q,NXF,NYE,ICOORD,INF,G(1),NF(INF,1),AO,AL,AM,AN
REAL COORD(ICOORD,1),RADIUS(1),DEPTH(1)
AO=(P-1)*(NYE+1)+Q
AL=AO+1
AM=P*(NYE+1)+Q
AN=AM+1
G(1)=NF(AL,1)
G(2)=NF(AL,2)
G(3)=NF(AO,1)
G(4)=NF(AO,2)
G(5)=NF(AM,1)
G(6)=NF(AM,2)
G(7)=NF(AN,1)
G(8)=NF(AN,2)
COORD(1,1)=RADIUS(P)
COORD(2,1)=RADIUS(P)
COORD(1,2)=DEPTH(Q+1)
COORD(4,2)=DEPTH(Q+1)
COORD(2,2)=DEPTH(Q)
COORD(3,2)=DEPTH(Q)
COORD(3,1)=RADIUS(P+1)
COORD(4,1)=RADIUS(P+1)
RETURN
END

```

```
SUBROUTINE PRINTW(U,V,L)
  INTEGER L
  REAL U(L),V(L)
  WRITE(3,1)U,V
1  FORMAT(1H ,3E12.4,34X,3E12.4)
  RETURN
END
```

APPENDIX B

SUMMARY TABLE OF WEIGHTING FACTORS



Ring 1 = Square 1

$$\text{Ring 2} = \frac{\text{Sq. 8} + \text{Sq. 9} + \text{Sq. 2}}{3}$$

$$\text{Ring 3} = \frac{\text{Sq. 14} + \text{Sq. 15} + \text{Sq. 10} + \text{Sq. 3}}{4}$$

$$\text{Ring 4} = \frac{\text{Sq. 19} + \text{Sq. 20} + \text{Sq. 21} + \text{Sq. 16} + \text{Sq. 17} + \text{Sq. 11} + \text{Sq. 4}}{7}$$

$$\text{Ring 5} = \frac{\text{Sq. 25} + \text{Sq. 26} + \text{Sq. 27} + \text{Sq. 22} + \text{Sq. 18} + \text{Sq. 12} + \text{Sq. 5}}{7}$$

$$\text{Ring 6} = \frac{\text{Sq. 30} + \text{Sq. 31} + \text{Sq. 32} + \text{Sq. 24} + \text{Sq. 13}}{5}$$

Square	Corner	Weighting Factor	= $\frac{(\text{Width})(\text{Factor})}{\text{Area}}$
1	1,1		0.55
	11,1		0.55
	1,2		0.026
	11,2		0.026
2	1,2		0.30
	11,1		0.45
	11,2		0.022
	13,1		0.047
	13,2		0.0022
3	1,2		0.222
	1,3		0.077
	13,1		0.27
	13,2		0.013
4	1,3		0.30
	13,1		0.27
	13,2		0.013
5	1,3		0.17
	1,4		0.13
	13,1		0.27
	13,2		0.013
6	1,4		0.42
	1,5		0.38
	13,1		0.13
	13,2		0.006
	14,1		1.0
	14,2		0.047
7		Contribution neglected	
8		Same as Square 2	
9	1,2		0.25
	3,2		0.0256
	11,2		0.25
	13,2		0.256
	2,2		0.547
	12,2		0.547
10	1,2		0.185
	1,3		0.064
	3,2		0.019
	3,3		0.0066
	13,2		0.149

(Continued)

(Sheet 1 of 4)

Square	Corner	Weighting Factor = $\frac{(\text{Width})(\text{Factor})}{\text{Area}}$
10	2,2	0.406
	2,3	0.141
11	1,3	0.25
	3,3	0.0256
	13,3	0.149
	2,3	0.547
12	1,3	0.142
	1,4	0.106
	3,3	0.015
	3,4	0.011
	13,2	0.149
	2,3	0.313
	2,4	0.234
13	1,4	0.35
	1,5	0.31
	3,4	0.25
	3,5	0.22
	13,2	0.13
	13,3	0.02
	2,4	0.77
	2,5	0.11
	14,2	0.15
	14,3	0.02
14		Same as Square 3
15		Same as Square 9
16	3,2	0.11
	3,3	0.04
	13,2	0.11
	13,3	0.04
17	3,3	0.15
	13,2	0.11
	13,3	0.04
18	3,3	0.09
	3,4	0.06
	13,2	0.11
	13,3	0.04
19		Same as Square 4
20		Same as Square 11

(Continued)

(Sheet 2 of 4)

Square	Corner	Weighting Factor = $\frac{(\text{Width})(\text{Factor})}{\text{Area}}$
21		Same as Square 17
22	3,3 13,3	0.15 0.15
23	3,3 3,4 13,3	0.09 0.06 0.15
24	3,4 3,5 13,3 13,4 14,3 14,4	0.42 0.38 0.12 0.03 0.86 0.23
25		Same as Square 5
26		Same as Square 12
27		Same as Square 18
28		Same as Square 23
29	3,3 3,4 13,3 13,4	0.09 0.06 0.09 0.06
30		Same as Square 6
31		Same as Square 13
32		Same as Square 24

1st subindex of corner:

- 1 - Beam 1
- 11 - Beam 1 from the other direction
- 2 - Beam 2
- 12 - Beam 2 from the other direction
- 3 - Grid 1
- 13 - Grid 1 from the other direction
- 4 - Grid 2
- 14 - Grid 2 from the other direction

(Continued)

(Sheet 3 of 4)

Square

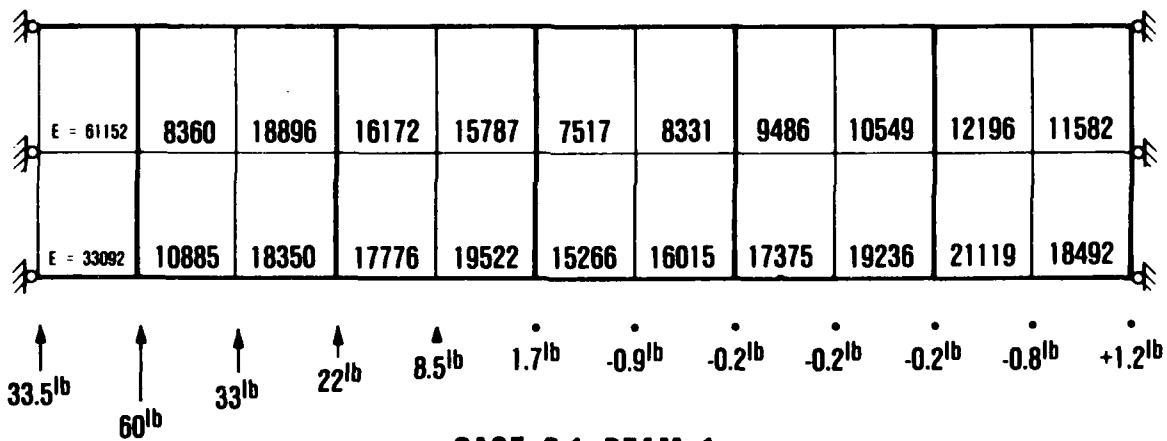
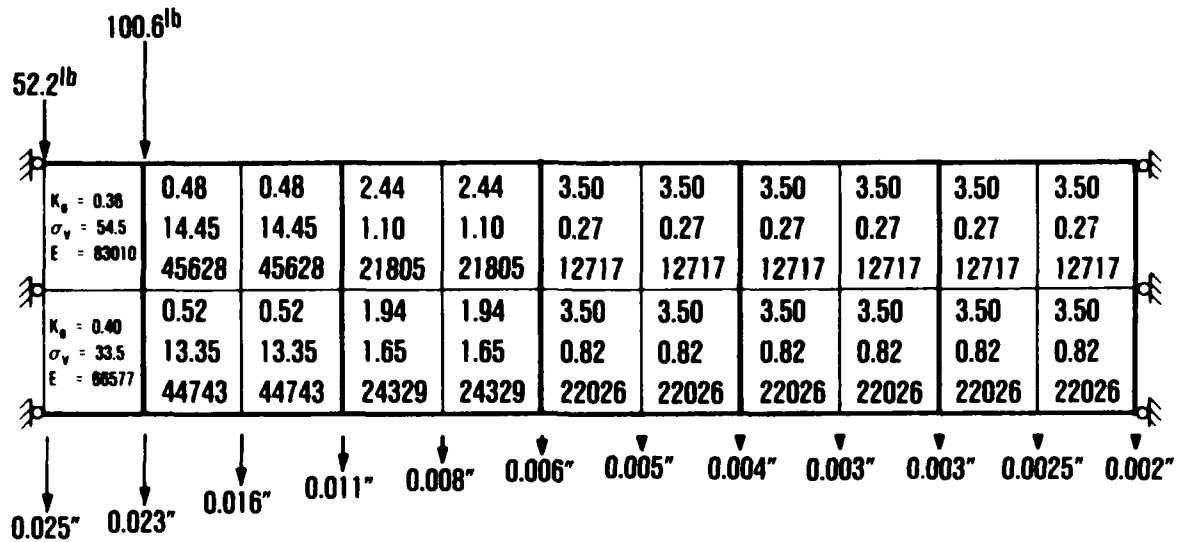
Corner

Weighting Factor = $\frac{(\text{Width})(\text{Factor})}{\text{Area}}$

2nd subindex of corner:
The corner number on the
beam referenced by the
first subindex

APPENDIX C

SUMMARY OF INPUT AND OUTPUT FOR SGRID ANALYSIS

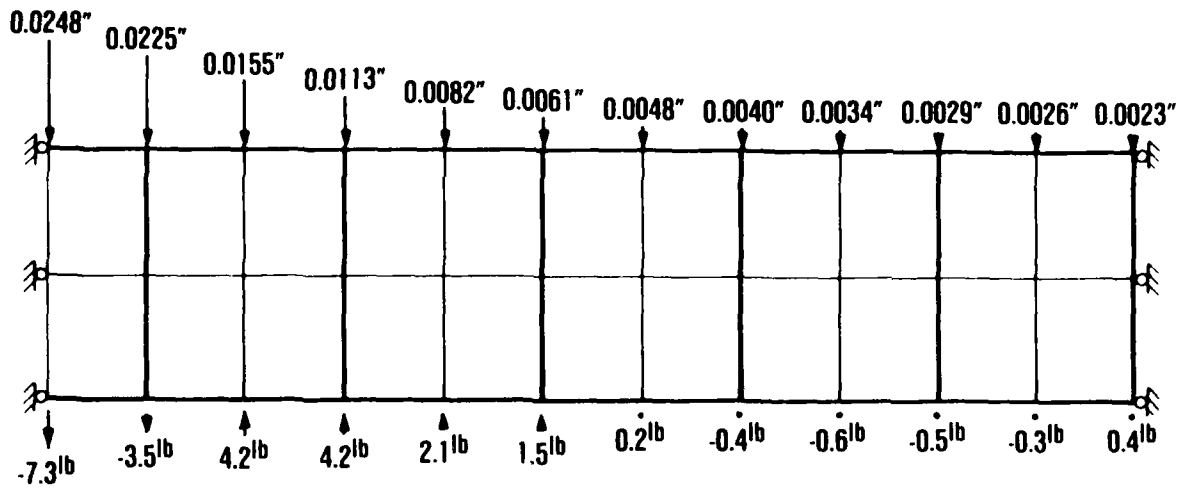


CASE 2-1 BEAM 1

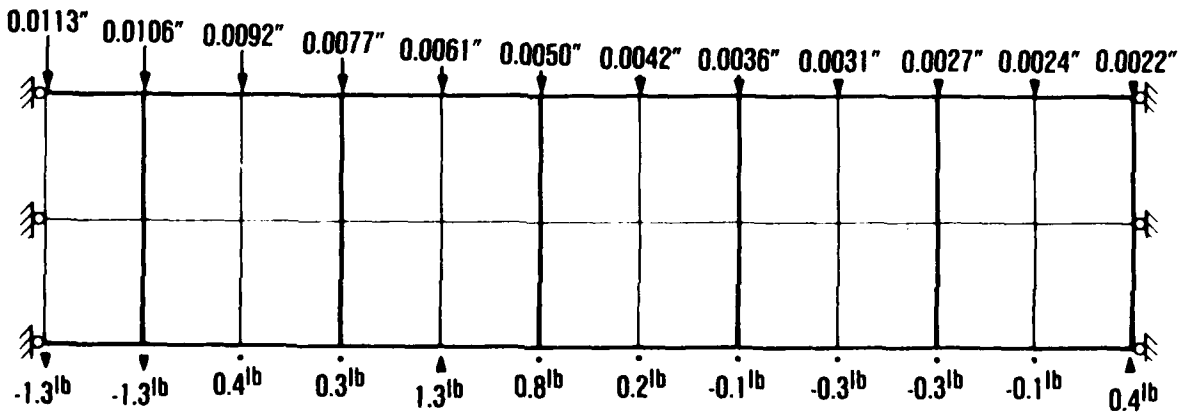
	19.5 ^{lb}	14.2 ^{lb}										
K_p	0.39	0.87	0.87	2.74	2.74	3.50	3.50	3.50	3.50	3.50	3.50	
σ_v	14.45	1.9	1.9	0.43	0.43	0.27	0.27	0.27	0.27	0.27	0.27	
E	43482	19562	19562	14312	14312	12717	12717	12717	12717	12717	12717	
K_p	0.43	0.68	0.68	1.47	1.47	2.11	2.11	2.11	2.11	2.11	2.11	
σ_v	13.35	4.1	4.1	1.28	1.28	0.82	0.82	0.82	0.82	0.82	0.82	
E	42723	26669	26669	19254	19254	17792	17792	17792	17792	17792	17792	
	0.016"	0.014"	0.012"	0.009"	0.007"	0.006"	0.005"	0.004"	0.003"	0.003"	0.002"	0.002"

E = 25627	7001	10200	9420	11821	10923	10152	10509	11889	11715	11653	
E = 26558	11755	13917	14459	15516	14724	14454	15127	16632	16575	14933	
3.0 ^{lb}	14.2 ^{lb}	5.6 ^{lb}	6.9 ^{lb}	2.2 ^{lb}	3.1 ^{lb}	0.5 ^{lb}	-0.5 ^{lb}	-0.8 ^{lb}	-1.0 ^{lb}	-0.5 ^{lb}	1.0 ^{lb}

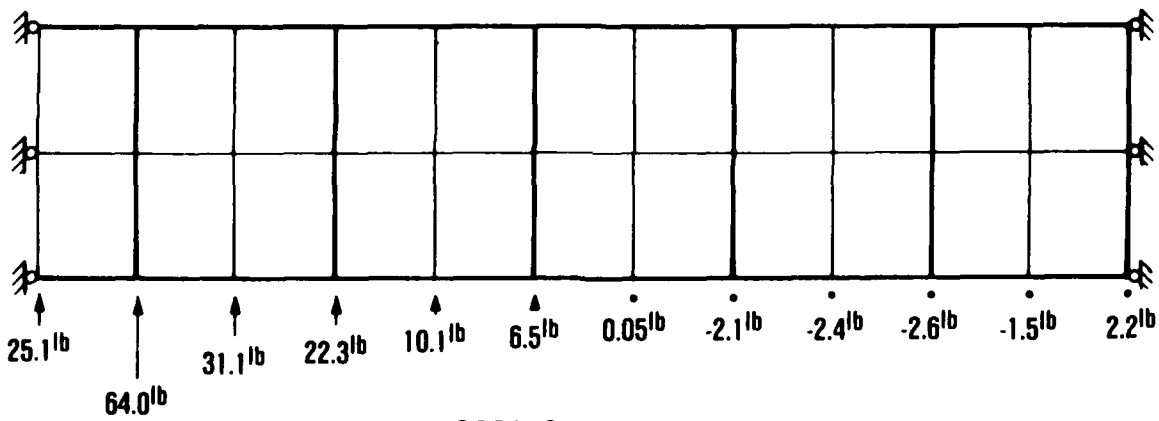
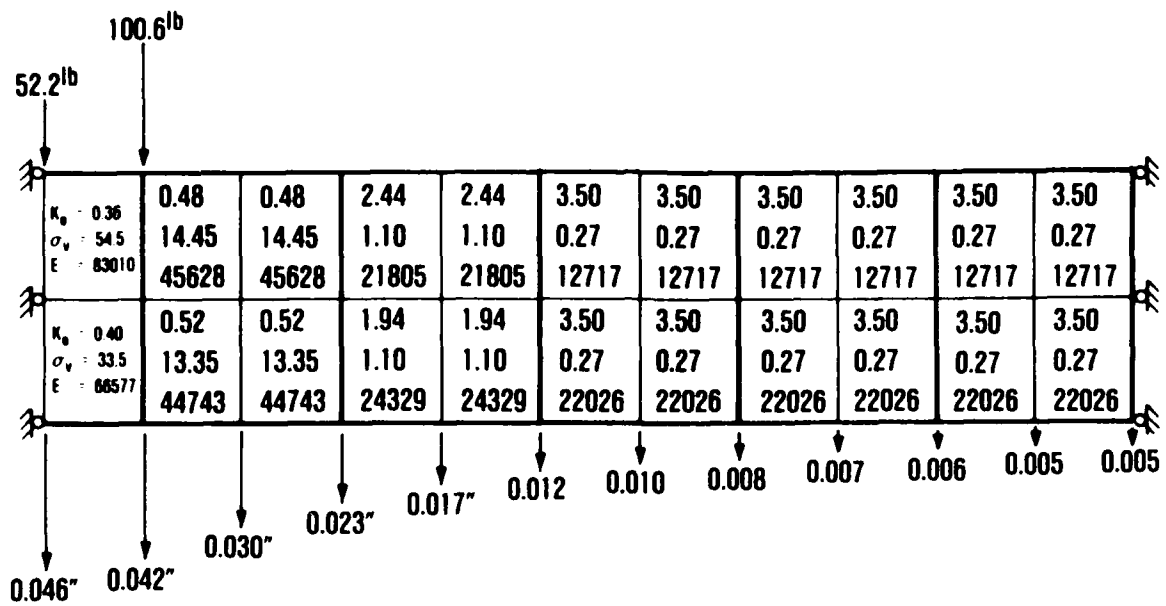
CASE 2-1 BEAM 2



GRID 1

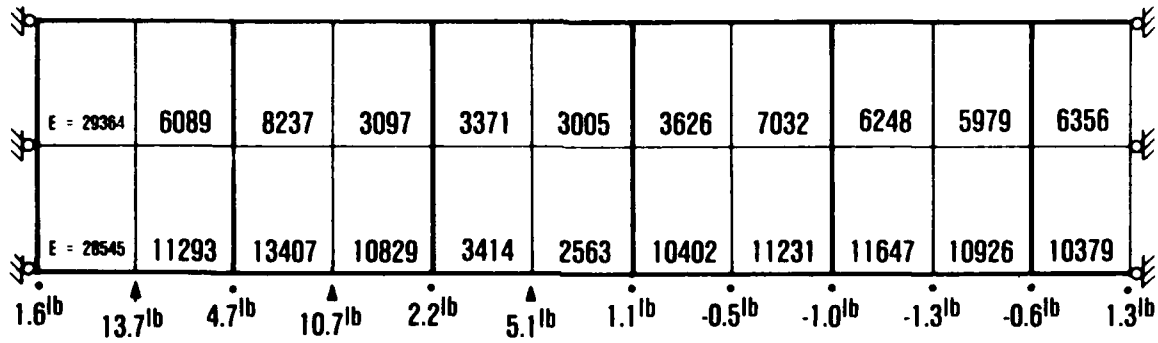
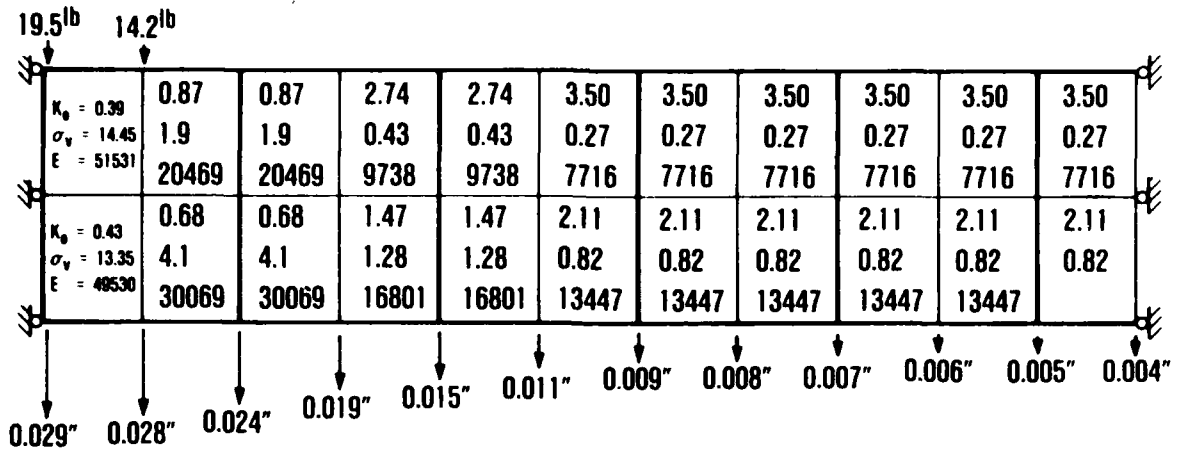


GRID 2
CASE 2-1

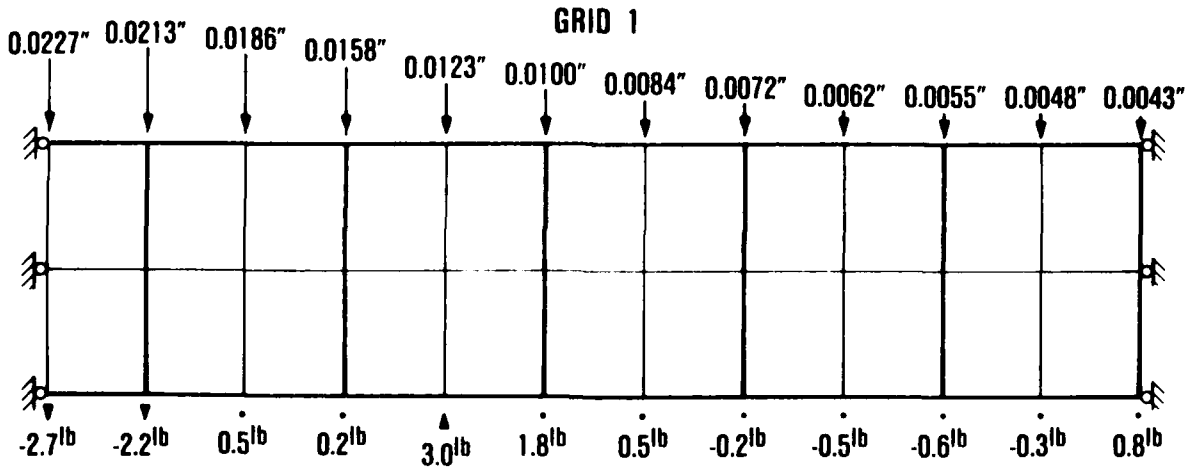
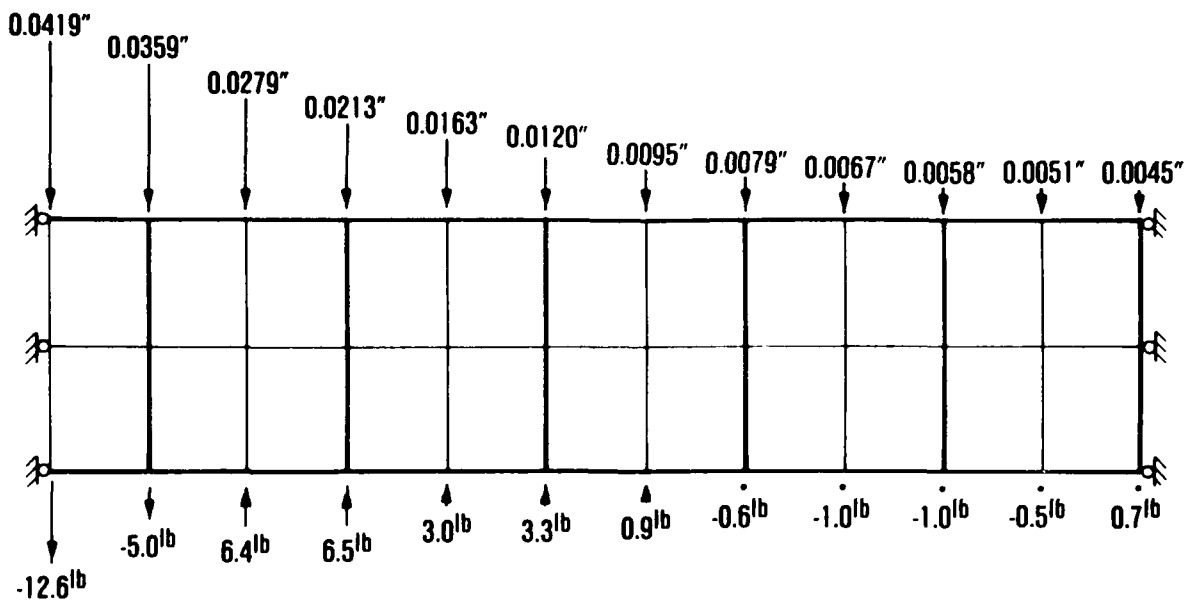


CASE 3-2 BEAM 1

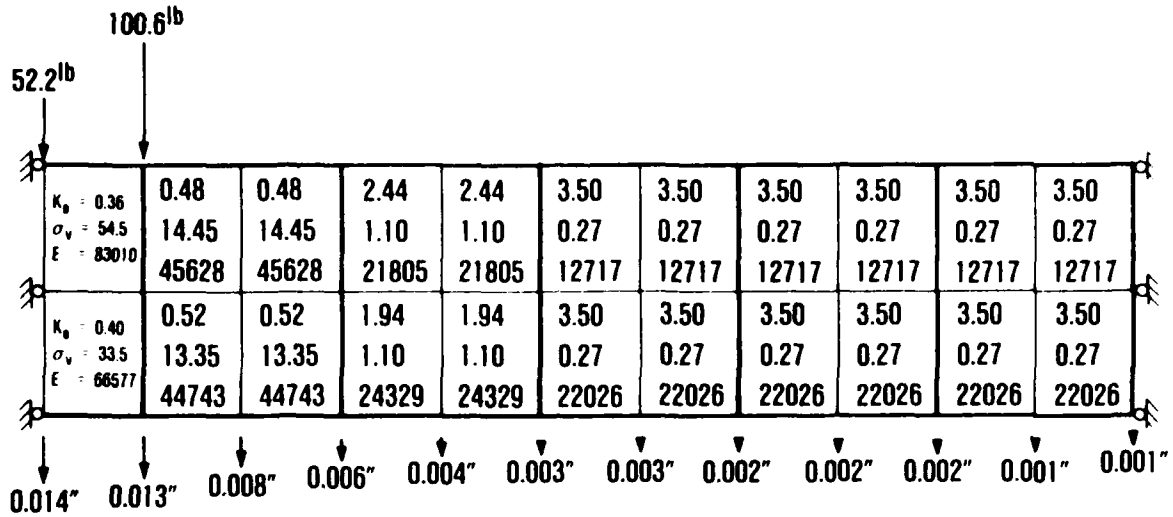
$K_b = 0.36$ $\sigma_v = 54.5$ $E = 83010$	0.48	0.48	2.44	2.44	3.50	3.50	3.50	3.50	3.50	3.50
	14.45	14.45	1.10	1.10	0.27	0.27	0.27	0.27	0.27	0.27
	45628	45628	21805	21805	12717	12717	12717	12717	12717	12717
$K_b = 0.40$ $\sigma_v = 33.5$ $E = 66577$	0.52	0.52	1.94	1.94	3.50	3.50	3.50	3.50	3.50	3.50
	13.35	13.35	1.10	1.10	0.27	0.27	0.27	0.27	0.27	0.27
	44743	44743	24329	24329	22026	22026	22026	22026	22026	22026



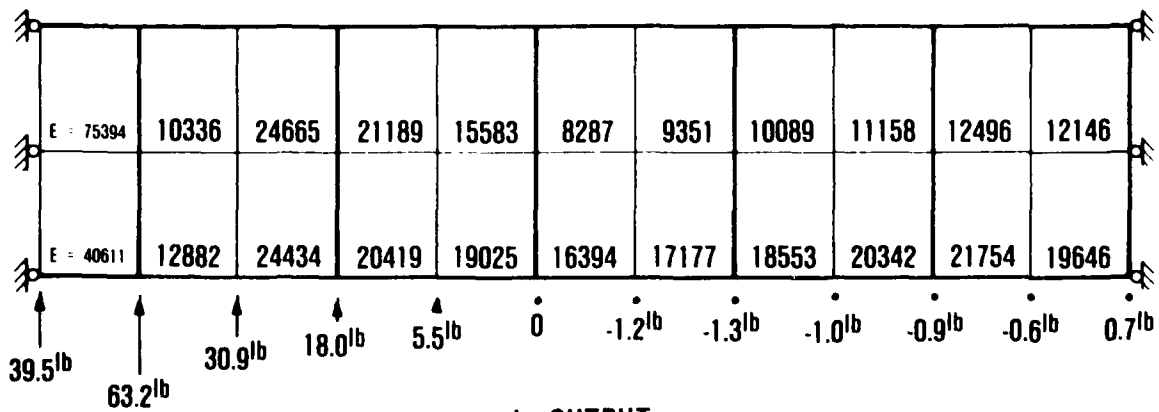
CASE 3-2 BEAM 2



CASE 3-2



a. INPUT

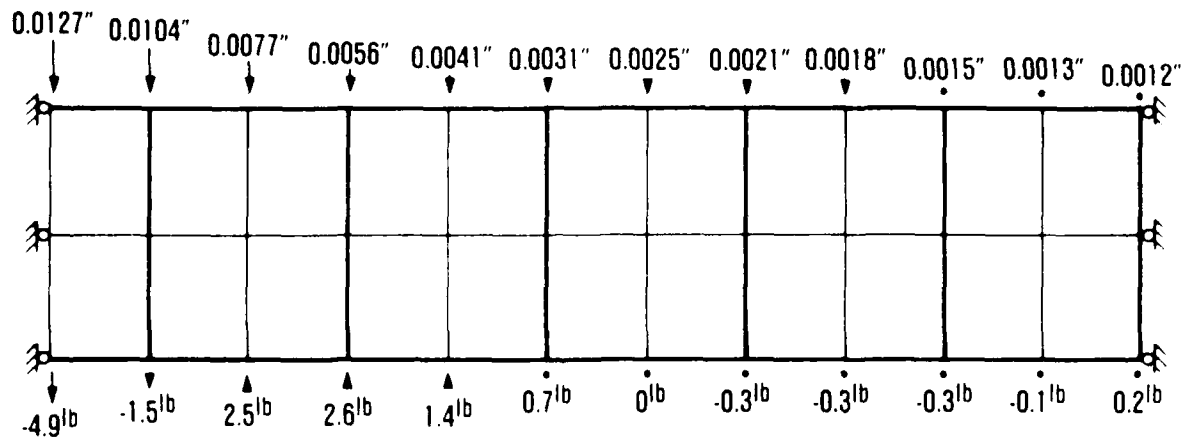


b. OUTPUT
CASE 4-3 BEAM 1

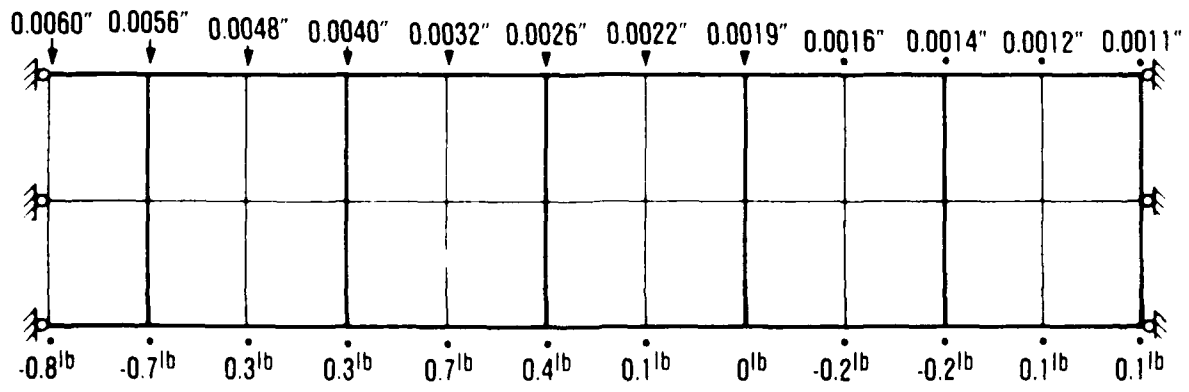
	19.5lb	14.2lb										
K_b	0.39	0.87	0.87	2.74	2.74	3.50	3.50	3.50	3.50	3.50	3.50	
σ_v	14.45	1.9	1.9	0.43	0.43	0.27	0.27	0.27	0.27	0.27	0.27	
E	43482	19562	19562	14312	14312	12601	12601	12601	12601	12601	12601	
K_b	0.43	0.68	0.68	1.47	1.47	2.11	2.11	2.11	2.11	2.11	2.11	
σ_v	13.35	4.1	4.1	1.28	1.28	0.82	0.82	0.82	0.82	0.82	0.82	
E	42723	26669	26669	19254	19254	17738	17738	17738	17738	17738	17738	
	0.008"	0.008"	0.006"	0.005"	0.004"	0.003"	0.002"	0.002"	0.002"	0.002"	0.001"	0.001"

E	27798	8701	12589	10969	13888	10804	10572	11046	12099	12058	12060	
E	30330	14161	16799	15814	18316	15205	15199	15987	17079	16999	16043	
	6.7lb	14.1lb	5.1lb	5.7lb	1.8lb	1.4lb	0.1lb	-0.4lb	-0.5lb	-0.6lb	-0.2lb	0.5lb

CASE 4-3 BEAM 2



GRID 1



GRID 2
CASE 4-3

END

1-87

DTIC